ABSTRACT

LU, YUAN. Distributed and Channel-Adaptive Spectrum Detection, Sensing, and Access for Rational Cognitive Radio Users. (Under the direction of Dr. Alexandra Duel-Hallen.)

Cognitive radio (CR) can potentially improve spectrum utilization while limiting disruption to and maintaining the existing communication infrastructure of the licensed, or primary-user (PU), network. In a multichannel CR network, unlicensed, or secondary users (SUs) strive to discover idle PU channels through spectrum sensing and have to share the available spectrum resources with other competing SUs.

In practice, SUs' sensing capabilities are usually limited in software-defined radio systems due to hardware limitations. Moreover, it is often necessary to make autonomous sensing decisions without the coordination of a central controller. Sensing strategy and medium access control (MAC) design objectives include high throughput, resolved competition, distributed implementation, user fairness, PU protection and robustness to non-ideal conditions.

We first study distributed sensing and access for multiple noncooperative SUs with one-shot sensing capabilities in Chapter 1. Our approach to this problem is to exploit heterogeneous SU preferences over potentially available channels, which naturally helps to randomize sensing decisions and thereby to relieve SU congestion. The proposed channel-aware sensing strategy is fully distributed and relies only on the local channel state information (CSI) of the SU-to-SU links, which can be obtained by using the proposed pilot-based prediction method. However, it cannot completely eliminate overlapped sensing decisions, and this issue is remedied by a novel first-come-first-served (FCFS) MAC scheme at negligible cost.

Chapter 2 is devoted to the underlying spectrum detection techniques. It is well-known that the capability to obtain reliable spectrum sensing results is vital for any CR system, with the goal of capturing as many spectrum opportunities as possible while maintaining guaranteed PU protection. However, conventional spectrum detection methods cannot achieve these goals when the average signal-to-noise ratio (SNR) of the fading channel between the PU transmitter and the SU sensor is low and this limitation is to a large degree due to the fixed sensing threshold, which is determined from the miss detection (MD) rate averaged over the fading distribution. This observation readily leads us to the proposed CSI-adaptive detection threshold approach. The resulting time-varying false alarm (FA) rate accurately reflects the concurrent PU-to-SU channel quality and thereby enables the SUs to select channels with clearly detectable PU traffic. Assuming sufficient spatial and frequency diversity, it also randomizes sensing decisions.

While the noncooperative approaches in Chapter 1–2 exploit multiuser and multichannel diversity gains inherent to a wireless environment, the possibility of SU cooperation brings in yet another degree of freedom for geographically separated SUs. However, fair payoff (spectrum

access) allocation has not been investigated for cooperative sensing in multichannel CR networks with heterogeneous PU signal quality at different SU sensors although such scenarios are prevalent in practice. It is proposed to decouple the coalition formation and the access (payoff) allocation problems by modeling these processes as a two-layer coalitional game. This game fosters cooperation by providing each SU with the access opportunities it deserves.

Finally, in Chapter 4, we shift our focus to the single-SU joint stopping rule and sensing order optimization problem assuming sequential sensing capability and perfect CSI. We show that it is optimal to stop at the first sensed idle channel when the optimal sensing order is employed. We develop a computationally efficient greedy algorithm to solve the simplified sensing order selection problem with myopic stopping. This algorithm closely approximates the optimal solution, runs in polynomial time, has negligible memory requirements and allows the SU to check the optimality of the output solution.

In summary, this thesis contributes to the CR research area with novel channel-aware sensing strategies, detection techniques, game models, and algorithms, which underscore the importance of taking the underlying CSI into account when designing a CR system.

Distributed and Channel-Adaptive Spectrum Detection, Sensing, and Access for Rational Cognitive Radio Users

by
Yuan Lu

A dissertation submitted to the Graduate Faculty of
North Carolina State University
in partial fulfillment of the
requirements for the Degree of
Doctor of Philosophy

Electrical Engineering

Raleigh, North Carolina

2016

APPROVED BY:

Dr. Brian Hughes	Dr. Hans Hallen
Dr. Wenye Wang	Dr. Alexandra Duel-Hallen Chair of Advisory Committee

BIOGRAPHY

Yuan Lu was born in Xi'an and moved to Shenzhen, China, when she was ten. She received the B.E. degree in electrical engineering from Southeast University, Nanjing, China, in 2008. In 2009, she enrolled in the M.S. program and transferred to the Ph.D. program one year after, in the Department of Electrical and Computer Engineering, North Carolina State University, Raleigh, NC, USA. Since then she has been working toward the Ph.D. degree under the supervision of Dr. Alexandra Duel-Hallen. Her research interests include cognitive radio, wireless and digital communications, signal detection and estimation, cross-layer design, multi-agent learning, and cooperative game theory. She won the NC State University outstanding graduate teaching assistant award in 2015.

ACKNOWLEDGEMENTS

I wish to thank a lot of people who have helped me through this educational adventure.

First and foremost to my advisor, Dr. Alexandra Duel-Hallen, for her knowledge, support, advices, thoughtfulness, keen insights and so much more. I am especially grateful for her encouragement and patient guidance during the most difficult time of my research. Thank you for having faith in me nonetheless, thank you for giving me the opportunity to be your student and helping me get started, and thank you for always keeping me on track and focused.

I would also like to thank the rest of my current and former committee members: Dr. Brian Hughes, Dr. Hans Hallen, Dr. Huaiyu Dai and Dr. Wenye Wang for their insightful comments and careful criticism on my research. My extended thanks to all professors who have taught me as a graduate student here in the NC State University.

I would like to again thank my advisor Dr. Alexandra Duel-Hallen, as well as Dr. Dror Baron, Dr. Keith Townsend, Mrs. Cecilia Townsend and, most importantly, my former students for nominating and supporting me to win the graduate teaching assistant award.

I appreciate the help and the provided computing resources from Dr. Gary Howell and the high-performance computing (HPC) group at the NC State University. Special thanks also go to Dr. Tao Jia for useful information and discussions on channel gain prediction.

I would also thank all my peer graduate students and friends studying and working in the engineering building II for the great conversations that we had, the happy moments that we shared, and also the stressful days we went through together during the past few years.

Last but not least, I thank my parents for bringing me to this world and being there for me all along. I thank my husband Jiwei Zhu and my best friend Shiyi Zhao for your company. I am very lucky to have you in my life.

TABLE OF CONTENTS

LIST OF TABLES

LIST OF FIGURES

LIST OF ABBREVIATIONS

***c*NBS** *coarse* Nash bargaining solution

***f*NBS** *fine* Nash bargaining solution

AWGN additive white Gaussian noise

BER bit error rate

BG backward-direction greedy

cdf cumulative distribution function

CDR constant detection rate

CR cognitive radio

CSI channel state information

DCA dynamic channel assignment

DP dynamic programming

FA false alarm

FCFS first-come-first-served

FG forward-direction greedy

i.i.d. independent and identically distributed

LRP long range prediction

MAC medium access control

MD miss detection

MMSE minimum mean square error

MS myopic stopping

NBS Nash bargaining solution

NMSE normalized mean square error

NTU nontransferable utility

OS optimal stopping

pdf probability density function

POMDP partially observable Markov decision process

PTU partially transferable utility

PU primary user

ROC receiver operating characteristic

SC selection combining

SNR signal-to-noise ratio

SU secondary user

TDFS time division fair share

TDMA time-division multiple access

TG two-pass greedy

TU transferable utility

Chapter 1

Spectrum Sensing and Access for Noncooperative Secondary Users with One-Shot Sensing Capabilities

In hardware-constrained cognitive radio (CR) ad hoc networks, secondary users (SUs) with limited sensing capabilities strive to discover and share available spectrum resources without impairing primary-user (PU) transmission. In this chapter, we assume each SU can sense only one channel within each time slot due to the hardware constraints. A novel noncooperative sensing strategy is analyzed in this chapter where the reward is adapted to the SU-link channel state information (CSI) prior to sensing, thus randomizing sensing decisions and boosting the network throughput. Moreover, CSI-aided sensing is combined with a novel first-come-first-served (FCFS) medium access control (MAC) scheme that resolves SU competition prior to sensing. Finally, a pilot-based CSI prediction method is developed to enable the proposed CSI-aided sensing strategies for mobile scenarios. Analytical and numerical results demonstrate that the proposed sensing and access methods significantly outperform nonadaptive sensing strategies for practical mobile CR scenarios with CSI mismatch, imperfect spectrum sensors, and pilot overhead.

1.1 Introduction

Resolving congestion among SUs is challenging in hardware-constrained autonomous CR networks. Traditionally, sensing decisions are made using channel availability information, e.g., a statistical model of PU traffic [1]. For example, the myopic sensing policy [2] bases sensing choices exclusively on PU occupancy. However, since the PU transmission range is typically larger than the SU range [3] as illustrated in Figure 1.1, all neighboring SUs make similar sens-

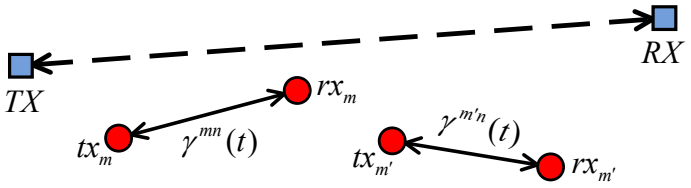

Figure 1.1: A PU TX–RX pair and SU tx–rx pairs m and m'.

ing decisions when the myopic strategy is employed, leading to potential SU collisions [4]. In principle, fair medium access for each idle channel can be accomplished using carrier sensing, random backoff, control message exchange, etc., so the SUs competing for the same channel are equally likely to gain access, and SU collisions at the physical layer are avoided. However, in a hardware-constrained CR network, a collision-avoidance MAC scheme alone is not sufficient since it results in poor spectrum utilization and low CR network throughput. To improve the throughput, a randomized sensing policy which spreads SUs' sensing decisions over different channels is necessary. Several strategies in the literature, e.g., [1, 4–8], address this issue by randomizing sensing decisions, using negotiation, or employing game theory, but these strategies provide limited throughput improvement because they reduce an SU's ability to sense its preferred channel.

One limitation of previously proposed sensing strategies is the choice of reward given by the channel bandwidth, which does not diversify sensing choices. We propose to *adapt the reward to the instantaneous channel gain of the SU transmitter–receiver link*. This reward varies over SU locations and frequencies due to channel fading and thus randomizes sensing decisions. Moreover, SUs boost their individual throughputs by favoring spectrum opportunities with high expected transmission rates.

The proposed strategy matches the reward employed by the SUs to the data rate achieved during transmission. We assume that the SU transmitter obtains the CSI and adapts to it. Adaptation to the CSI of the secondary link to improve channel access and/or transmission rate has been proposed in, e.g., [9–11]. However, in these references, adaptation took place after sensing and thus did not help to alleviate SU congestion when making sensing decisions. To the best of our knowledge, adaptation to SU link CSI prior to sensing was explored only in [12–14]. However, in [12] and [13], SUs sense multiple channels prior to transmission while in this chapter we focus on one-shot sensing to reduce the sensing load. Moreover, collision resolution requires excessive message exchange on the control channel in [13] and is not included in [12, 14]. In contrast, we propose to combine CSI-aided sensing with novel FCFS MAC and demonstrate throughput advantages of this combination as well as its optimality under a fair time-share constraint.

The investigations [12, 13] employ idealistic assumptions, including static SUs and perfect CSI knowledge at the sensor while [14] presents a two-dimensional partially observable Markov decision process (POMDP) framework for CSI tracking assuming pedestrian speeds. We investigate vehicular CR systems where fading CSI quickly becomes outdated. To enable the proposed CSI adaptation prior to sensing, we develop a CR-specific pilot-based multipath fading prediction method and analyze its overhead requirements. Moreover, we evaluate the impact of frequency correlation on multichannel diversity provided by CSI-adaptive strategies.

Contributions:

- Propose and analyze a novel distributed sensing strategy for a hardware-constrained CR system that adapts the reward to the channel gain of the SU link.
- Combine the proposed CSI-adaptive sensing policy with FCFS MAC and demonstrate significant throughput gains over nonadaptive sensing strategies.
- Demonstrate robustness of the CSI-aided sensing strategy to mobile speed, correlated fading, and pilot overhead.

The rest of this chapter is organized as follows. The notation is summarized in Table 1.1. The proposed CSI-aided sensing strategy is described in Section 1.2. This strategy is combined with an efficient MAC method and analyzed in Section 1.3. Section 1.4 contains numerical performance comparison of several sensing strategies and analysis of a pilot-based CSI prediction method for mobile CR networks. Finally, Section 1.5 concludes this chapter.

1.2 Channel-Adaptive Myopic Sensing

We consider an overlay CR ad hoc network [15] where M SU pairs seek spectrum opportunities on N non-overlapping channels in a fully distributed manner. We assume CR network traffic is backlogged initially and remains backlogged over the entire time horizon.[1] The PU traffic is modeled as a stationary Markov process [16, 17] with independently evolving channels. The transition probabilities are assumed known to all SUs. Both the primary and the CR networks share the same slotted structure and are perfectly synchronized [2].[2]

In a typical CR network, the transmission range of the PUs is normally much larger than that of the SUs, so we assume that for each SU pair, both the transmitter and the receiver are affected by the same set of PUs and experience the same spectrum opportunities. SUs are required to sense the spectrum before accessing any channel, and can transmit only if the

[1] The routing and connection-level scheduling of SU traffic for minimizing the queueing delay is beyond our scope.

[2] Even if the PU traffic is unslotted, i.e., continuous, it can be converted into an equivalent slotted traffic model with certain collision constraints [18]. In practice, perfect synchronization may be hard to achieve and PU activity state might change during SU transmission [19]. This problem can be partially corrected by using short SU packets [20] and/or in-band sensing [19].

Table 1.1: Significant Notation in Chapter 1

Notation	Explanation
N	Number of channels.
M	Number of SU pairs.
T	Number of slots over the whole time horizon [2]. Slot duration is 1 ms.
B^n	Bandwidth of channel n.
$S^{mn}(t)$	$S^{mn}(t) \in \{0(\text{busy}), 1(\text{idle})\}$. PU traffic state on channel n for SU m at time slot t.
p_{ij}^{mn}	PU Markov chain transition probability on channel n for SU m: $p_{ij}^{mn} = \Pr[S^{mn}(t) = j \mid S^{mn}(t-1) = i]$, where $i, j \in \{0, 1\}$; assume $p_{ii}^{mn} = 0.8$ and $p_{ij}^{mn} = 0.2$, $\forall m, n$ and $i \neq j$.
$n_*^m(t)$	$n_*^m(t) \in \{1, \ldots, N\}$. Sensing decision of SU m at time slot t.
$a^m(t)$	Sensing result of SU m at time slot t: $a^m(t) = 1$ if the channel is sensed idle and $a^m(t) = 0$ otherwise.
$\theta^{mn}(t)$	Belief probability $\theta^{mn}(t) = \Pr[S^{mn}(t) = 1 \mid n_*^m(1), a^m(1), \ldots, n_*^m(t-1), a^m(t-1)]$, i.e., the conditional probability of channel n being available for SU m given past observations.
$\gamma^{mn}(t), \bar{\gamma}^{mn}$	Received instantaneous and average SNR for SU m on channel n.
$R^{mn}(t)$	Reward for SU m sensing channel n at time slot t.
$H^{mn}(\gamma^{mn}(t))$	Expected achievable throughput of SU m for sensing channel n at time slot t.
H_π^m, H_π	Average expected individual and normalized network throughputs for sensing policy π.

channel is sensed idle. We assume each SU can sense only one channel within each time slot due to the hardware constraints.

Each SU maintains a belief vector $\boldsymbol{\theta}^m(t) = [\theta^{m1}(t), \ldots, \theta^{mN}(t)]$ to infer the current PU traffic state [2]. Consider a myopic, or greedy, sensing policy in [2]. At the first time slot $t = 1$, the initial belief vector is given by the stationary probabilities of the Markov process. Then for each $t > 1$, SU m chooses to sense the channel $n_*^m(t)$ by maximizing the expected reward $\mathbb{E}[R^{mn}(t)]$:

$$n_*^m(t) = \arg\max_n \theta^{mn}(t) R^{mn}(t). \tag{1.1}$$

Assuming perfect spectrum detection, the belief vector is updated as [2]:

$$\theta_r^{mn}(t) = \begin{cases} a^m(t), & \text{if } n_*^m(t) = n \\ \theta^{mn}(t), & \text{if } n_*^m(t) \neq n \end{cases} \tag{1.2}$$

$$\theta^{mn}(t+1) = p_{11}^{mn}\theta_r^{mn}(t) + p_{01}^{mn}(1-\theta_r^{mn}(t)). \tag{1.3}$$

The process is repeated over the time horizon $t \in [1, T]$.

The myopic policy in [2] has good performance for a single SU pair scenario. However, it ignores competing SUs, and its performance degrades when multiple SUs in the neighborhood are active; since the belief vectors $\boldsymbol{\theta}^m(t)$ of these SUs converge to similar values as t increases. One reason why the myopic policy is degraded in traffic-congested scenarios is the conventional reward choice given by the channel bandwidth

$$R_{\text{conv}}^{mn}(t) = B^n \tag{1.4}$$

which results in similar sensing decisions for all SUs. For example, when all channels have the same bandwidth (often normalized to 1), all SUs sense the most likely channel to be idle in the current time slot. This results in congestion and poor throughput. Moreover, when SUs compete for the same channel, they leave other channels unexploited, thus degrading the network throughput. Most randomized strategies in the literature [1,4–8] also employ the reward (1.4), but modify the myopic channel selection (1.1) to diversify sensing decisions of different SUs. However, these methods compromise SUs' chances to sense their favorite channels.

On the other hand, *we propose to adapt the reward to the power of the link between the transmitting and receiving secondary network nodes.* Consider the mth SU transmitter–receiver pair. At time slot t, the received signal-to-noise ratio (SNR) of the link between these two SUs on the nth channel is given by $\gamma^{mn}(t) = |g^{mn}(t)|^2 P/(N_0 B^n)$ as illustrated in Figure 1.1, where $g^{mn}(t)$ is the complex-valued received channel gain (the CSI), P is the transmission power, and N_0 is the power spectral density of complex additive white Gaussian noise (AWGN). Suppose $\gamma^{mn}(t)$ is perfectly known at the mth SU transmitter and is fixed for the slot duration. In the proposed CSI-aided policy, the reward is given by the channel capacity

$$R_{\text{cap}}^{mn}(t) = C^{mn}(t) = B^n \log_2(1+\gamma^{mn}(t)). \tag{1.5}$$

This reward is a function of the instantaneous CSI and differs among the SU pairs due to their spatial separation and channel fading. Thus, *the proposed strategy randomizes sensing decisions and improves the individual throughput.*

The reward choice (1.5) attempts to match the anticipated throughput prior to sensing to the actual throughput achieved if the channel is used for transmission. In this case, the expected achievable throughput is given by

$$H^{mn}(\gamma^{mn}(t)) = \theta^{mn}(t) R_{\text{cap}}^{mn}(t). \tag{1.6}$$

Since the rate (1.5) is not attainable in practice, we also investigate a realistic cross-layer design that combines CSI-aided sensing with *adaptive modulation during transmission*. For simplicity we confine our attention to continuous-rate adaptation [21] although this approach can be easily extended to discrete-rate adaptation. Assuming adaptive quadrature amplitude modulation with fixed transmission power, we employ adaptively adjusted data rate as the reward

$$R_{\mathrm{AM}}^{mn}(t) = B^n k^{mn}(t) \tag{1.7}$$

where $k^{mn}(t)$ is the maximum spectral efficiency that the system can support under a certain bit error rate (BER) constraint $\mathrm{BER_T}$ [21],

$$k^{mn}(t) = \log_2(1 - 1.5\gamma^{mn}(t)/\ln(5\mathrm{BER_T})). \tag{1.8}$$

In this case, the reward is matched to the expected throughput

$$H^{mn}(\gamma^{mn}(t)) = \theta^{mn}(t) R_{\mathrm{AM}}^{mn}(t). \tag{1.9}$$

Note that unlike CSI-aided rewards (1.5) and (1.7), the conventional reward (1.4) is not matched to the expected transmission rate when channel adaptation is employed during transmission.

1.3 First-Come-First-Served Channel-State-Information-Aided Sensing and Access and Performance Analysis

1.3.1 FCFS MAC

While the proposed CSI-aided strategy randomizes sensing decisions, it is still possible for several SUs to choose the same channel. However, when an idle channel is found, only one of the SUs that have participated in sensing it can transmit successfully. To avoid SU collisions, perfect *access decision resolution after sensing* has been adopted in many related references, e.g., [2, 4, 22] and is assumed in several methods evaluated in this chapter.

However, in a hardware-constrained CR network, it may be desirable to avoid overlapped sensing decisions prior to sensing to prevent wasted sensing effort and to improve spectrum utilization [20]. For example, a distributed competition resolution scheme is proposed in [6] which pre-ranks the SUs and tries to evolve them onto orthogonal channels for sensing. In [7], time division fair share (TDFS) MAC is investigated, where time slots are reserved for different SUs to make individual sensing decisions in a round-robin manner from the most to the least rewarding. These two schemes are designed under the assumption that the achievable throughput on each channel is SU-invariant. However, the reward choices (1.5) and (1.7) do not satisfy

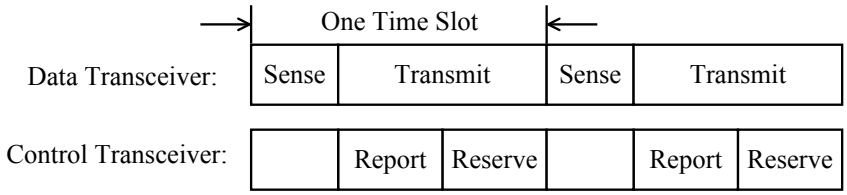

Figure 1.2: Slot structure.

this assumption. Thus the MAC methods in [6, 7] do not guarantee full contention resolution prior to sensing for CSI-aided sensing strategies and might require additional management of access requests after sensing.

To overcome this limitation, we exploit a multichannel MAC scheme based on the dynamic channel assignment (DCA) protocol [23]. DCA was intended for non-CR multichannel ad hoc networks and is often used in CR networks to resolve access requests after an available channel is found. We modified it to resolve contention prior to sensing in hardware-constrained CR networks, as illustrated in Figure 1.2. Each SU is equipped with a local database and two transceivers: the control transceiver is always tuned to an out-of-band control channel [24], and the data transceiver can be tuned to any one of the N data channels. During the *reserve* phase in Figure 1.2, SUs exchange control packets on the control channel prior to sensing with random backoff times to indicate the channels to be reserved for sensing according to the proposed sensing policy, as opposed to access request resolution in the original DCA MAC. SUs become aware of neighboring SUs' sensing decisions by overhearing these control messages. The current reserved channel list of all neighboring SUs is stored in the local database, which is updated when SUs learn about their neighbors' channel reservations. Unlike in DCA, reserving SUs will only transmit over the reserved channels if they are sensed idle. We assume distinct backoff time values for different SUs, resulting in perfect and sequential competition resolution on the control channel prior to sensing [24]. Moreover, low-overhead transmission of the control packets is assumed. In our proposed multichannel MAC, each channel is reserved by the first SU that requests it. Therefore, we refer this scheme as FCFS MAC. Finally, we emphasize that FCFS can be easily superimposed onto almost any existing contention-based multichannel non-CR MAC, so it adds negligible overhead and energy consumption.

1.3.2 Analytical Results for i.i.d. PU Traffic

Next, we compare several sensing strategies analytically in Table 1.2. Assume B^n equals 1 Hz, the independent and identically distributed (i.i.d.) traffic model [6,7], and perfect CSI knowledge prior to sensing. All SUs are subject to the same set of PUs and thus experience the same channel availabilities, which reduces the PU state $S^{mn}(t)$ to $S^n(t)$. The PU traffic on each channel

Table 1.2: Summary of Sensing Strategies for Arbitrary M, N Values

No	**Strategy π**	**CSI-Adaptation (Y/N)**	**MAC (Before/After Sensing)**
i	Random selection	N	After
ii	Myopic [2]	N	After
iii	Myopic with TDFS [7] ($N \geq M$)	N	Before
iv	Myopic with FCFS	N	Before
v	Randomized [4]	N	After
vi	CSI-aided myopic (Section 1.2)	Y	After

Expected Individual Throughput H_π^m for i.i.d. PU Traffic Model
(i) $H^m_{\text{Random}} = \sum_{n=1}^{N}\sum_{j=1}^{M} \frac{1}{j}\binom{M-1}{j-1}\left(\frac{1}{N}\right)^j\left(1-\frac{1}{N}\right)^{M-j}\mathbb{E}\left[H^{mn}\right]$
(ii) $H^m_{\text{My}} = \frac{1}{M}\mathbb{E}[H^{m1}]$
(iii) $H^m_{\text{My-TDFS}} = \frac{1}{M}\sum_{n=1}^{M}\mathbb{E}[H^{mn}] \geq H^m_{\text{My}}$
(iv) $H^m_{\text{My-FCFS}} = H^m_{\text{My-TDFS}}$
(v) $H^m_{\text{Randomized}} = \sum_{n=1}^{N}\sum_{j=1}^{M} \frac{1}{j}\binom{M-1}{j-1}\left(\frac{\beta^n}{\sum_k \beta^k}\right)^j\left(1-\frac{\beta^n}{\sum_k \beta^k}\right)^{M-j}\mathbb{E}[H^{mn}]$
(vi) $H^m_{\text{CSI}} = \sum_{n=1}^{N}\sum_{j=1}^{M} \frac{1}{j}\binom{M-1}{j-1}(q_n)^j(1-q_n)^{M-j}\mathbb{E}[\max\{H^{m1},\ldots,H^{mN}\}]$

evolves as an i.i.d. Bernoulli process with known availability probability $\beta^n = \Pr[S^n = 1], \forall n$ (omitting the time index t). First, we assume heterogeneous PU traffic statistics. Without loss of generality, let $\beta^1 > \cdots > \beta^N$. Since the PU traffic exhibits no time correlation in this case, the belief probability of each SU is set equal to the channel availability probability, i.e., $\theta^{mn}(t) = \beta^n$.

We assume that all SU pairs *achieve their channel capacity with perfect CSI feedback during transmission*. Thus, when an SU m chooses channel n, the expected throughput $H^{mn}(\gamma^{mn}(t)) = \beta^n \log_2(1+\gamma^{mn}(t))$ for all m, n (or simply H^{mn} whenever the context is clear). For sensing

strategy π, the average expected individual throughput of SU m and the normalized network throughput are defined as

$$H_\pi^m \triangleq \sum_{n=1}^{N} \sum_{j=1}^{M} \frac{1}{j} \Pr[n_*^m = n, J_n^m = j-1] \mathbb{E}[H^{mn} | n_*^m = n, J_n^m = j-1] \tag{1.10}$$

and

$$H_\pi \triangleq \frac{1}{M} \sum_{m=1}^{M} H_\pi^m \tag{1.11}$$

respectively, where J_n^m is the number of SUs sensing channel n excluding SU m, the channel n_*^m is selected according to the sensing strategy π, the expectation in (1.10) is over the channel SNR $\gamma^{mn}(t)$, and the $(1/j)$ factor is justified by the assumption of perfect access request resolution in Section 1.3.1. Assuming i.i.d. Rayleigh fading over all channels and SU links with the average SNR $\bar{\gamma}^{mn} = \bar{\gamma}$, the cumulative distribution function (cdf) of H^{mn} is given by (cf. Appendix A.1)

$$F_{H^{mn}}(x) = 1 - \exp\left(\frac{-1}{\bar{\gamma}} \left(2^{x/\beta^n} - 1 \right) \right). \tag{1.12}$$

The six sensing strategies in Table 1.2 are classified by their rewards and MAC methods. Strategies (i–v) do not adapt to CSI prior to sensing and employ the conventional bandwidth reward (1.4) although they utilize adaptive transmission after sensing. Note that the expected value $\mathbb{E}[H^{mn}] = \int_0^\infty [1 - F_{H^{mn}}(x)]\, dx$. On the other hand, the proposed strategy (vi) is CSI-adaptive prior to sensing, and the reward (1.5) is matched to the expected achievable throughput (1.6). The formulas in Table 1.2 are proved in Appendix A.3. The probability in H_{CSI}^m

$$q_n \triangleq \Pr[n_*^m = n] = \Pr[\arg\max_n H^{mn} = n] \tag{1.13}$$

and

$$\mathbb{E}[\max\{H^{m1}, \ldots, H^{mN}\}] = \int_0^\infty [1 - \prod_{n=1}^{N} F_{H^{mn}}(x)] dx. \tag{1.14}$$

We also derived in Appendix A.2 the average expected individual throughputs H_π^m of CSI-aided myopic sensing with TDFS and FCFS (labeled as policies vii and viii, respectively) as well as that of the centralized sum-rate optimal policy (ix) assuming $M = N = 2$. In the sum-rate optimal policy (ix), the SUs are coordinated by a central controller (e.g., an access point or a base station), and the throughput of this policy provides an upper bound on the throughputs of the distributed policies (i–viii). The three policies (vii–ix) employ CSI-adaptation and contention resolution prior to sensing. We were not able to obtain the throughput expressions of these policies for arbitrary $N, M \geq 2$.

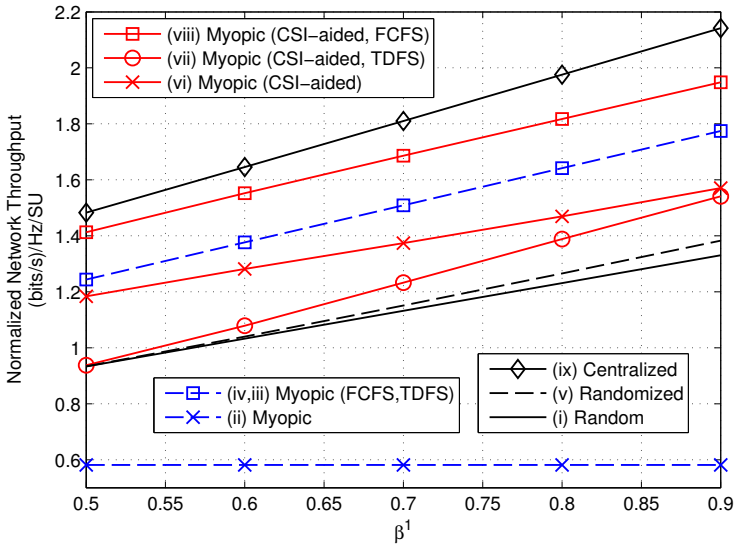

Figure 1.3: Analytical throughput vs. β^1; $\beta^2 = 0.4$; capacity reward; 2 SU pairs; 2 channels; i.i.d. Rayleigh fading; average SNR = 10 dB.

Assuming $M = N = 2$ and $\beta^2 = 0.4$, the normalized network throughputs (1.11) are compared as a function of β^1 in Figure 1.3. First, we compare performance of the policies that employ contention resolution after sensing. Note that the myopic policy (ii) performs even worse than the naïve random channel selection approach (i) since in the former both SUs favor channel 1 and always compete to gain access, leaving channel 2 unexploited. The randomized sensing policy (v) reduces overlapped sensing decisions, but it reduces the SUs' chances of sensing their favorite channels and sacrifices the individual throughput to compensate for possible SU collisions, so has small performance gain over the random selection approach (i). The proposed CSI-aided myopic sensing policy (vi) achieves better performance than the policies above.

Next, we consider MAC prior to sensing. When applied to the myopic policy, the proposed FCFS scheme (Section 1.3.1) and the TDFS scheme [7] achieve identical throughputs and on average provide equal share of spectrum opportunities to the two SUs (iii and iv). On the other hand, when applied to the CSI-aided myopic policy, TDFS (vii) actually degrades performance while FCFS (viii) results in significant improvement. FCFS can still identify overlapped SU sensing decisions through control message exchange in this case, while TDFS requires SUs to cede its preferred channel to the other SU for half of the time to combat anticipated SU competition. However, in CSI-aided sensing strategies, the channel preference depends on the local CSI of each SU. Thus, the nonpreferred channel of the ceding SU can be the preferred channel of the other SU, resulting in a conflicted sensing decision. Therefore, TDFS undermines the randomizing effect of CSI-aided sensing and reduces its throughput.

Note also that while the centralized policy (ix) outperforms the CSI-aided myopic policy with FCFS (viii), the latter is more fair since it provides SUs with the opportunity to sense their preferred channels at any time with equal probabilities while in (ix) these chances are compromised to achieve the optimal sum-rate. We found that numerical results for i.i.d. PU traffic and larger N, M values do not provide additional insights (cf. Appendix A.2–A.3).

Finally, we quantify the benefits of multiuser and multichannel diversity for the proposed CSI-aided sensing policy in Section 1.2 assuming a homogeneous environment where all Rayleigh fading channels are i.i.d. with the average SNR $\bar{\gamma}^{mn} = \bar{\gamma}$ and the PU traffic follows i.i.d. Bernoulli process with $\beta^n = \beta$.[3] From Appendix A.4,

$$H^m_{\text{CSI}} = \mathbb{E}\left[\max\{H^{m1}, \ldots, H^{mN}\}\right] g^{MN} \tag{1.15}$$

where the expectation is given by (1.14) and

$$g^{MN} \triangleq N \sum_{j=1}^{M} \frac{1}{j} \binom{M-1}{j-1} \left(\frac{1}{N}\right)^j \left(1 - \frac{1}{N}\right)^{M-j} \tag{1.16}$$

quantifies each SU's share of spectrum opportunities in a multi-SU setting. The expression in (1.15) balances the multichannel diversity gain vs. SU competition tradeoff. For example, when $M = N$, (1.16) reduces to $g^{MM} = 1-(1-1/M)^M$, which decreases with M (cf. Appendix A.4), thus indicating more intense SU competition for larger M. On the other hand, the expectation in (1.15) corresponds to selection combining (SC) diversity gain [25], which increases with M. Note that (1.15) provides guidelines for CR network design. For example, if the SU network capacity (M) is fixed, the number of channels (N) can be optimized using (1.15) exploiting the tradeoff between SC diversity gain (which saturates for large M) and the cost of network setup or channel leasing [22]. Similarly, for fixed N, the optimal M can be determined based on (1.15) to prevent extremely high SU competition.

1.4 Numerical Simulation Results

In Section 1.4.1–1.4.3, we present simulation results for a network with $M = 3$ SUs and $N = 10$ channels. It represents a small hardware-constrained network, for example, a sparse rural CR network. However, small network size does not preclude SU competition since the number of available channels is also small. In Section 1.4.4, we investigate performance trends for varying

[3]Note that it is generally difficult to analyze diversity systems in closed-form for a heterogeneous environment, and thus identical statistics for all diversity branches are often assumed in the study of diversity combining, e.g., [25]. Moreover, the homogeneous assumption is useful when the CR network is not yet or being constructed because SUs may not have sufficient knowledge of the PU traffic or fading statistics at that time.

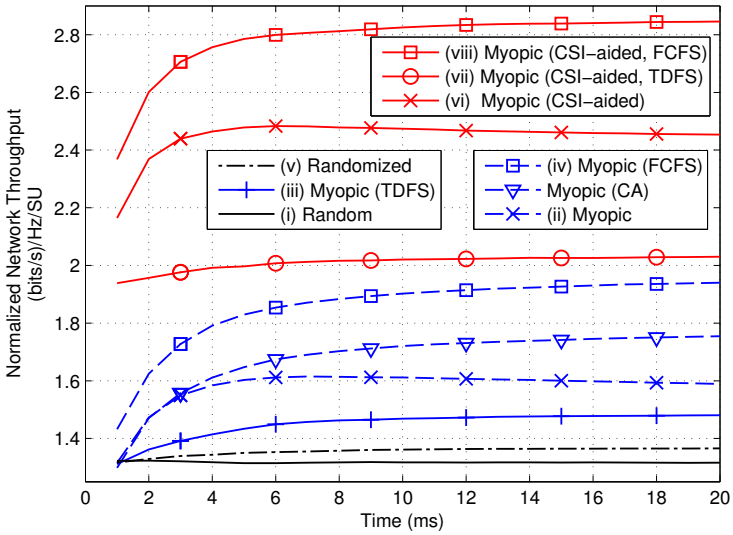

Figure 1.4: Throughput vs. time; capacity reward; 3 SU pairs; 10 channels; i.i.d. Rayleigh fading; average SNR = 10 dB; $f_{dm} = 40$ Hz.

M and N parameters. Finally, we study the effect of spatial correlation in Section 1.4.5 under shadow fading.

We assume the average SNR for all SU pairs and channels is 10 dB unless stated otherwise. The instantaneous SNR $\gamma^{mn}(t)$ is fixed over the duration of one time slot (1 ms). A Markovian PU traffic model is employed (see Table 1.1).

1.4.1 Performance Comparison under Ideal Assumptions

In Figure 1.4, the throughputs of policies (i–viii) in Section 1.3.2 and the modified myopic policy with collision avoidance (myopic/CA) [5] are compared over the time interval of 20 ms. In the latter strategy, each SU maintains a variable-length list of candidate channels based on the past history of MAC-layer SU collisions (or conflicting sensing decisions) and uniformly selects one channel on the list for sensing at each time slot. We assume perfect CSI knowledge at the sensor and ideal spectrum sensing. The maximum Doppler shift f_{dm} is 40 Hz although the performance is not sensitive to f_{dm} under the perfect CSI assumption.

Note that the throughputs of all strategies approach their asymptotic values as time increases. The sensing history and the belief vectors (1.2) and (1.3) of different SUs differ slightly in the Figure 1.4 scenario, as SUs attempt to predict channel availabilities with partially observed PU traffic states. Thus, unlike in Figure 1.3, the myopic policy (ii) provides about 0.3 (bits/s)/Hz/SU improvement over the random selection approach (i) because different SUs make similar, but not identical sensing decisions. This observation also provides insight into

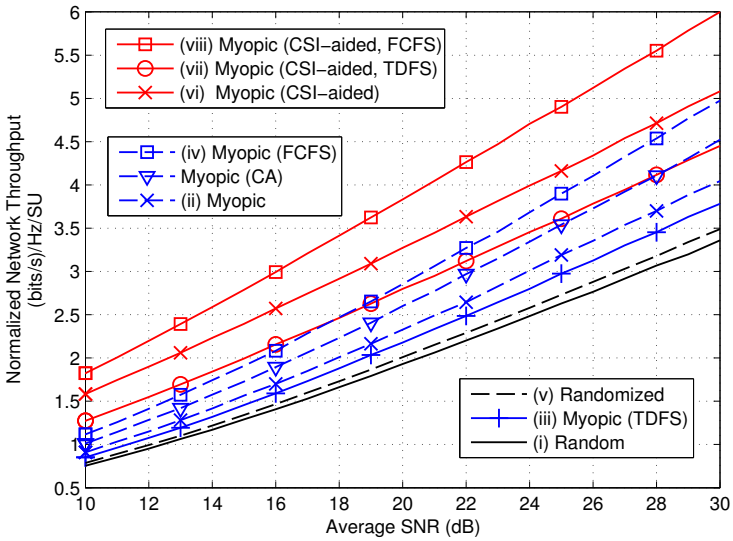

Figure 1.5: Throughput vs. average SNR; continuous-rate adaptation; fixed transmission power; $\text{BER}_{\text{T}} = 10^{-3}$; 3 SU pairs; 10 channels; i.i.d. Rayleigh fading; $T = 20$ slots.

relatively poor performance of the myopic policy with TDFS (iii) when compared with that in Figure 1.3. Note that an SU senses its favorite channel for $1/M$ of the time using TDFS MAC, so its throughput loss is exacerbated by a larger number of SUs M in Figure 1.4 relative to Figure 1.3.

The myopic/CA policy effectively reduces SU collisions and restores the gain obtained from PU traffic cognition. However, it acts only after SUs collide whereas the CSI-aided myopic policy (vi) takes advantage of fading variation to randomize sensing decisions and to boost the individual throughput. Due to a larger number of channels N, SUs achieve greater benefit from multichannel diversity and thus higher throughput gain of CSI-aided sensing than in Figure 1.3. *The gains of the CSI-aided myopic strategy (vi) over the myopic (ii) and myopic/CA strategies are about 0.9 and 0.7 (bits/s)/Hz/SU (or about 50% and 40%), respectively. An additional gain of about 0.4 (bits/s)/Hz/SU (or over 15%) can be achieved by applying the FCFS MAC with the CSI-aided strategy (viii vs. vi).* We also note that FCFS offers a gain of 0.35 (bits/s)/Hz/SU (or 20%) when used with the conventional myopic strategy (iv vs. ii) and outperforms other nonadaptive strategies.

In Figure 1.5, we investigate the throughput averaged over 20 slots vs. the average SNR for the sensing strategies that employ adaptive modulation during transmission. In this case, the reward for the CSI-adaptive strategies is given by (1.7) and the throughput during transmission is given by (1.9) for all strategies. We observe that the proposed CSI-aided policy (vi) outperforms the myopic policy (ii) by at least 5 dB. The gain over the myopic/CA policy [5] decreases

with the average SNR, but is *at least 3 dB* for a practical average SNR ≤ 30 dB. Moreover, the FCFS scheme provides *2–4 dB* performance gain over the CSI-aided myopic strategy (viii vs. vi) and up to 4 dB gain over the conventional myopic strategy (iv vs. ii). Similar SNR gains were observed when the adaptation is to the channel capacity [see (1.5)–(1.6)]. Guided by the results in Figure 1.4 and Figure 1.5, we consider only the CSI-adaptive and the nonadaptive myopic policies with/without FCFS, i.e., (ii,iv,vi,viii), in the remainder of this chapter since other strategies do not significantly improve upon (ii). Also, we assume that all strategies achieve the expected throughput (1.6) and all CSI-aided policies use the capacity reward (1.5).

1.4.2 Imperfect Sensing

To analyze performance of CSI-aided sensing in the presence of *sensing errors*, we employ the belief update process that incorporates the reliability of the spectrum sensor, which is characterized by the miss detection (MD) rate p_m (when the sensor fails to detect the PU signal) and the false alarm (FA) rate p_f (when the sensor misidentifies the PU presence). Assuming energy detection [26],

$$p_m = 1 - \int_0^\infty Q_\nu(\sqrt{2\nu\lambda}, \sqrt{\tau}) f(\lambda) d\lambda \tag{1.17}$$

$$p_f = \frac{\Gamma(\nu, \tau/2)}{\Gamma(\nu)} \tag{1.18}$$

where ν is the number of collected samples, τ is the detection threshold, $f(\lambda)$ is the probability density function (pdf) of the PU signal SNR observed at the sensor, $\Gamma(\cdot)$ and $\Gamma(\cdot,\cdot)$ are complete and incomplete gamma functions, respectively, and $Q_\nu(\cdot,\cdot)$ is the generalized Marcum Q-function. Suppose the node-level constraint [15] on the collision probability between the SU and the PU networks is known. Given p_m, the detection threshold τ is determined by inverting (1.17), and the FA rate p_f is then computed from (1.18).

After sensing, the belief is corrected by the reliability of the spectrum sensor [27]:

$$\theta_r^{mn}(t) = \begin{cases} \frac{(1-p_f)\theta^{mn}(t)}{(1-p_f)\theta^{mn}(t)+p_m(1-\theta^{mn}(t))}, & \text{if } n_*^m(t) = n \text{ and } a^m(t) = 1 \\ \frac{p_f\theta^{mn}(t)}{p_f\theta^{mn}(t)+(1-p_m)(1-\theta^{mn}(t))}, & \text{if } n_*^m(t) = n \text{ and } a^m(t) = 0 \\ \theta^{mn}(t), & \text{if } n_*^m(t) \neq n \end{cases} \tag{1.19}$$

and then updated according to the Markov chain as in (1.3).

In Figure 1.6, the throughput vs. allowed collision probability is compared for the proposed CSI-aided myopic strategies (vi) and (viii) and their non-adaptive counterparts (ii) and (iv) assuming moderate received PU signal strength. The average normalized maximum achievable

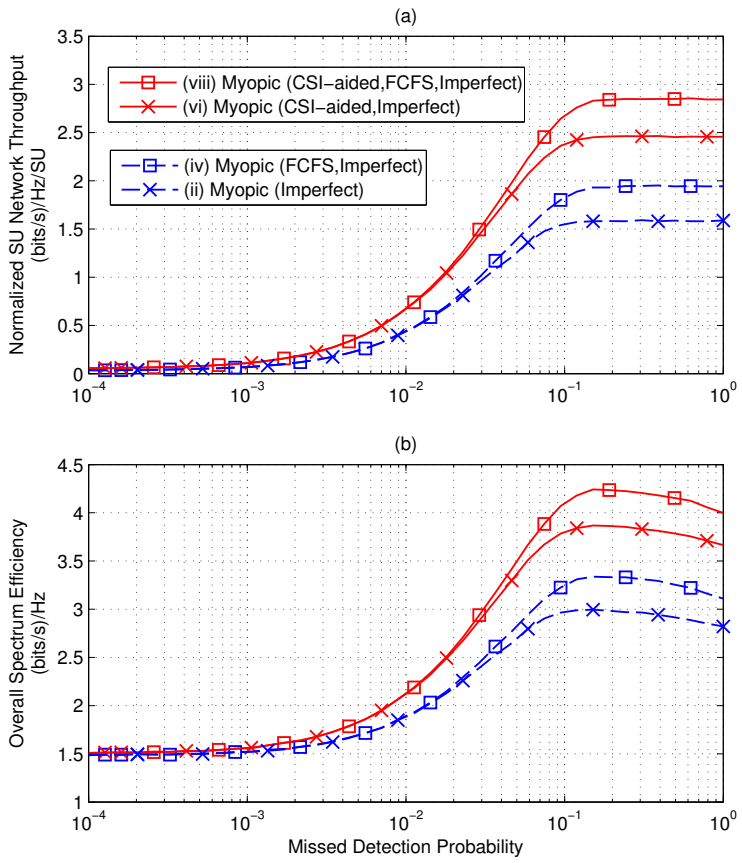

Figure 1.6: Throughput vs. p_m under imperfect sensing; capacity reward; 3 SU pairs; 10 channels; i.i.d. Rayleigh fading; average SNR = 10 dB; $\nu = 5$; $T = 20$ slots.

rate *of the SU network* is illustrated in (a) and the overall throughput (normalized by the number of channels) for *both PU and CR networks* is shown in (b). As we increase the allowed collision probability with the PU network, the average throughput of the SUs increases and eventually saturates to the ideal spectrum sensor case for each sensing strategy. However, for large p_m, the PU transmission is frequently interrupted by the SUs, causing the overall spectral efficiency to decline. For all policies, the SU network can approximate the ideal throughput in the presence of sensing error unless the collision constraint is extremely tight. In this scenario, the maximum spectrum efficiency is achieved by setting $p_m \approx 0.1$. We observe that *the proposed CSI-aided strategy maintains about 0.8 (bits/s)/Hz/SU gain* over the conventional myopic strategy while the FCFS MAC makes an extra gain of over 0.3 (bits/s)/Hz/SU for $p_m \geq 0.1$.

1.4.3 Adaptation to Multipath Fading CSI

The proposed sensing strategy relies on accurate prediction of the fading SNR $\gamma^{mn}(t)$ for the upcoming time slot prior to sensing. Such prediction is particularly challenging for CR systems since the signals of each SU transmitter–receiver pair are not confined to predefined frequency bands or time slots. Thus, it is important to ensure that the proposed policies are robust to *CSI mismatch*. In this section, we explore adaptation to a short-term, or multipath, fading component of SNR $\gamma^{mn}(t)$. We assume that the sensing policy employs the minimum mean square error (MMSE) estimate of the actual SNR $\gamma^{mn}(t)$ conditioned on its mismatched observation $\hat{\gamma}^{mn}(t) = |\hat{g}^{mn}(t)|^2 P/N_0 B^n$ where $\hat{g}^{mn}(t)$ is the complex-valued predicted CSI. Below, we suppress the indices m, n and t for brevity. First, we investigate theoretical throughput degradation to CSI mismatch. Given $\hat{\gamma}$, the reward for each SU link is computed as

$$R(\hat{\gamma}) = \int_0^\infty R(\gamma) f(\gamma|\hat{\gamma}) d\gamma \tag{1.20}$$

where $R(\gamma)$ is given by (1.5) or (1.7), and $f(\gamma|\hat{\gamma})$ is the pdf of γ conditioned on $\hat{\gamma}$. For Rayleigh fading channels [28]

$$f(\gamma|\hat{\gamma}) = \frac{1}{\bar{\gamma}\sigma^2} I_0\left(\frac{2\sqrt{\gamma\hat{\gamma}}}{\bar{\gamma}\sigma^2}\right) \exp\left(\frac{-1}{\bar{\gamma}\sigma^2}(\gamma + \hat{\gamma})\right) \tag{1.21}$$

where $I_0(\cdot)$ is the zeroth order modified Bessel function, $0 \leq \sigma^2 \leq 1$ is the normalized mean square error (NMSE) of the SNR estimation, and $\bar{\gamma}$ is the average SNR.

Figure 1.7 illustrates robustness of the proposed CSI-aided myopic sensing (vi) and FCFS (viii) policies to *CSI mismatch*. Since CSI estimation during channel exploration is likely to be more accurate than prior to sensing, we assume perfect CSI at the transmitter and focus on the impact of the CSI error on the performance of channel-adaptive sensing. We observe that for mismatched CSI, CSI-aided sensing policies (vi) and (viii) still benefit from multiuser diversity and approximate the optimal values when NMSE $\sigma^2 < 0.1$. Note that $\sigma^2 = 0.1$ corresponds to severely degraded CSI prediction accuracy in conventional adaptive transmission applications [29]. The throughputs of the CSI-aided strategies (vi) and (viii) converge to the non-adaptive counterparts (ii) and (iv), respectively, as the NMSE σ^2 approaches 1, i.e., when the CSI information is not available. *Thus the proposed approaches are robust to CSI errors and degrade gracefully when CSI become unreliable.*

Above, we have assumed that the NMSE σ^2 is fixed and independent of the SUs' transmission patterns. Such assumption is valid for traditional non-CR wireless systems, where the pilots are sent according to a fixed and regular schedule over time and frequency, and current CSI is predicted based on outdated CSI extracted from previously received pilot signals [29]. However, in CR, SUs can send pilots only on channels that are free of PU transmission. We propose the

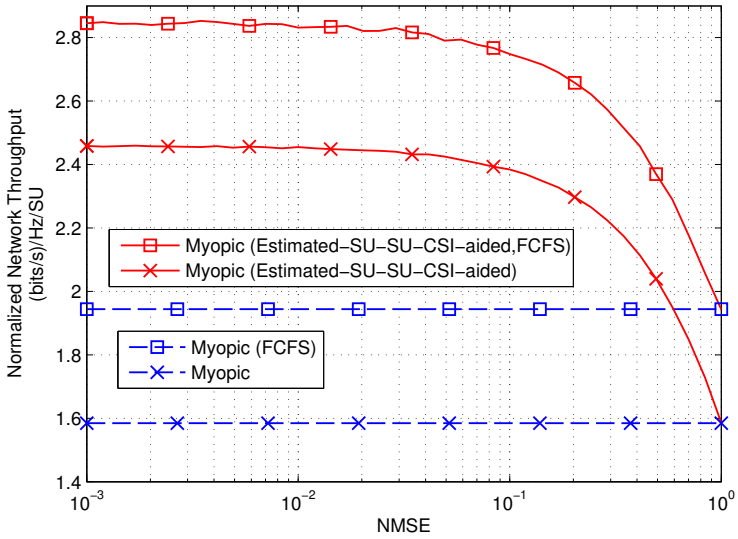

Figure 1.7: Throughput vs. NMSE prior to sensing under CSI error; capacity reward; 3 SU pairs; 10 channels; i.i.d. Rayleigh fading; average SNR = 10 dB; $T = 20$ slots.

following pilot placement method to aid CSI prediction prior to sensing. In this method, all SUs report their sensing results using a control channel as in the *reporting* phase of [30, Fig. 3–4] at the beginning of each time slot after spectrum sensing (cf. Figure 1.2). Thus, SUs learn which channels are idle in the current time slot. Note that exchange of CSI is not required for the proposed method. Each SU receiver sends pilots on the idle channels discovered by itself and its neighbors. When a pilot is sent by the receiver of the mth SU pair over channel n at time slot t, the mth SU sensor (transmitter) obtains a noisy observation of the actual channel gain by reciprocity (Figure 1.1), denoted as $\tilde{g}^{mn}(t)$. To predict the channel coefficient $\hat{g}^{mn}(t)$, SU transmitter m collects all such received noisy pilots on the nth channel and its adjacent channels within a time window $\{t-W,\ldots,t-1\}$ and a frequency window of width $2L+1$ centered at channel n. Some channels might have fewer than L neighbors on one side and thus reduced window size. The time lags (in slots) of these pilots and the corresponding channel indices are $\boldsymbol{u}^{mn}(t) = [u_1^{mn}(t),\ldots,u_i^{mn}(t),\ldots,u_{p^{mn}(t)}^{mn}(t)]$ and $\boldsymbol{v}^{mn}(t) = [v_1^{mn}(t),\ldots,v_i^{mn}(t),\ldots,v_{p^{mn}(t)}^{mn}(t)]$ respectively, where $u_i^{mn}(t) \in [t-W, t-1]$, $v_i^{mn}(t) \in [n-L, n+L]$, and $p^{mn}(t)$ is the number of pilots falling into the observation window. For the ease of notation, let us put all these noisy pilots into one $p^{mn}(t) \times 1$ vector $\tilde{\boldsymbol{p}}^{mn}(t)$, in which $[\tilde{\boldsymbol{p}}^{mn}(t)]_i = \tilde{g}^{m,v_i^{mn}(t)}(t-u_i^{mn}(t))$ and denote the corresponding actual fading coefficients $\boldsymbol{p}^{mn}(t)$, in which $[\boldsymbol{p}^{mn}(t)]_i = g^{m,v_i^{mn}(t)}(t-u_i^{mn}(t))$. For example, consider the pilot transmission pattern in Figure 1.8. To obtain the predicted channel coefficient at $t=7$ on the fifth channel, or $\hat{g}^{m,5}(7)$ (marked as "?" in Figure 1.8), SU transmitter m extracts the CSI from the received pilots within the observation window shown

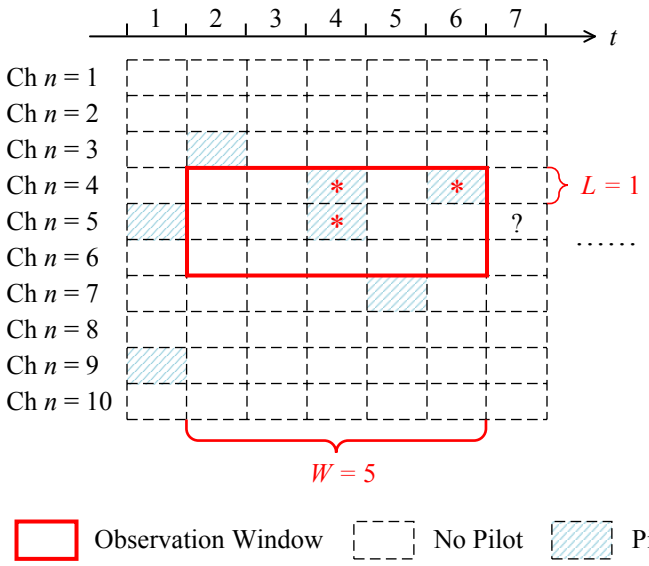

Figure 1.8: Observation window of SU m for predicting $\gamma^{m,5}(7)$ (marked "?").

by the solid rectangular box with $W = 5$ and $L = 1$ in Figure 1.8, i.e., $\boldsymbol{u}^{m5}(7) = [1, 3, 3]$, $\boldsymbol{v}^{m5}(7) = [4, 4, 5]$ and $\tilde{\boldsymbol{p}}^{mn}(t) = [\tilde{g}^{m,4}(6), \tilde{g}^{m,4}(4), \tilde{g}^{m,5}(4)]$. The collected pilots' locations are marked with "$*$" in Figure 1.8. Then, the MMSE long range prediction (LRP) algorithm [31] is used to calculate the predicted channel coefficient and the expected reward (1.20) at the beginning of each time slot based on the observations of these pilots:

$$\hat{g}^{mn}(t) = (\boldsymbol{d}^{mn}(t))^{\mathsf{H}} \tilde{\boldsymbol{p}}^{mn}(t) \tag{1.22}$$

with the optimal prediction coefficient vector given by

$$\boldsymbol{d}^{mn}(t) = (\boldsymbol{R}^{mn}(t))^{-1} \boldsymbol{r}^{mn}(t) \tag{1.23}$$

where the $p^{mn}(t) \times p^{mn}(t)$ autocorrelation matrix of the collected pilots and the $p^{mn}(t) \times 1$ cross-correlation vector between the collected pilots and the CSI to be predicted are given by

$$\boldsymbol{R}^{mn}(t) = \mathbb{E}[\tilde{\boldsymbol{p}}^{mn}(t)(\tilde{\boldsymbol{p}}^{mn}(t))^{\mathsf{H}}] = \mathbb{E}[\boldsymbol{p}^{mn}(t)(\boldsymbol{p}^{mn}(t))^{\mathsf{H}}] + \frac{N_0 \boldsymbol{I}}{2} \tag{1.24}$$

and

$$\boldsymbol{r}^{mn}(t) = \mathbb{E}[g^{mn}(t)(\boldsymbol{p}^{mn}(t))^{*}] \tag{1.25}$$

respectively, in which $\boldsymbol{I}$ is a $p^{mn}(t) \times p^{mn}(t)$ identity matrix and the resulting time-varying

Table 1.3: Number of Operations of LRP for CSI

	Number of Multiplications	**Number of Additions/Subtractions**
$(\boldsymbol{R}^{mn}(t))^{-1}$	$(p^{mn}(t))^3$	$(p^{mn}(t))^3 - 2(p^{mn}(t))^2 + p^{mn}(t)$
$\boldsymbol{d}^{mn}(t) = (\boldsymbol{R}^{mn}(t))^{-1}\boldsymbol{r}^{mn}(t)$	$(p^{mn}(t))^2$	$(p^{mn}(t)-1)^2$
$\hat{g}^{mn}(t) = (\boldsymbol{d}^{mn}(t))^{\mathsf{H}}\tilde{\boldsymbol{p}}^{mn}(t)$	$p^{mn}(t)$	$p^{mn}(t)-1$

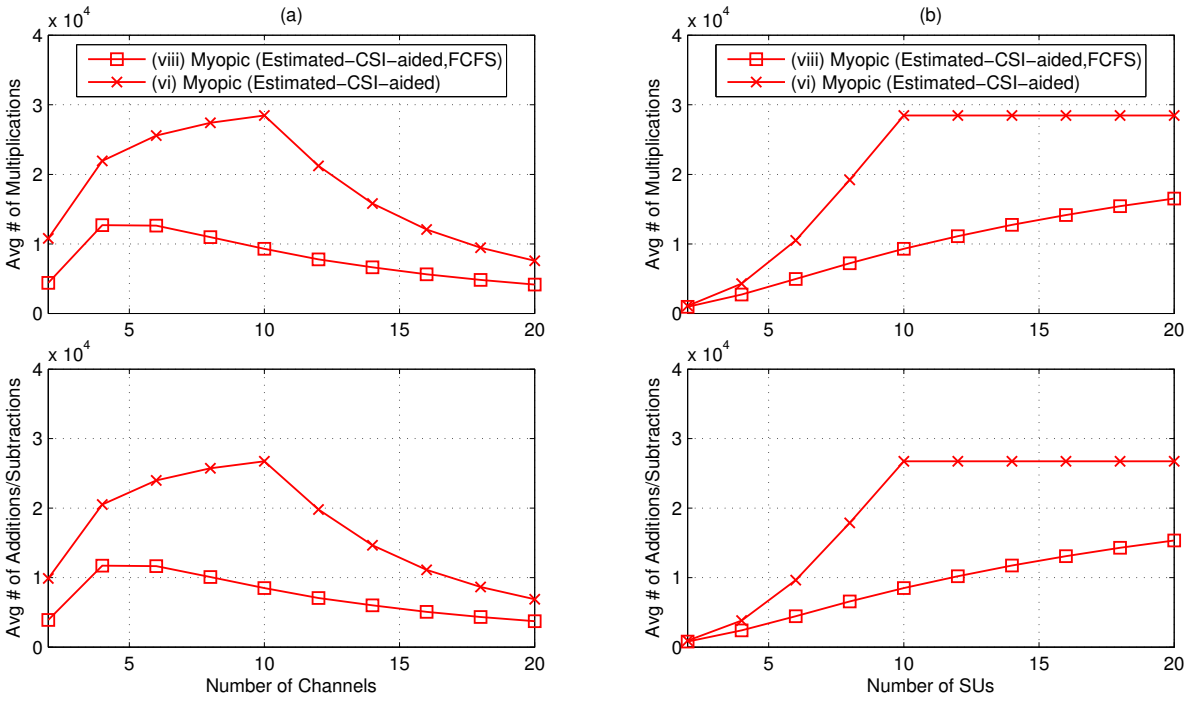

Figure 1.9: Number of operations for CSI prediction: (a) varying N with $M = 10$ (b) varying M with $N = 10$; ETSI Vehicular-A channel model; average SNR $= 10\,\text{dB}$; $f_{dm} = 75\,\text{Hz}$; $B^n = 200\,\text{kHz}$; $L = 1$; $W = 20$; $T = 10^5$ slots.

NMSE is given by

$$(\sigma^{mn}(t))^2 = \mathbb{E}\left[|\hat{g}^{mn}(t) - g^{mn}(t)|^2\right] = 1 - (\boldsymbol{r}^{mn}(t))^{\mathsf{H}}(\boldsymbol{R}^{mn}(t))^{-1}\boldsymbol{r}^{mn}(t). \tag{1.26}$$

Note that the complexity the proposed sensing policy is dominated by that of the CSI prediction process. Table 1.3 lists the number of operations for each step in the LRP algorithm using the Gauss-Jordan method for matrix inversion [32, Page 119]. Therefore, the total number of multiplications is $(p^{mn}(t))^3 + (p^{mn}(t))^2 + p^{mn}(t)$ and the total number of additions/subtractions is $(p^{mn}(t))^3 - (p^{mn}(t))^2$. Preliminary results on computational complexity are shown in Figure 1.9.

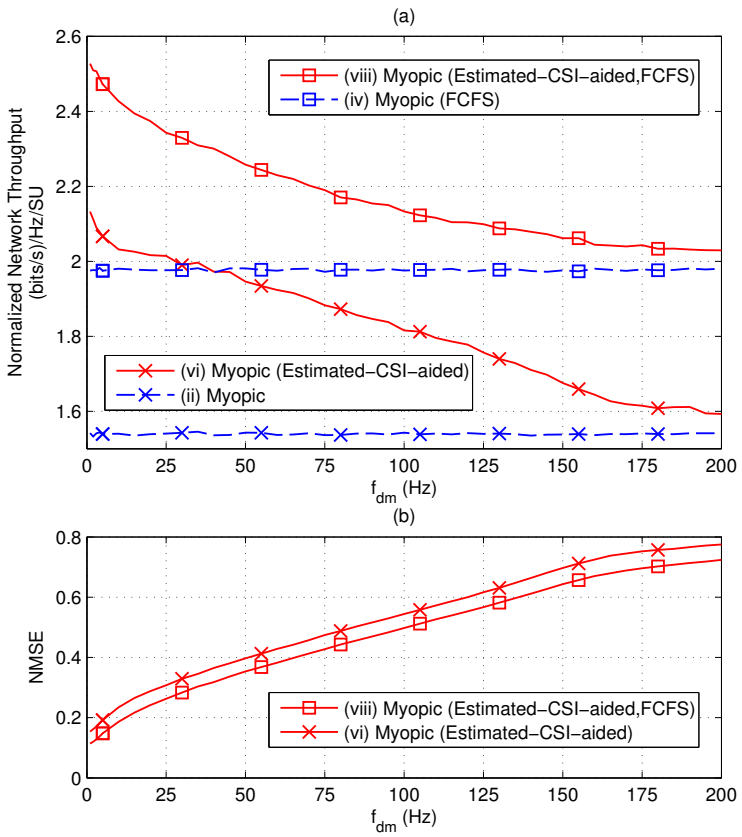

Figure 1.10: Performance of CSI-adaptive strategies with predicted CSI vs. f_{dm}: (a) throughput comparison with nonadaptive strategies (b) prediction NMSE; 3 SU pairs; 10 channels; ETSI Vehicular-A channel model; average SNR = 10 dB; $B^n = 200$ kHz; $L = 1$; $W = 20$; $T = 10^5$ slots.

We assume a known channel autocorrelation matrix. In practice, adaptive prediction methods can be used to track fading parameter variation [29]. We employ the ETSI Vehicular-A channel [33] which has six paths and an root-mean-square delay of 633 ns. Each channel is subject to frequency-flat fading. The time-varying channel coefficients are generated independently on each path and for each SU pair using the deterministic modified Jakes model [34], and thus we consider a longer time horizon of $T = 10^5$. Perfect pilot transmission scheduling among the SUs and negligible pilot overhead are assumed. In Figure 1.10, the throughputs of the CSI-aided sensing policies (vi,viii) and the NMSEs of CSI prediction (averaged over the whole time horizon and all SUs) are compared as a function of f_{dm} for $B^n = 200$ kHz. We observe that the averaged NMSEs in Figure 1.10(b) grow with f_{dm} (or the mobile speed), thus degrading the throughputs of the CSI-aided myopic sensing policies in Figure 1.10(a). As f_{dm} approaches 200 Hz, the latter converge to their nonadaptive counterparts (ii,iv), respectively. The FCFS MAC com-

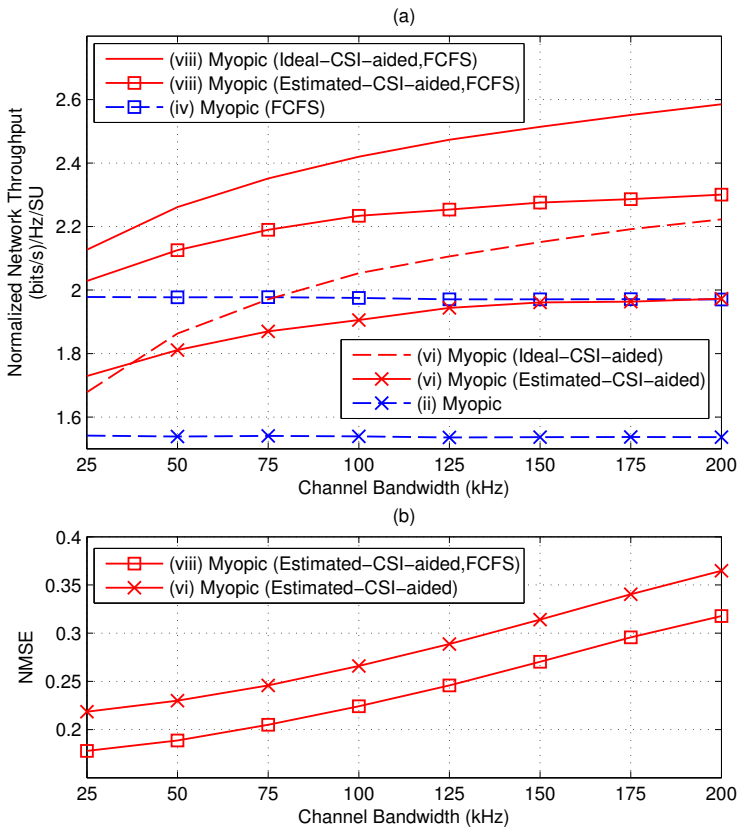

Figure 1.11: Performance of CSI-adaptive strategies with predicted CSI vs. channel bandwidth: (a) throughput of adaptive and nonadaptive policies (b) prediction NMSE; 3 SU pairs; 10 channels; ETSI Vehicular-A channel model; average SNR $= 10\,\text{dB}$; $f_{dm} = 40\,\text{Hz}$; $L = 1$; $W = 20$; $T = 10^5$ slots.

pletely eliminates overlapped sensing decisions so SUs can potentially discover additional idle channels for pilot transmissions. Thus, the FCFS MAC improves CSI estimation accuracy [see Figure 1.10(b)] and provides an additional throughput gain of about 0.4 (bits/s)/Hz/SU over the CSI-aided myopic sensing policy alone for mismatched CSI (viii vs. vi) in Figure 1.10(a).

In Figure 1.11, we compare these policies as a function of the channel bandwidth for $f_{dm} = 40\,\text{Hz}$. We first note from Figure 1.11(b) that the predicted CSI is more accurate for smaller channel bandwidths since frequency correlation between future channel gains and past observations collected from adjacent channels decreases with channel bandwidth. Thus, for CSI-aided sensing policies (vi,viii), the gap between the throughput curves for ideal and mismatched CSI widens as the bandwidth increases in Figure 1.11(a). However, better CSI prediction does not lead to improved throughput in Figure 1.11(a). This seemingly conflicting result is mainly due to the tradeoff between the CSI prediction accuracy and multichannel diversity. As the

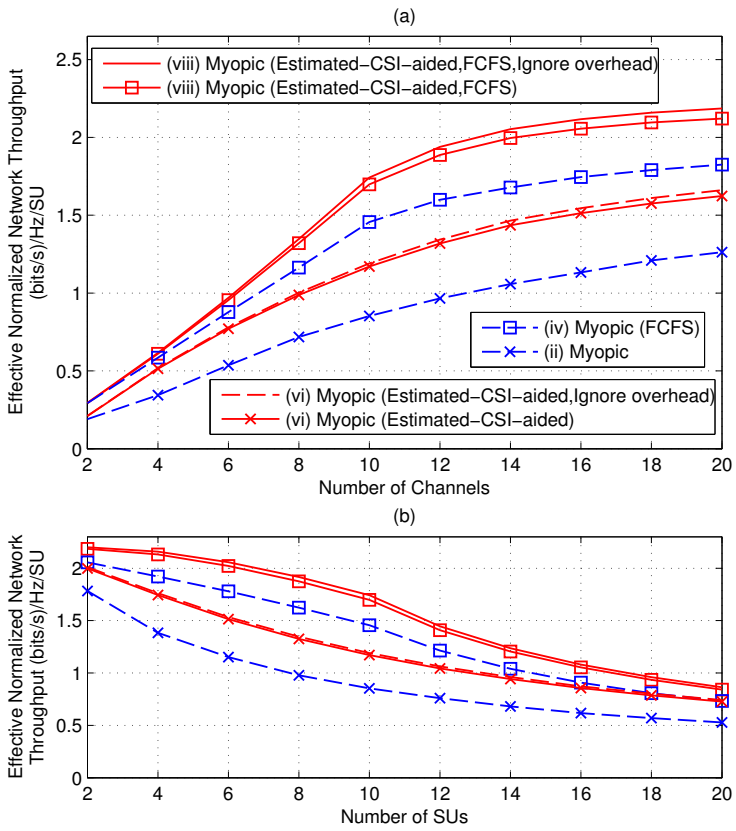

Figure 1.12: Performance of CSI-adaptive strategies with pilot overhead: (a) varying N with $M = 10$ (b) varying M with $N = 10$; ETSI Vehicular-A channel model; average SNR $= 10\,\text{dB}$; $f_{dm} = 75\,\text{Hz}$; $B^n = 200\,\text{kHz}$; $L = 1$; $W = 20$; $T = 10^5$ slots.

channel bandwidth grows, the correlation between the channels decreases, and the throughput gain of CSI-adaptation increases, compensating for decreased prediction accuracy. Overall, our proposed CSI-adaptive sensing policies (vi,viii) outperform their nonadaptive counterparts (ii,iv) for $f_{dm} \leq 200\,\text{Hz}$ and $B^n \in [25, 200]\,\text{kHz}$ for the Vehicular-A channel model. The gain is on the order of 0.4 (bits/s)/Hz/SU for typical system parameters and modest mobile speed, i.e., for $B^n \geq 75\,\text{kHz}$ and $f_{dm} \leq 75\,\text{Hz}$ (or when the carrier frequency $\leq 1\,\text{GHz}$ and the mobile speed $\leq 50\,\text{mph}$ [29]).

1.4.4 Effects of System Parameters and Pilot Overhead

We vary the number of channels (N) and SUs (M) in Figure 1.12(a) and (b), respectively. Note that the SU throughput increases with the amount of spectrum resources (N) and decreases with the number of competitors (M). Moreover, Figure 1.12 shows the effect of pilot overhead. In the proposed method, each SU sends one pilot symbol per slot in each channel that was sensed

to be idle. The symbol interval $T_{\text{sym}} = 1/B^n = 5\,\mu$s. At each time slot t, the total number of pilot transmissions in the CR system is $N_p(t) \times M$, and the total number of transmitted symbols is $N_p(t) \times 1\,\text{ms}/T_{\text{sym}}$, where $N_p(t)$ is the number of sensed available channels and 1 ms is the slot duration (cf. Table 1.1). Thus, the results in Figure 1.12 show very negligible pilot overhead since $M \in [2, 20]$ is much smaller than $1\,\text{ms}/T_{\text{sym}} = 200$.

In practice, pilot overhead increases with M, mobile speed, and reduced number of symbols per slot. To compensate, the proposed method can be enhanced by low-power pilot signals transmitted under the noise level of the PU network during the busy slots [35] or by channel gain estimation in the presence of sensing errors [36]. Moreover, each SU can reduce its pilot rate or choose only a subset of channels for CSI tracking since multichannel diversity saturates as the number of diversity branches increases [25]. Finally, in case of bursty SU traffic, SUs can transmit pilots only when they have data to transmit or shortly before transmission to reduce pilot overhead. On the other hand, high PU activity, low channel correlation, or hardware constraints result in insufficient pilot availability and limit prediction accuracy. If prediction of the multipath fading component becomes infeasible due to fast mobile speed (see Figure 1.10), the proposed strategies can adapt to slowly varying long-term (shadow) fading CSI. Using statistical and realistic physical shadow fading channel models, we demonstrate in the next section that CSI-aided strategies retain significant gains over conventional sensing policies and are robust to spatial and frequency correlation in CR ad hoc networks.

1.4.5 Adaptation to Shadow Fading CSI

In this section we explore adaptation to log-normal shadow fading where short-term fading is removed using diversity techniques. We investigate short-term Rayleigh fading model and the long-term shadow fading models separately for the following reasons [37]. At lower speeds, log-normal shadowing remains almost constant for the duration of transmission, and Rayleigh fading changes sufficiently slowly to allow prediction and adaptation prior to sensing as discussed in Section 1.4.3 and Section 1.4.4. As the speed increases, prediction of the Rayleigh fading component might become infeasible, but it is still beneficial to adapt to shadow fading [37]. Thus, estimation and tracking of shadow fading CSI is simpler and more practical than for short-term fading CSI.

However, the shadow fading components of different SUs are likely to be correlated. To analyze the impact of spatial correlation on the performance of the proposed CSI-aided policies (vi,viii), we employ the correlated lognormal shadowing model [38] for a simple CR network topology with one common SU receiver and $M = 20$ equally spaced SU transmitters placed uniformly on a linear track with minimum separation d as shown in Figure 1.13. We assume the shadow fading coefficients are uncorrelated across different channels. For each channel, the

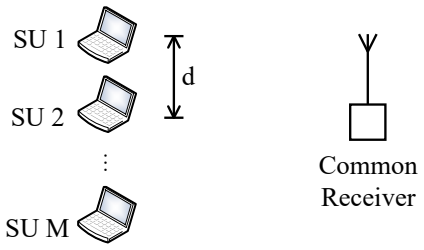

Figure 1.13: Network topology for the lognormal shadowing model.

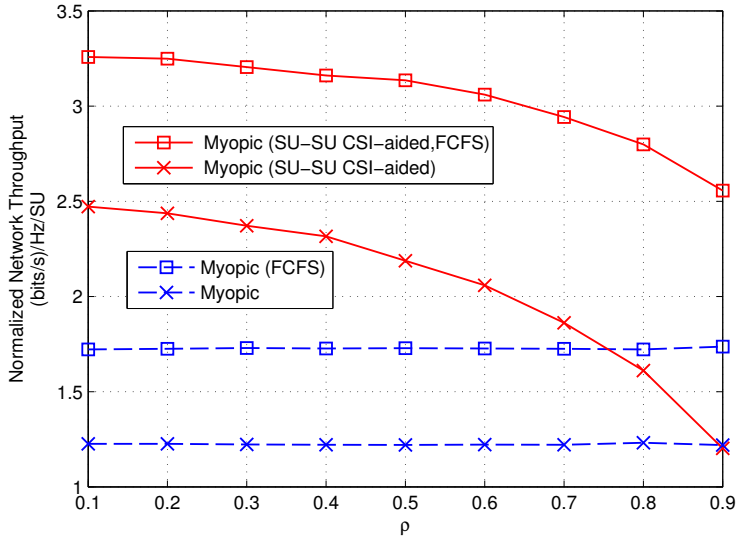

Figure 1.14: Throughput vs. spatial correlation ρ; capacity reward; 20 SU pairs; 40 channels; log-normal fading; average SNR= 10 dB; $\sigma_{\gamma_{\text{dB}}} = 5$ dB; $T = 20$ slots.

correlation coefficient between any two links m and m' is given by [39]

$$\rho_{mm'} = \rho^{|m-m'|} \tag{1.27}$$

with

$$\rho = e^{-\alpha d} \tag{1.28}$$

where α is a constant that depends on the environment. According to [39], $\alpha \approx 0.12$ and $\alpha \approx 0.002$ in urban and suburban cellular radio scenarios, respectively.

The impact of different values of ρ is shown in Figure 1.14. Each link is modeled using the lognormal distribution with average dB-scale SNR $\mu_{\gamma_{\text{dB}}} = 10$ dB and the dB-spread $\sigma_{\gamma_{\text{dB}}} = 5$ dB. Perfect CSI and sensing results are assumed.

Note that the throughputs of the CSI-aided sensing strategies (vi,viii) degrade as ρ increases. For smaller values of ρ, these strategies randomize decisions and benefit from multiuser diversity.

However, when the SU links are highly correlated, i.e., for $\rho \geq 0.9$, the performance of the proposed CSI-aided sensing policy (vi) approaches that of the myopic policy (ii). In this case, all SU links actually experience almost the same shadow fading patterns, so the multiuser diversity gained from adaptation to the channel conditions is lost. From (1.28), $\rho \geq 0.9$ corresponds to the case when $d \leq 0.88\,\text{m}$ in urban environments or $d \leq 52.68\,\text{m}$ in suburban environments. However, the model in [38] is applicable to cellular scenarios and does not accurately characterize channel propagation in vehicle-to-vehicle ad hoc networks. Spatial correlation among ad hoc network links was investigated in [40] and shown not to exceed $\rho = 0.3$ in most scenarios. *The proposed CSI-aided policies (vi) and (viii) maintain most of their potential gains for such correlation values.* Moreover, note that the CSI-aided myopic sensing policy with FCFS (viii) is less sensitive to the variation of ρ than the CSI-adaptive myopic strategy (vi). Using FCFS MAC, SUs yield to each other to avoid SU collisions while still benefiting from sensing channels with good channel quality. As a result, this method still exhibits 0.8 (bits/s)/Hz/SU gain over nonadaptive FCFS myopic sensing method (iv) for $\rho = 0.9$.

1.5 Conclusion

A channel-aware sensing strategy was investigated for distributed hardware-constrained mobile CR networks. To achieve effective collision resolution, this strategy was combined with a novel multichannel FCFS MAC algorithm. Analysis and simulations showed that adaptation to the CSI of the secondary link prior to sensing randomizes sensing decisions and improves both the individual and network throughputs. The throughput and energy gains of the proposed CSI-aided myopic strategy were on the order of 40% and 3 dB, respectively, relative to sensing policies in the literature. Moreover, combining this strategy with FCFS MAC provided additional gains of approximately 15% and 2–4 dB, respectively. Finally, a pilot-based fading prediction method was developed to enable CSI-aided sensing strategies, and it was demonstrated that the proposed sensing strategies are robust to CSI mismatch, spatial and frequency correlation, and sensing errors in practical mobile CR ad hoc networks.

In the next chapter, we will propose combined adaptive threshold control and channel-aware sensing strategies to improve the sensing quality and the SU throughput for very low PU signal SNR. Moreover, in the extreme cases where our proposed CSI-aided sensing policies is impaired due to the lack of diversity (cf. Section 1.4.3 and Section 1.4.5), the cooperative game in Chapter 3 can be employed to balance the SU traffic across different channels.

Chapter 2

Spectrum Detection for Noncooperative Secondary Users with One-Shot Sensing Capabilities

In Chapter 1, we assumed perfect or, at least, sufficiently accurate sensing results and focused on adaptation to the CSI of the SU links. In this chapter, we complete the discussion of CSI-adaptive sensing strategies by addressing the challenges of designing reliable spectrum sensors. We propose a threshold adaptation approach to the instantaneous PU-to-SU CSI under the prescribed collision constraint and a novel sensing strategy, which incorporates the resulting time-varying FA probability into the belief update and the reward computation. It is demonstrated that the proposed sensing approach improves SU confidence, randomizes sensing decisions, and significantly improves SU network throughput while satisfying the collision probability constraint to the PUs in the low average PU-to-SU SNR region. Moreover, the proposed adaptive sensing strategy is robust to mismatched and correlated fading CSI. In addition, threshold adaptation at a single SU sensor outperforms conventional cooperative sensing unless the number of cooperating SUs is very large. Finally, joint adaptation to PU channel gain and SU link CSI is proposed to further improve CR throughput and to reduce SU collisions.

2.1 Introduction

A spectrum detection method is an integral component of any sensing strategy. Classical detection approaches include matched filtering and energy detection [41]. To provide sufficient protection to the PU receivers and to avoid the "hidden node" problem, a constant detection rate (CDR) of the PU signals [42] is required even when the signal from the PU transmitter to the SU detector is weak (low PU-to-SU SNR) [43]. However, individual SU sensing decisions

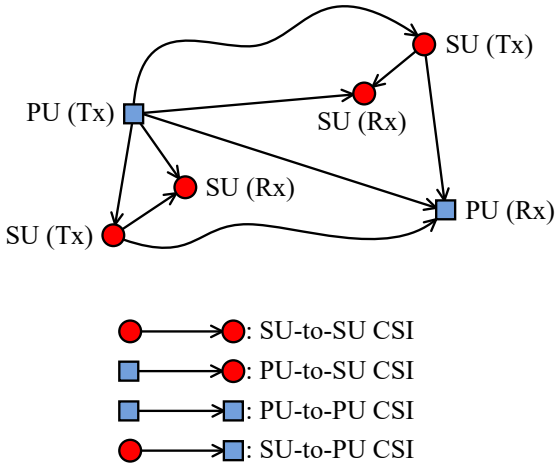

Figure 2.1: Types of CSI in a typical CR scenario.

become unreliable for fading PU-to-SU channels with low average SNR. Previously proposed advanced detection techniques only partially alleviate this problem. Cooperative sensing [44] can combat channel fading, but requires a large number of cooperating SUs and/or diversity branches. Thus, conventional cooperative sensing is not feasible for small networks, e.g., rural CR ad-hoc networks.

Related work: In [45], PU-to-SU channel gain (see Figure 2.1) is employed as a criterion in choosing channels for sensing. However, uniform PU activity across a wide band of channels was assumed. Moreover, a fixed threshold based on the FA rate constraint was employed although in practice the threshold should be chosen to satisfy an MD rate constraint [42]. Sensing threshold adaptation for single channel CR networks was investigated based on SU transmission power [46], the CSI between SU pairs [47], the amount of interference caused to PUs in case of missed detection [48], and the sensed SNR [49]. *However, threshold adaptation has not been incorporated into sensing strategy design for multichannel CR networks.*

In Chapter 1, we explained the importance of a randomized sensing policy which spreads SUs' sensing decisions over different channels and have investigated myopic sensing strategy where the reward is adapted to the SU-to-SU CSI (Figure 2.1) prior to sensing. This strategy was shown to reduce SU congestion and boost network throughput. However, this adaptation cannot salvage the detection accuracy loss due to low SNR of the PU signal at the sensor, which severely deteriorates performance of all sensing strategies in the literature. Thus, *randomized sensing strategies robust to low PU-to-SU SNR should be investigated.*

Contribution: We design a sensing strategy for overlay CR networks that adapts the threshold to the instantaneous SNR of the signal between the PU transmitter and the SU sensor, i.e., PU-to-SU CSI illustrated in Figure 2.1. To the best of our knowledge, only [49] has explored

such threshold adaptation. However, in [49], only one PU pair, one SU pair, and one channel were assumed, and unrealistic constraints that require the knowledge of the PU-to-PU SNR statistics and the instantaneous channel gain between the SU transmitter and the PU receiver at the SU (SU-to-PU CSI in Figure 2.1) was employed. We consider multiple SU pairs that compete for available channels under the hardware constraints. To offer sufficient protection to the primary network, we impose a constraint on the instantaneous MD probability at each SU. The resulting instantaneous FA probability is incorporated into the belief update and reward computation of the sensing strategy. By selecting to sense channels with high instantaneous PU-to-SU SNR, *this policy reduces FA rate, improves sensing decisions, and increases the CR network throughput.*

Moreover, the proposed adaptive sensing strategy randomizes sensing decisions of different SU detectors and helps to resolve SU collisions since the received channel gain from the PU transmitter varies over SU locations and frequencies. Thus, *the proposed detection method converts the conventional myopic strategy into a randomized sensing strategy.* Moreover, we combine sensing threshold adaptation with the channel-aware myopic sensing strategy in Chapter 1 that adapts the reward to the CSI of the SU link.

We also investigate practical feasibility of adaptive sensing threshold control. First, the knowledge of the PU-to-SU channel gain prior to sensing is necessary for threshold adaptation. It is also required for several cooperative sensing approaches [50, 51]. This CSI can be obtained directly from a channel gain map [52] if available. However, this method requires a large number of SUs, so will not be appropriate for small CR networks, highly dynamic systems, base station PU transmitters, etc. Otherwise, such information can be acquired from previous spectrum sensing or during the "silence" phase [53] when an SU does not have data to transmit and/or has sensed a channel that is occupied by a PU. Blind PU link CSI estimation was also proposed in [50]. This CSI is likely to be noisy and outdated, requires estimation and prediction, and CSI mismatch at the sensor is likely. To maintain the MD rate constraint, we incorporate the CSI error into the sensing strategy design and *investigate robustness to CSI mismatch.* Second, we validate performance of the proposed strategy for *multipath and correlated shadow fading channel models.* Finally, adaptive threshold control at a single SU is *compared with conventional cooperative sensing detection* for realistic network scenarios, and the advantages of the proposed sensing method for small CR networks, e.g., rural networks, are demonstrated.

The rest of this chapter is organized as follows. In Section 2.2, we formulate the problem and discuss sensing threshold adaptation. Myopic PU-to-SU CSI-aided sensing strategy is described and combined with reward adaptation to the CSI of the SU link in Section 2.3. Numerical results are presented in Section 2.4. Finally, we draw conclusions in Section 2.5.

2.2 Adaptive Sensing Threshold Control

In this chapter, we consider an overlay CR network [41] with M SU transmitter–receiver pairs and N orthogonal channels. The SUs can only access spectrum when active PUs are not detected in the neighborhood and are required to sense the spectrum before accessing any channel. All SUs make their own sensing and access decisions autonomously without the coordination of a central controller.

Suppose $\mathbf{y}^{mn}(t) = [y_1^{mn}(t), \ldots, y_\nu^{mn}(t)]$ is the signal received by the sensor of the mth SU on the nth channel at the time slot t, where ν is the number of collected samples. The components $y_i^{mn}(t)$ contain i.i.d. Gaussian noise terms with unit variance. If the PU transmitter is active, they also contain the PU signal. The instantaneous PU-to-SU SNR per sample λ^{mn} has the distribution $f_{\lambda^{mn}}(\lambda^{mn})$. Assume energy detection [44]. If the PU signal is not present during the sensing period (null hypothesis H_0), the output decision statistic $S(\mathbf{y}^{mn}(t))$ follows a central Chi-square distribution with 2ν degrees of freedom. If the PU signal is present (alternative hypothesis H_1), $S(\mathbf{y}^{mn}(t))$ follows a noncentral Chi-square distribution with 2ν degrees of freedom and a non-centrality parameter $2\nu\lambda^{mn}(t)$. If the decision statistic $S(\mathbf{y}^{mn}(t))$ is larger than the detection threshold $\tau^{mn}(t)$, the spectrum sensor accepts the alternative hypothesis H_1 and vice versa.

The instantaneous MD probability $p_{\mathrm{MD}}^{mn}(t)$ and the instantaneous FA probability $p_{\mathrm{FA}}^{mn}(t)$ are given by

$$p_{\mathrm{MD}}^{mn}(t) = \Pr[S(\mathbf{y}^{mn}(t)) < \tau^{mn}(t)|H_1] = 1 - Q_\nu\left(\sqrt{2\nu\lambda^{mn}(t)}, \sqrt{\tau^{mn}(t)}\right) \tag{2.1}$$

and

$$p_{\mathrm{FA}}^{mn}(t) = \Pr[S(\mathbf{y}^{mn}(t)) > \tau^{mn}(t)|H_0] = \frac{\Gamma(\nu, \tau^{mn}(t)/2)}{\Gamma(\nu)} \tag{2.2}$$

where $Q_\nu(.,.)$ is the generalized Marcum Q-function, $\Gamma(.,.)$ and $\Gamma(.)$ are the upper incomplete gamma function and the complete gamma function, respectively.

Conventionally the threshold is fixed, so $\tau^{mn}(t) = \tau^{mn}$. In this case the probability of MD is given by the expectation

$$p_{\mathrm{MD}}^{mn} = 1 - \int_{\lambda^{mn}} Q_\nu(\sqrt{2\nu\lambda^{mn}}, \sqrt{\tau^{mn}}) f_{\lambda^{mn}}(\lambda^{mn}) d\lambda^{mn} \tag{2.3}$$

and the probability of FA is

$$p_{\mathrm{FA}}^{mn} = \frac{\Gamma(\nu, \tau^{mn}/2)}{\Gamma(\nu)}. \tag{2.4}$$

We propose to adjust the threshold according to the instantaneous PU-to-SU CSI. Assuming the ideal CSI knowledge, the detector employs *the instantaneous FA and MD probabilities*

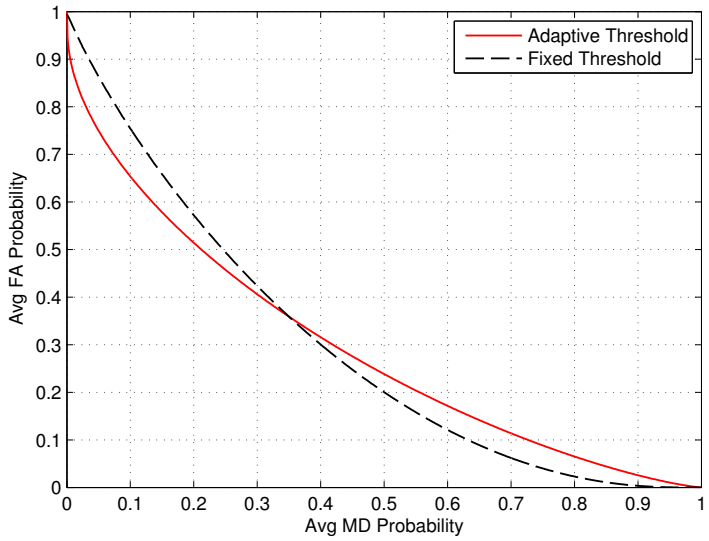

Figure 2.2: ROC curves for energy detection with fixed vs. adaptive threshold selection; Rayleigh fading; $\bar{\lambda} = -10\,\text{dB}$; $\nu = 100$.

(2.1)–(2.2) instead of averaging these probabilities over the fading distribution.

Both the conventional and the adaptive detectors must satisfy the MD rate constraint $p_{\text{MD,Target}}$. The detection threshold is computed by inverting the MD probability:

$$\tau^{mn}(t) = {p_{\text{MD}}^{mn}}^{-1}(p_{\text{MD,Target}}) \tag{2.5}$$

where p_{MD}^{mn} is given by (2.3) for the traditional energy detector and by $p_{\text{MD}}^{mn}(t)$ in (2.1) for the adaptive threshold selection.

Since the range of the PUs is usually much larger than the range of the SUs, all SUs in the neighborhood have similar PU SNR statistics. Thus, in the fixed threshold case, the FA probability and the threshold are time-invariant and are likely to take on similar values for neighboring SUs. However, for the proposed method, these parameters are time-variant and *will have different values across the CR spectrum for different SUs* due to spatial and frequency diversity in fading scenarios. Moreover, as the received power at the SU sensor increases, that SU can raise the detection threshold in (2.1) while maintaining a certain collision probability constraint in (2.5), and abrupt fluctuations in the received power caused by noise or interference will not be misidentified as PU signals. Thus, from (2.1)–(2.2), $p_{\text{FA}}(t)$ decreases with $\lambda^{mn}(t)$ given $p_{\text{MD,Target}}$, resulting in fewer wasted spectrum opportunities relative to the conventional detector case.

The receiver operating characteristic (ROC) curves of the energy detector with fixed and adaptive threshold selection under Rayleigh fading are compared in Figure 2.2. The average

PU-to-SU SNR $\bar{\lambda} = -10\,\text{dB}$. When the prescribed probability of MD is under 0.3, computing the threshold adaptively provides a lower average FA probability and thus *improves sensing reliability*.

2.3 Myopic Sensing with Adaptive Threshold Selection

The PU traffic is modeled as a stationary Markov process with known transition probabilities evolving independently on each channel. For channel n at the mth SU location, p_{ij}^{mn} denotes the probability of transition from state i to state j, where $i, j \in \{0(\text{busy}), 1(\text{idle})\}$. All PUs and SUs share the same slotted structure and are perfectly synchronized [2]. We assume that each SU can sense and then access only one channel at each time slot due to the hardware constraints. The belief vector $\boldsymbol{\theta}^m(t) = [\theta^{m1}(t), \theta^{m2}(t), \ldots, \theta^{mN}(t)]$ is employed by the SUs to infer the current state of the PU traffic, where $\theta^{mn}(t)$ is the conditional probability that channel n is available at time t for the mth SU pair based on past sensing history [2]. The sensing result $a^m(t) = 1$ if a spectrum opportunity is correctly detected or if an MD occurs, and $a^m(t) = 0$ if a PU activity is correctly detected or when an FA occurs.

As in Chapter 1, we consider noncooperative sensing policies where each SU makes sensing decisions selfishly without taking into account possible collisions with other CR users. Suppose the reward for SU m on channel n is $R^{mn}(t)$. At the first time slot $t = 1$, the initial belief vector is given by the stationary probabilities of the Markov process. Then at each time slot $t > 1$, SU m chooses to sense the channel $n_*^m(t)$ by maximizing the expected reward

$$n_*^m(t) = \arg\max_n \mathbb{E}[R^{mn}(t)] \tag{2.6}$$

where $\mathbb{E}[R^{mn}(t)] = \theta^{mn}(t) R^{mn}(t)$.

In the equations below, the probabilities of FA and MD are given by (2.1)–(2.2) for the proposed adaptive threshold and (2.3)–(2.4) for the conventional fixed threshold energy detection, respectively. After sensing, the belief is corrected by the reliability of the spectrum sensor [27]:

$$\theta_r^{mn}(t) = \begin{cases} \frac{(1-p_{\text{FA}}^{mn})\theta^{mn}(t)}{(1-p_{\text{FA}}^{mn})\theta^{mn}(t) + p_{\text{MD}}^{mn}(1-\theta^{mn}(t))}, & \text{if } n_*^m(t) = n \text{ and } a^m(t) = 1 \\ \frac{p_{\text{FA}}^{mn}\theta^{mn}(t)}{p_{\text{FA}}^{mn}\theta^{mn}(t) + (1-p_{\text{MD}}^{mn})(1-\theta^{mn}(t))}, & \text{if } n_*^m(t) = n \text{ and } a^m(t) = 0 \\ \theta^{mn}(t), & \text{if } n_*^m(t) \neq n \end{cases} \tag{2.7}$$

and then updated according to the Markov chain:

$$\theta^{mn}(t+1) = p_{11}^{mn}\theta_r^{mn}(t) + p_{01}^{mn}(1 - \theta_r^{mn}(t)) \tag{2.8}$$

where the process is repeated over the time horizon $t \in [1, T]$ [2]. When the instantaneous

reliability parameter $p_{\mathrm{FA}}^{mn}(t)$ is employed in (2.7)–(2.8) instead of the average p_{FA}^{mn}, more accurate estimation of the current PU traffic states results.

Finally, the reward is modified by the instantaneous probability of FA in the proposed policy. Suppose the reward for a fixed threshold strategy is given by $R_{\mathrm{FT}}^{mn}(t)$. The corresponding sensing strategy with adaptive threshold control employs the reward

$$R_{\mathrm{AT}}^{mn}(t) = (1 - p_{\mathrm{FA}}^{mn}(t))R_{\mathrm{FT}}^{mn}(t). \tag{2.9}$$

Thus, $R^{mn}(t)$ in (2.6) is given by $R_{\mathrm{FT}}^{mn}(t)$ when the conventional sensing method is employed and by (2.9) for adaptive threshold selection.

By taking into account the sensing reliability when selecting channels to sense, *SUs will favor stronger PU-to-SU channels* since $p_{\mathrm{FA}}^{mn}(t)$ decreases with $\lambda^{mn}(t)$. This approach increases SU confidence relative to the conventional sensing method where the individual SU throughput is sacrificed to protect the PUs. Moreover, due to geographical separation that provides spatial and frequency diversity, SUs perceive distinct sensing reliabilities on each channel, resulting in different sensing decisions. *Thus, the proposed policy randomizes sensing decisions and reduces SU congestion.*

Conventionally the reward is given by the channel bandwidth, i.e.,

$$R_{\mathrm{FT}}^{mn} = B^n. \tag{2.10}$$

However, when this reward is employed in the myopic policy, it results in severe CR network congestion and poor throughput. To reduce congestion, several strategies in the literature, e.g., [4], randomize sensing decisions or use negotiation while retaining the reward given by the channel bandwidth. However, the gains of these strategies are limited.

In Chapter 1, we proposed to *adapt the reward to the maximum achievable rate of the SU link*, i.e.,

$$R_{\mathrm{FT}}^{mn}(t) = C^{mn}(t) = B^n \log_2(1 + \gamma^{mn}(t)) \tag{2.11}$$

where $\gamma^{mn}(t)$ is the instantaneous SNR of the mth SU pair on the nth channel, and $C^{mn}(t)$ is the channel capacity. This sensing strategy exploits spatial and frequency diversity, randomizes sensing decisions, and boosts the network throughput. This myopic (SU-to-SU CSI-aided) sensing strategy significantly outperforms other randomized policies even when they employ adaptive transmission as illustrated in Section 1.3–1.4. This gain is due to adaptation to the SU link CSI prior to sensing. We showed that this approach is robust to CSI mismatch and fading correlation and retains its gain when the reward is computed using realistic adaptive modulation.

In practice, sensing errors significantly degrade the throughput of all strategies in the lit-

erature under a realistic collision probability constraint, especially in the low PU-to-SU SNR region [43]. To remedy this problem, we can employ adaptive threshold control. These two types of adaptation prior to sensing, i.e., adaptation to PU-to-SU and SU-to-SU CSI, are tested individually and jointly in the numerical results below. Thus, *we evaluate the benefits of adaptive threshold control for both conventional and channel-aware myopic strategies and the gain of combined adaptation prior to sensing to the PU-to-SU and the SU-to-SU link CSI.*

2.4 Numerical Results

Consider a CR network with $M = 20$ SU pairs and $N = 40$ channels with the same bandwidth $B^n = 1\,\text{Hz}$, $\forall n$. The transition probabilities of the PU traffic on all channels at all SU locations are $p_{01}^{mn} = 0.2$ and $p_{11}^{mn} = 0.8$, $\forall m, n$. All SU-to-SU, PU-to-SU, and PU-to-PU channels are subject to independent Rayleigh fading unless stated otherwise. All SU-to-SU links are identically distributed on all channels with the average SNR $\bar{\gamma}$. Similarly, at all SU sensors the average PU signal SNR $\bar{\lambda}$ is the same on all channels. In this chapter we focus on low average SNR from the PU transmitter to the SU sensor (PU-to-SU SNR in Figure 2.1). Note that the PU receiver can still be close to the SU transmitter, so the interference to the PU network (SU-to-PU SNR) can still be significant. We assume an overlay scenario where an MD results in a collision between the SU and the PU transmissions.

We employ a MAC scheme similar to [54] where an SU will transmit over a channel if it is sensed idle or go to sleep during the current time slot if it is sensed busy. If multiple SU pairs choose to sense the same channel and if that channel is idle, only one of them can transmit successfully. Moreover, we assume that SUs always have data to transmit. Finally, the *SU network throughput for any sensing strategy in this section is computed under the assumption that adaptive transmission is employed after sensing with the accumulated reward given by the channel capacity.*

Since the generalized Marcum Q-function in (2.1) and its inverse in (2.5) are very computationally complex, we employ the Gaussian approximation that holds for $\nu \gg 1$ [41].

2.4.1 Throughput Gain of PU-to-SU CSI Adaptation

We compare the average secondary network throughput (normalized by M) and the primary network throughput (normalized by N) assuming average PU-to-PU SNR $= 10\,\text{dB}$ over $T = 20$ time slots, as a function of $p_{\text{MD,Target}}$ in Figure 2.3(a) and (b), respectively, for four sensing policies. The first two policies employ fixed threshold selection in (2.3)–(2.4): the conventional myopic sensing policy with the bandwidth reward in (2.10) (myopic, imperfect) [2] and the myopic sensing policy that adapts to SU link SNR with the reward (2.11) (SU–SU CSI-aided,

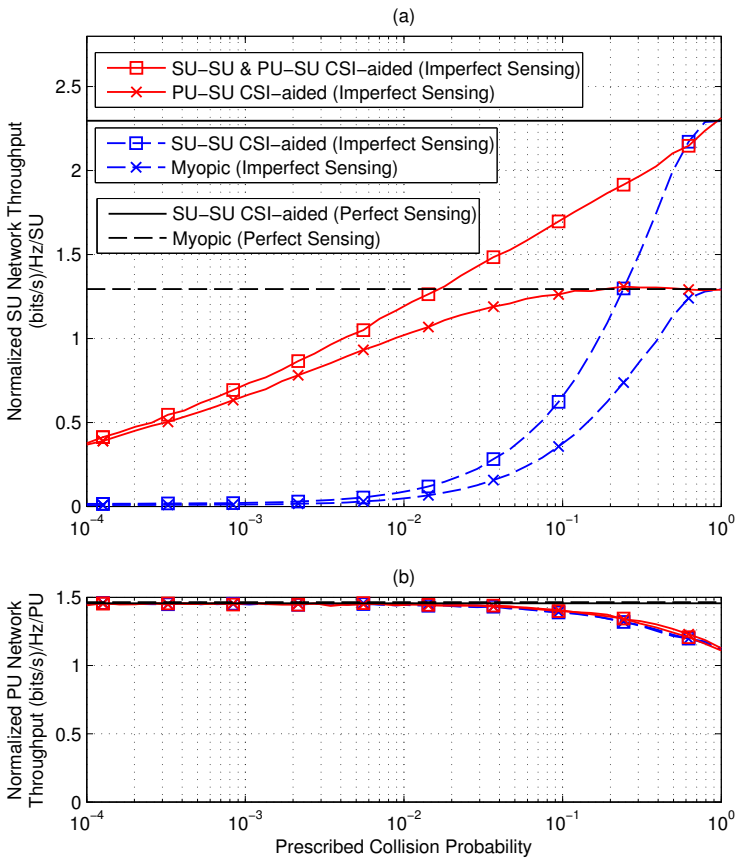

Figure 2.3: Throughput vs. $p_{\mathrm{MD,Target}}$: (a) SU network (b) PU network; 20 SU pairs; 40 channels; i.i.d. Rayleigh fading; PU-to-PU SNR = SU-to-SU SNR $\bar{\gamma} = 10\,\mathrm{dB}$; PU-to-SU SNR $\bar{\lambda} = -10\,\mathrm{dB}$; $T = 20$; $\nu = 100$.

imperfect) proposed in Chapter 1. The other two policies employ adaptive threshold selection (2.2), (2.5) and the reward (2.9), where $R_{\mathrm{FT}}^{mn}(t)$ is given by (2.10) for the myopic PU–SU CSI-aided policy and (2.11) for the combined PU–SU and SU–SU CSI-aided myopic sensing policy. Moreover, the throughputs of the conventional and SU–SU CSI-adaptive strategies under perfect sensing are also plotted in Figure 2.3.

Due to the MD rate constraint our proposed policy offers the same long-term protection to the PUs as conventional sensing strategies as demonstrated by overlapped PU performance curves in Figure 2.3(b). The throughput of the PU network is compromised severely when $p_{\mathrm{MD,Target}} > 10^{-1}$ and approaches its optimal value as the prescribed collision probability tends to 10^{-2}. However, from Figure 2.3(a), the SU network throughput degrades rapidly for $p_{\mathrm{MD,Target}} \leq 10^{-1}$ when conventional fixed threshold detection is employed. *The proposed threshold adaptation results in 0.4–1 (bits/s)/Hz/SU throughput gain over the fixed threshold policy*

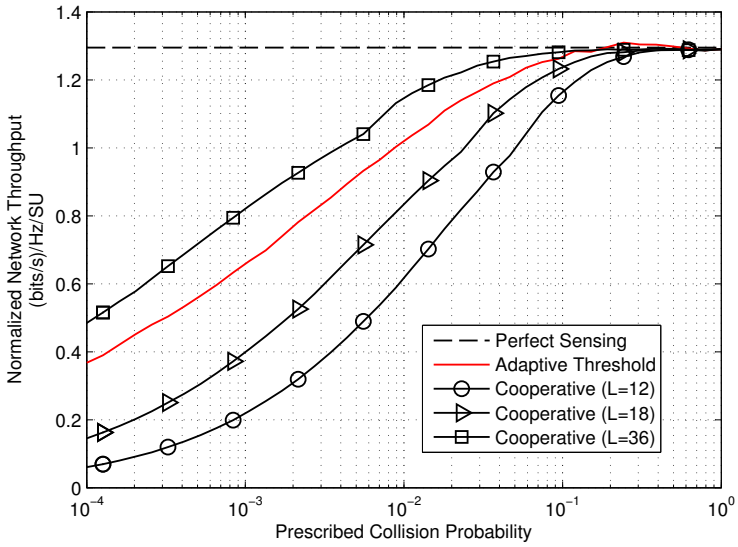

Figure 2.4: Throughput of adaptive threshold selection and of cooperative sensing; 20 SU pairs; 40 channels; i.i.d. Rayleigh fading; $\bar{\gamma} = 10\,\text{dB}$; $p_{\text{MD,Target}} = 0.1$; $\bar{\lambda} = -10\,\text{dB}$; $T = 20$; $\nu = 100$.

in the small $p_{\text{MD,Target}}$ *region.* Both strategies converge to their ideal counterparts as $p_{\text{MD,Target}}$ increases. *The combined adaptation provides up to 0.4 (bits/s)/Hz/SU additional gain relative to adaptive sensing threshold selection alone for* $p_{MD,Target} \leq 10^{-1}$. Since both policies employ adaptive transmission, this gain is due to adaptation to SU link CSI prior to sensing.

However, in the low $p_{\text{MD,Target}}$ region adaptive threshold selection is more beneficial for the conventional myopic strategy than for the strategy that also adapts to the CSI of the SU link. First, the former strategy reaches the ideal sensor case for $p_{\text{MD,Target}}$ as small as 0.1 while the latter converges to the ideal case only for $p_{\text{MD,Target}} = 1$. Moreover, at $p_{\text{MD,Target}} = 10^{-2}$, the throughput gain provided by threshold adaptation is about 75% of the ideal throughput for the conventional myopic policy and is only 43% for the SU-to-SU CSI adaptive strategy. The lower relative gain in the latter strategy is due to reward adaptation that randomizes sensing decisions, so additional multiuser and multichannel diversity provided by sensing threshold adaptation has lower impact than for the conventional myopic strategy.

In Figure 2.4, we evaluate the myopic policy using two spectrum detection approaches: sensing threshold adaptation and cooperative sensing. In the latter method, we assume OR-rule hard decision combining [44] where a fusion center collects independent individual sensing decisions from L SUs and decides H_1 if any of the L local decisions is H_1. The MD and FA probabilities of the final decisions are $P_{\text{MD}}^{mn} = (p_{\text{MD}}^{mn})^L$ and $P_{\text{FA}}^{mn} = 1 - (1 - p_{\text{FA}}^{mn})^L$, respectively, where p_{MD}^{mn} and p_{FA}^{mn} are given by (2.3)–(2.4), respectively, and the threshold can be determined by inverting P_{MD}^{mn}, i.e., $\tau^{mn} = P_{\text{MD}}^{mn\,-1}(p_{\text{MD,Target}})$, $\forall m, n$.

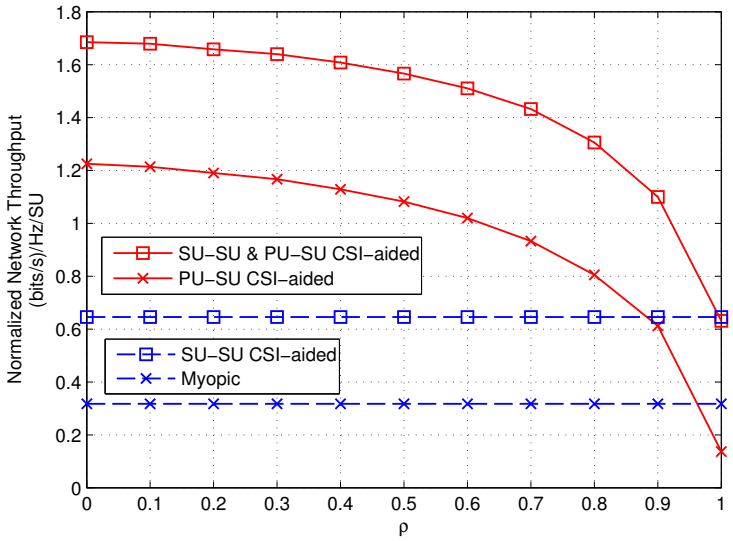

Figure 2.5: Throughput vs. spatial correlation ρ; 20 SU pairs; 40 channels; log-normal fading; $\mu_{\gamma_{\mathrm{dB}}} = 10\,\mathrm{dB}$; $\mu_{\lambda_{\mathrm{dB}}} = -10\,\mathrm{dB}$; $\sigma_{\gamma_{\mathrm{dB}}} = \sigma_{\lambda_{\mathrm{dB}}} = 5\,\mathrm{dB}$; $p_{\mathrm{MD,Target}} = 0.1$; $T = 20$; $\nu = 100$.

Cooperative sensing has lower throughput than the proposed PU-to-SU CSI-aided myopic policy unless the number of diversity branches is very large. We found that at least $L = 30$ independent sensing observations are required to match the throughput of adaptive threshold selection at a single SU detector. Thus, *throughput improvement and multiuser diversity gain of the proposed method outweigh the benefits of cooperative sensing for realistic hardware-constrained CR networks, e.g., rural CR ad hoc networks where the number of cooperating SUs or diversity branches is likely to be small while competition for available spectrum might still be severe.*

2.4.2 Impact of Correlated Shadow Fading and CSI Error

We explore adaptation to the log-normal shadow fading where the short-term (multipath) fading is removed using diversity techniques. While estimation and tracking of shadow fading CSI is simpler and more practical than of short-term fading CSI for high speeds, the shadow fading signals from the PU transmitter to different SU sensors are likely to be correlated in space and frequency. To validate robustness to spatial correlation, we employ the correlated lognormal shadowing model [38] for the network with one PU transmitter and $M = 20$ equally spaced SU detectors placed on a linear track[1]. The shadow fading coefficients are assumed uncorrelated in frequency across different channels and for all SU-to-SU links. For each channel, the spatial

[1]We assume that SU transmitter is responsible for spectrum sensing. In practice, sensing can also be carried out at the receiver side or at both ends of the SU link (equivalent to cooperative sensing with $L = 2$).

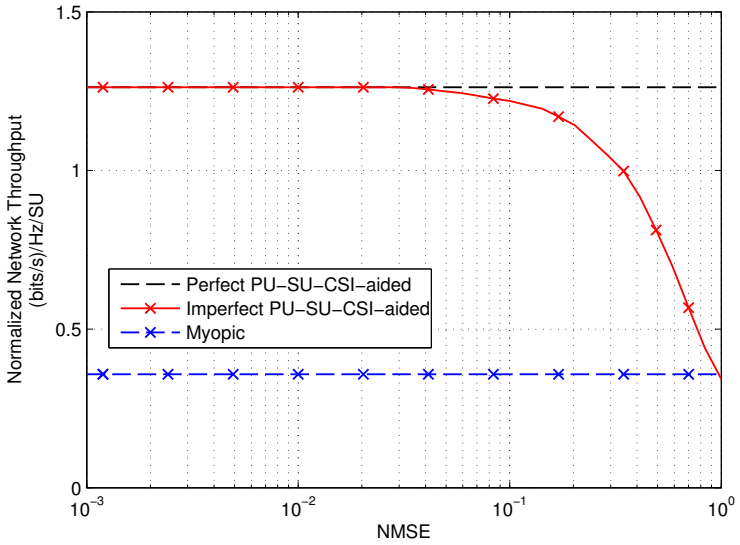

Figure 2.6: Throughput vs. NMSE of CSI estimation; 20 SU pairs; 40 channels; i.i.d. Rayleigh fading; $\bar{\gamma} = 10\,\text{dB}$; $\bar{\lambda} = -10\,\text{dB}$; $p_{\text{MD,Target}} = 0.1$; $T = 20$; $\nu = 100$.

correlation coefficient between any two PU-to-SU links observed at detectors m and m' is given by $\rho_{mm'} = \rho^{|m-m'|}$, where ρ is the shadow fading correlation for two adjacent detectors. Each channel is modeled using the lognormal distribution with average dB-scale SNR $\mu_{\gamma_{\text{dB}}} = 10\,\text{dB}$, $\mu_{\lambda_{\text{dB}}} = -10\,\text{dB}$ and the dB-spread $\sigma_{\gamma_{\text{dB}}} = \sigma_{\lambda_{\text{dB}}} = 5\,\text{dB}$. The impact of different values of ρ is shown in Figure 2.5. Note that the throughput of the proposed PU-to-SU CSI-aided sensing strategy degrades to that of conventional myopic sensing as the correlation ρ increases. However, CSI-aided sensing provides significant throughput gain even for relatively high values of ρ. These results show that *the proposed method is useful in practical shadow fading scenarios* [38, 40].

As discussed in the introduction, estimated PU-to-SU channel gain will result in CSI mismatch, and CSI estimation errors can also degrade performance of the proposed sensing threshold adaptation. Robustness to the SU-to-SU CSI errors was validated in Chapter 1. Below we investigate the effect of PU-to-SU CSI mismatch. We assume that the detector employs the MMSE estimate of the actual PU-to-SU SNR λ conditioned on its mismatched observation $\hat{\lambda}$ (omitting the indices m, n and t for simplicity). The threshold is calculated using the expected MD rate,

$$\hat{p}_{\text{MD}}(t) = \int_0^\infty p_{\text{MD}}(t) f(\lambda|\hat{\lambda}) d\lambda \tag{2.12}$$

$$\hat{\tau}(t) = \hat{p}_{\text{MD}}^{-1}(p_{\text{MD,Target}}) \tag{2.13}$$

where $p_{\text{MD}}(t)$ is given by (2.1) and $f(\lambda|\hat{\lambda})$ is the conditional pdf of λ given $\hat{\lambda}$, e.g., [28]. The FA probability is computed using the threshold (2.13), and the reward is computed using (2.9)

where $R_{\mathrm{FT}}^{mn}(t)$ is given by (2.10). We illustrate the throughput vs. NMSE of SNR estimation for the myopic strategy with adaptive threshold selection in Figure 2.6.

We observe that the proposed approach approximates the ideal PU-to-SU CSI case when NMSE ≤ 0.1 and degrades gracefully to the conventional myopic policy with fixed threshold when the PU-to-SU CSI becomes unreliable. Note that NMSE ≥ 0.1 corresponds to severely degraded CSI prediction accuracy in conventional communication systems [29]. Thus, we conclude that the *proposed scheme is robust to PU-to-SU CSI mismatch.*

2.5 Conclusion

Adaptation of the detection threshold to the instantaneous SNR of the PU signal was proposed for CR spectrum sensing. The instantaneous MD probability constraint was imposed, and the resulting time-variant FA probability was incorporated into the sensing strategy design. It was demonstrated that the proposed sensing strategy randomizes sensing decisions and provides 0.4–1 (bits/s)/Hz/SU throughput gain over the fixed threshold policy for small prescribed collision probabilities with the PU network and low average PU-to-SU SNR. Additional 0.4 (bits/s)/Hz/SU can be gained by combined adaptation to PU-to-SU and SU-to-SU CSI. Moreover, cooperative sensing with at least 30 independent sensing results is necessary to match the throughput of proposed threshold adaptation at a single detector. Finally, it is shown that the proposed adaptive strategy is robust to shadow fading correlation and to CSI mismatch for practical CR network parameters.

Chapter 3

Cooperative Secondary Users with One-Shot Sensing Capability

To improve the sensing accuracy under weak PU signal SNR, we have introduced a channel-adaptive approach by adjusting the local detection thresholds in Chapter 2. Yet another viable alternative is to foster cooperative sensing among the SUs. In this chapter, a two-layer coalitional game model is investigated for cooperative SUs, in which the coalition formation and the payoff allocation problems are decoupled: in the top-layer hedonic game, SUs form disjoint coalitions over potentially available channels while in the bottom-layer game, SUs negotiate over the payoff allocation within each coalition. The cooperatively detected spectrum opportunities are then shared among the coalition members in a coordinated manner according to their binding agreement on payoff allocation. The proposed game is decentralized and fosters cooperation by providing each SU with the transmission opportunities it deserves. Moreover, we propose a new physical-layer approach to distribute the network-level MD constraints fairly among the interfering SUs for guaranteed PU protection. We demonstrate the performance advantages of the AND-rule combining of spectrum sensing results for heterogeneous SUs. Numerical results show that the proposed game outperforms previously investigated collaborative sensing and multichannel access approaches in terms of energy efficiency, throughput, SU fairness, and computational complexity. Finally, the effect of mobility on the computational complexity of the proposed game is discussed.

3.1 Introduction

Cooperative sensing exploits spatial diversity to improve sensing accuracy in CR systems [55]. While most investigations assume a fixed number of fully cooperative SUs with identical sensing capabilities monitoring a single channel, in practice, there are many possible channels for sensing

and transmission, and the sensing accuracy varies over the spectrum and among the SUs. Under the hardware constraints, SUs need to choose both the channels to sense and their collaborators[1] for spectrum sensing.

Game theory has been utilized recently to model and analyze SU interactions in cooperative sensing [57–64] and opportunistic access [18, 64, 65], but, to the best of our knowledge, only the game in [64] takes into account transmission (spectrum access) opportunities when making channel sensing and collaboration decisions in a multichannel CR network. However, in the one-layer game of [64], the SUs sensing the same channel are forced to cooperate, and all coalition members have the same probability of transmission over the channel that has been sensed idle. Thus, the game in [64] is not suitable for the heterogeneous environment where the contributions of different SUs within a coalition can vary significantly. For example, an SU located closer to the PU tends to obtain more accurate sensing results and, thus, its contribution to the cooperative sensing accuracy is greater than that of a more distant SU. Such heterogeneous scenarios are typical in wireless networks. To provide incentives for cooperation, the payoff of each player should match its contribution. In this chapter, we propose a two-layer coalitional game where channel sensing decisions and access agreements are guided by a fair payoff allocation method among the SUs.

Moreover, to facilitate efficient spectrum sensing, we develop constraints on MD rates of coalition members and provide novel insights into the performance of fusion rules of sensing results for heterogeneous networks under the CDR [42] constraints.

The *contributions* of this chapter are:

- Development and analysis of a two-layer coalitional game that includes:
  - (i) An efficient, stable, and distributed coalition formation algorithm across and within the channels.
  - (ii) A contribution-based payoff allocation scheme to promote individual incentives for cooperation.
- Improved spectrum sensing approaches:
  - (i) A fair distribution method of the integrated network-level primary collision probability constraint among the coalitions and member SUs sharing the same channel.
  - (ii) Demonstration of performance advantages of the AND-rule combining for heterogeneous sensing environments under the CDR constraints.

The rest of this chapter is organized as follows. Table 3.1 summarizes significant notation. In Section 3.2, we introduce the system model and formulate the proposed two-layer game, which is then analyzed in Section 3.3 using coalitional game theory. Simulation results and comparison with [64] are presented in Section 3.4, and conclusions are drawn in Section 3.5.

[1] We consider only cooperation among the SUs. The PU–SU cooperation [56] is out of the scope of this thesis.

Table 3.1: Significant Notation in Chapter 3

Notation	Explanation
$\mathcal{M}$, $\mathcal{N}$	Set of all SUs and set of all channels.
$C = (S, n)$	A top-layer coalition C is a two-tuple, where $C(1)$ is a set of SUs $S \subseteq \mathcal{M}$ and $C(2)$ is the operating channel n.
$\mathcal{P}$	A top-layer partition of $\mathcal{M}$ defines a set of disjoint top-layer coalitions $\mathcal{P} = \{C^1, C^2, \ldots, C^N\}$ with cardinality N, where $\forall n \neq \tilde{n}$, $C^n(1) \cap C^{\tilde{n}}(1) = \phi$, $C^n(2) \neq C^{\tilde{n}}(2)$, $\cup_{n=1}^{N} C^n(1) = \mathcal{M}$ and $\cup_{n=1}^{N} \{C^n(2)\} = \mathcal{N}$.
n_*^m	Sensing decision of SU m.
$\Pi(\mathcal{M}, \mathcal{N})$	Set of all N^M possible top-layer partitions.
x^{mC}	Top-layer utility, given by the expected data rate of SU $m \in C(1)$ operating on channel $C(2)$.
a^{mC}	Bottom-layer payoff for SU $m \in C(1)$ on channel $C(2)$, given by the probability that m transmits successfully.
R^{mn}	Transmission rate of SU pair m on channel n.
γ^{mn}	SU-to-SU SNR of SU pair m on channel n.
B^n, β^n	Bandwidth and availability probability of channel n.
(S, U^n)	Bottom-layer game among a set of SUs S on channel n with the value function U^n.
η	A bottom-layer coalition η is a subset of SUs sensing the same channel, i.e., $\eta \subseteq C(1)$ for some $C \in \mathcal{P}$.
ρ	A bottom-layer partition is a set of disjoint subsets of $C(1)$ with their union equal to $C(1)$ for some $C \in \mathcal{P}$.
$U^n(\eta; \rho)$	Value of bottom-layer coalition η, as given by η's overall successful transmission probability on channel n under the bottom-layer partition ρ where $\eta \in \rho$.
$U(\mathcal{P})$	The total partition value $U(\mathcal{P}) \triangleq \sum_{C \in \mathcal{P}} U^{C(2)}(C(1))$.
$P_{\mathrm{MD}}^n(\eta)$, $P_{\mathrm{FA}}^n(\eta)$	Cooperative MD and FA probabilities of a bottom-layer coalition η regarding the PU presence.
$P_{\mathrm{MD}}^{\mathrm{Ch}}$	Integrated MD (or PU collision) probability constraint on each channel.
$P_{\mathrm{MD}}^n(m)$, $P_{\mathrm{FA}}^n(m)$	Individual MD constraint and FA probability of SU m on channel n.
τ^{mn}	Adaptive detection threshold of SU m on channel n.
λ^{mn}	PU-to-SU SNR per sample at SU m on channel n.
ν	Number of collected samples for spectrum sensing.

3.2 System Model and Two-Layer Game Formulation

We consider an overlay slotted[2] CR ad hoc network with multiple SU pairs and multiple channels under i.i.d. Bernoulli PU traffic. An SU can sense and access only one channel at each time slot due to the hardware constraints.

3.2.1 The Top-Layer Game

The top-layer game is played by all SUs in $\mathcal{M} = \{1, \ldots, M\}$ across all channels in $\mathcal{N} = \{1, \ldots, N\}$. The set of SUs S sensing and transmitting over the same channel n forms a top-layer coalition $C = (S, n)$[3], i.e., the sensing decision of each SU $m \in S$ is

$$n_*^m = n \Leftrightarrow \{m \in C(1) \text{ and } C(2) = n\}. \tag{3.1}$$

Consequently, the set of all SUs $\mathcal{M}$ is partitioned into a total number of N disjoint top-layer coalitions on different channels, resulting in a top-layer partition $\mathcal{P} = \{C^1, C^2, \ldots, C^N\}$. Every possible top-layer coalition $C = (S, n)$ generates a partially transferable utility (PTU) measured by the expected data rate

$$x^{mC} = a^{mC} R^{mn} \tag{3.2}$$

for each member SU $m \in S$, where the successful transmission probability a^{mC} is a transferable utility (TU) [66] given by the allocated individual payoff provided by the bottom-layer game (cf. Section 3.3.1), and the data rate of SU m on channel n given by $R^{mn} = B^n \log_2(1 + \gamma^{mn})$ is a nontransferable utility (NTU) [66], which can vary greatly across different SU pairs due to their spatial separation. We define a preference relation that guides an SU when choosing a top-layer coalition. An SU m prefers to move from channel n to $\tilde{n}$ if the following preference relation is satisfied:

$$\tilde{C}^{\tilde{n}} \succ_m C^n \Leftrightarrow \begin{cases} x^{m\tilde{C}^{\tilde{n}}} > x^{mC^n} \\ \sum\limits_{i \in \tilde{C}^n(1)} a^{i\tilde{C}^n} + \sum\limits_{i \in \tilde{C}^{\tilde{n}}(1)} a^{i\tilde{C}^{\tilde{n}}} > \sum\limits_{i \in C^n(1)} a^{iC^n} + \sum\limits_{i \in C^{\tilde{n}}(1)} a^{iC^{\tilde{n}}} \end{cases} \tag{3.3}$$

where $\tilde{C}^n = (C^n(1) \backslash \{m\}, n)$ and $\tilde{C}^{\tilde{n}}$ are the top-layer coalitions that form on channels n and $\tilde{n}$, respectively, if SU m makes the move, and C^n and $C^{\tilde{n}} = (\tilde{C}^{\tilde{n}}(1) \backslash \{m\}, \tilde{n})$ are the existing top-layer coalitions on these channels. Thus, the top-layer coalition $\tilde{C}^{\tilde{n}}$ is preferable to C^n for SU m if (i) its expected data rate (3.2) improves and (ii) the combined successful transmission probabilities of all SUs on channels n and $\tilde{n}$ improve. For example, in Figure 3.1, SU $m = 4$

[2] Our results can be extended to continuous PU traffic by adjusting the primary collision constraints [18].

[3] Note that a top-layer coalition is a two-tuple specifying both the set of SUs S and the channel index n because the same set of SUs S can achieve different throughputs on different channels.

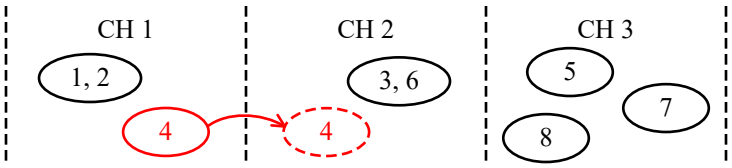

Figure 3.1: An example of the two-layer coalition structure and SU movements with 8 SUs and 3 channels. The top-layer partition is $\mathcal{P} = \{(\{1,2,4\},1),(\{3,6\},2),(\{5,7,8\},3)\}$ and the bottom-layer partitions are $\rho^1 = \{\{1,2\},\{4\}\}$, $\rho^2 = \{\{3,6\}\}$ and $\rho^3 = \{\{5\},\{7\},\{8\}\}$. SU $m = 4$ prefers to move from channel $n = 1$ to $\tilde{n} = 2$ if (3.3) is satisfied with $C^n = (\{1,2,4\},1)$, $C^{\tilde{n}} = (\{3,6\},2)$, $\tilde{C}^n = (\{1,2\},1)$ and $\tilde{C}^{\tilde{n}} = (\{3,6,4\},2)$.

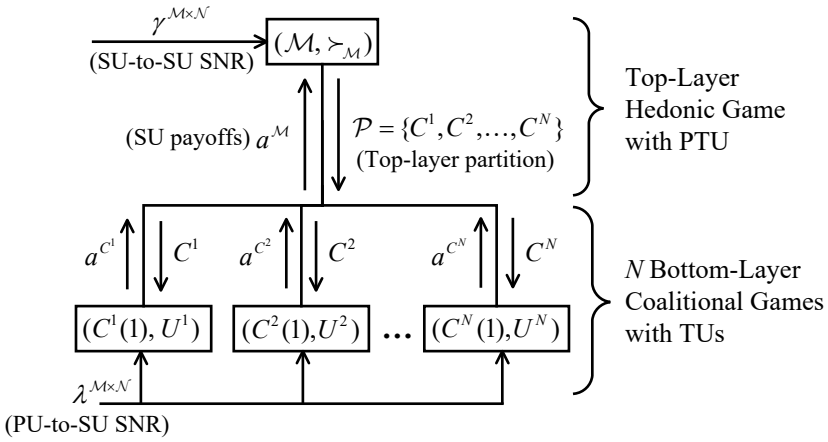

Figure 3.2: Two-layer coalitional game.

prefers to switch from channel 1 to channel 2 if this movement improves not only its individual throughput, but also the overall successful transmission probability of all SUs currently residing on these channels, i.e., SUs 1, 2, 3, 4 and 6. Using the preference relation (3.3), which combines the social and individual objectives, the top-layer game can be modeled as a hedonic game $(\mathcal{M}, \succ_{\mathcal{M}})$ [67]. Given $(\mathcal{M}, \mathcal{N}, a^{\mathcal{M}}, \gamma^{\mathcal{M}\times\mathcal{N}})$, the top-layer game generates a partition $\mathcal{P}$ as shown in Figure 3.2. We will describe the partition formation algorithm of the top-layer game and prove its convergence to a Nash-stable partition [67] in Section 3.3.2.

3.2.2 The Bottom-Layer Game

An output partition $\mathcal{P}$ of the top-layer game determines the set of SUs that can sense and transmit over each channel. The SUs sensing the same channel can further form disjoint bottom-layer coalitions, resulting in a bottom-layer partition ρ, as illustrated in Figure 3.1. Within each bottom-layer coalition, the SUs exchange and combine their sensing results to improve the overall successful transmission probability of this coalition. The detected spectrum opportunities

are then shared among the bottom-layer coalition members in a coordinated manner using a payoff allocation rule, which determines an SU's share of the slot for transmission and provides collision avoidance. We formulate N coalitional games (S, U^n) at the bottom layer, which are played on different channels, where $S = C(1)$ and $n = C(2)$ for some $C \in \mathcal{P}$, and U^n is a value function for all subsets of S. In Section 3.3.1, we prove the efficiency [68] of the grand coalitions on all channels and discuss several payoff allocation rules for the bottom-layer games.

Since SUs coordinate channel access within each bottom-layer coalition, there is no need to use a MAC scheme. In contrast, MAC would be needed if multiple bottom-layer coalitions formed since several such coalitions could simultaneously detect a spectrum opportunity correctly and, therefore, would compete for access. As in [7], we consider the following two MAC options:

1. 0/X-model: All competing SUs fail to transmit successfully.
2. 1/X-model: All competing SUs have equal access probability, and the overhead cost is ignored. After gaining the right to access, the winning SU will transfer its transmission opportunity to its bottom-layer coalition's members as required by their binding agreement on payoff allocation (cf. Section 3.3.1).

The performance of a chosen MAC option is impacted by the players' noncooperation cost, which measures how SU collisions and overhead affect the transferable successful transmission probability. Due to space limitations, we consider only the 0/X- and 1/X-models since they correspond to the maximum and minimum noncooperation cost, respectively. In practice, fair distributed MAC can be realized through random backoff and control message exchange at the cost of some control overhead and/or missed transmission opportunities. In Section 3.3.1, we prove the formation of the grand coalition assuming both MAC models, and we expect this property to hold under the assumption of other MAC options with moderate noncooperation costs, eliminating the need for SU competition and, thus, for actual MAC utilization in the proposed game. However, MAC needs to be assumed hypothetically to determine the payoff allocation (cf. Section 3.3.1).

Next, we consider computation of the value function U^n for a coalition $\eta \subseteq S$ on channel n, defined as the overall successful transmission probability of η on this channel. Given a partition ρ on channel n, label all other bottom-layer coalitions in $\rho \backslash \{\eta\}$ as

$$\rho \backslash \{\eta\} = \{\xi_1, \xi_2, \ldots, \xi_{|\rho|-1}\} \tag{3.4}$$

and define a binary-valued random vector of length $|\rho|-1$

$$\mathbf{X}_{\rho \backslash \{\eta\}} = (X_{\xi_1}, X_{\xi_2}, \ldots, X_{\xi_{|\rho|-1}}) \in \{0,1\}^{|\rho|-1} \tag{3.5}$$

where $X_{\xi_i} \in \{0,1\}$ is an indicator variable for the event that the coalition ξ_i experiences an FA, i.e.,

$$\Pr(X_{\xi_i} = x_i) = \begin{cases} P_{\mathrm{FA}}^n(\xi_i), & \text{if } x_i = 1 \\ 1 - P_{\mathrm{FA}}^n(\xi_i), & \text{if } x_i = 0. \end{cases} \tag{3.6}$$

The coalition values for the two MAC models can be expressed as:

$$U_{0/\mathrm{X}}^n(\eta;\rho) = \beta^n(1 - P_{\mathrm{FA}}^n(\eta)) \cdot \prod\nolimits_{i=1}^{|\rho|-1} P_{\mathrm{FA}}^n(\xi_i) \tag{3.7}$$

and

$$\begin{aligned} U_{1/\mathrm{X}}^n(\eta;\rho) &= \beta^n(1 - P_{\mathrm{FA}}^n(\eta)) \cdot \mathbb{E}\left[\frac{|\eta|}{|\eta| + J_{\rho\setminus\{\eta\}}\left(\mathbf{X}_{\rho\setminus\{\eta\}}\right)}\right] \\ &= \beta^n(1 - P_{\mathrm{FA}}^n(\eta)) \cdot \sum_{\mathbf{x}\in\{0,1\}^{|\rho|-1}} \left\{ \frac{|\eta| \prod_{i=1}^{|\rho|-1} \Pr(X_{\xi_i} = x_i)}{|\eta| + J_{\rho\setminus\{\eta\}}(\mathbf{x})} \right\} \end{aligned} \tag{3.8}$$

where β^n and $P_{\mathrm{FA}}^n(\eta)$ are defined in Table 3.1, and the number of competing SUs for cognitive access is given by

$$J_{\rho\setminus\{\eta\}}(\mathbf{x}) = \sum\nolimits_{i=1}^{|\rho|-1} (1 - x_i)|\xi_i|. \tag{3.9}$$

Since the bottom-layer coalition value $U^n(\eta;\rho)$ depends not only on the actions of the coalition members, but also on the actions of other SUs on channel n, this coalitional game is in partition form [66]. We assume the overall successful transmission probabilities (3.7) and (3.8) of a bottom-layer coalition are dividable and can be transferred among coalition members according to the allocated payoff probability a^{mC} [cf. (3.2)], so that the bottom-layer game has TU. To illustrate, consider the following example. Suppose the overall successful transmission probability of a two-SU bottom-layer coalition $\eta = \{1,2\}$ on channel n is $U^n(\eta) = 0.8$, and both SUs agree on a payoff probability allocation of $a^{1n} = 0.2$ and $a^{2n} = 0.6$. Under the 0/X-model, the coalition η acquires a transmission opportunity when η discovers an idle time slot. On the other hand, under the 1/X-model, the coalition η acquires a transmission opportunity when η discovers an idle time slot, possibly competes with other coalitions, and finally wins a right to transmit. The acquired transmission opportunities are then shared between the two SUs according to their payoff allocation agreement, either in a probabilistic manner, with the conditional probabilities that SU 1 and SU 2 are allowed to transmit for the entire time slot given by $a^{1n}/(a^{1n}+a^{2n}) = 1/4$ and $a^{2n}/(a^{1n}+a^{2n}) = 3/4$, respectively, or in a time-division multiple access (TDMA) manner, for 1/4 and 3/4 of the time, respectively[4]. In either case, it is not hard to show that the successful transmission probability of SU 1 and SU 2 are $1/4 \times U^n(\eta) = 0.2$

[4]SU transmissions might be unsuccessful either due to SU collisions (under the 0/X-model) or MD of PU traffic (under both MAC models).

and $3/4 \times U^n(\eta) = 0.6$, as desired.

3.2.3 Cooperative Sensing

Next, we present the cooperative sensing scheme at the physical layer. Consider a certain top-layer coalition $C = (S, n)$ and a bottom-layer partition ρ of S. The individual MD and FA probabilities for each SU $m \in S$ can be approximated as [44]

$$P^n_{\mathrm{MD}}(m) = 1 - Q\Big((\tau^{mn}/2\nu - \lambda^{mn} - 1) \sqrt{\nu/(2\lambda^{mn}+1)} \Big) \tag{3.10}$$

$$P^n_{\mathrm{FA}}(m) = Q\left((\tau^{mn}/2\nu - 1)\sqrt{\nu} \right) \tag{3.11}$$

respectively, where λ^{mn}, τ^{mn} and ν are defined in Table 3.1, and $Q(\cdot)$ is the Q-function [69, eq. (B.20)]. Since MD of the PU presence leads to undesired primary collisions, we impose constraints on the $P^n_{\mathrm{MD}}(m)$ values. The individual detection threshold τ^{mn} is obtained by inverting (3.10), resulting in the individual false-alarm probability $P^n_{\mathrm{FA}}(m)$ in (3.11). It is not hard to show that the resulting $P^n_{\mathrm{FA}}(m)$ decreases with the PU-to-SU SNR λ^{mn}, indicating stronger sensing capability of closer SUs to the PUs.

The PU transmission is interrupted if one or more bottom-layer coalitions in ρ fail to detect its presence, so the integrated MD probability on channel n is given by

$$P^n_{\mathrm{MD}}(\rho) = 1 - \prod_{\eta \in \rho} \left(1 - P^n_{\mathrm{MD}}(\eta)\right). \tag{3.12}$$

To provide uniform protection to the PUs across the potentially available spectrum, ensure fairness among the SUs, and improve spectrum detection, we impose the following constraints:
Network-level constraint (C.1): $P^n_{\mathrm{MD}}(\rho) = P^{\mathrm{Ch}}_{\mathrm{MD}}$ (cf. Table 3.1)
Coalition-level constraint (C.2): All equal-sized bottom-layer coalitions should maintain the same MD rate.
Node-level constraint (C.3): All SUs within a bottom-layer coalition must satisfy the same MD constraint.

Constraints (C.1) and (C.2) are satisfied by requiring: $\forall \eta \in \rho$,

$$P^n_{\mathrm{MD}}(\eta) = 1 - (1 - P^{\mathrm{Ch}}_{\mathrm{MD}})^{|\eta|/|S|}. \tag{3.13}$$

Next, we evaluate performance of the AND- and the OR-combining rules for the proposed constrained spectrum sensing approach. The FA probabilities of these fusion rules are given

by [42, eq. (10–17)][5]:

$$P^n_{\mathrm{FA,AND}}(\eta) = \prod_{m\in\eta} P^n_{\mathrm{FA,AND}}(m) = \prod_{m\in\eta} Q\left(\sqrt{2\lambda^{mn}+1}\phi + \sqrt{\nu}\lambda^{mn}\right) \tag{3.14}$$

$$P^n_{\mathrm{FA,OR}}(\eta) = 1 - \prod_{m\in\eta}(1 - P^n_{\mathrm{FA,OR}}(m)) = 1 - \prod_{m\in\eta}\left(1 - Q(\sqrt{2\lambda^{mn}+1}\tilde{\phi} + \sqrt{\nu}\lambda^{mn})\right) \tag{3.15}$$

respectively, with [cf. (3.13) and (C.3)]

$$\phi \triangleq Q^{-1}\big(1 - P^n_{\mathrm{MD,AND}}(m)\big) = Q^{-1}\big((1 - P^n_{\mathrm{MD}}(\eta))^{\frac{1}{|\eta|}}\big) = Q^{-1}\big((1 - P^{\mathrm{Ch}}_{\mathrm{MD}})^{\frac{1}{|S|}}\big) \tag{3.16}$$

$$\begin{aligned}\tilde{\phi} &\triangleq Q^{-1}\big(1 - P^n_{\mathrm{MD,OR}}(m)\big) = Q^{-1}\big(1 - (P^n_{\mathrm{MD}}(\eta))^{\frac{1}{|\eta|}}\big)\\ &= Q^{-1}\Big(1 - \big(1 - (1 - P^{\mathrm{Ch}}_{\mathrm{MD}})^{|\eta|/|S|}\big)^{\frac{1}{|\eta|}}\Big)\end{aligned} \tag{3.17}$$

where $m \in \eta \in \rho$ and all other notation is defined in Table 3.1. First, from (3.16)–(3.17), the individual MD constraint $P^n_{\mathrm{MD}}(m)$ depends on the size of the bottom layer coalition to which an SU belongs for the OR-rule, but not for the AND-rule. Thus, when using the AND-rule, SUs do not have to update the MD constraints when computing their values within different bottom-layer coalitions as long as the SU population $|S|$ on channel n does no change. Second, for both rules, as $|S|$ increases, each coalition η reduces its MD rate $P^n_{\mathrm{MD}}(\eta)$ in (3.13), leading to increased FA probability $P^n_{\mathrm{FA}}(\eta)$ in (3.14)–(3.15) and decreased coalition values in (3.7)–(3.8). Thus, large values of $|S|$ are penalized, balancing SU competition on all channels.

Finally, our extensive simulation results using (3.14)–(3.17) show that the AND-rule is more suitable when cooperative SUs have heterogeneous sensing capabilities (i.e., different PU-to-SU SNRs) while the OR-rule provides better performance in homogeneous scenarios. Intuitively, if there is at least one SU $m \in \eta$ with favorable PU-to-SU SNR λ^{mn}, and thus with small FA probability $P^n_{\mathrm{FA,AND}}(m)$, the resulting $P^n_{\mathrm{FA,AND}}(\eta)$ is very small since $P^n_{\mathrm{FA,AND}}(\eta) \leq \min_{m\in\eta} P^n_{\mathrm{FA,AND}}(m)$ in (3.14). In contrast, for the OR-rule, if only one member SU has very poor sensing capacity, the entire bottom-layer coalition η suffers since $P^n_{\mathrm{FA,OR}}(\eta) \geq \max_{m\in\eta} P^n_{\mathrm{FA,OR}}(m)$ in (3.15). For example, in Figure 3.3 we compare the integrated FA probabilities (3.14) and (3.15) for coalition $\eta = \{1, 2\}$ on channel n when the average PU-to-SU SNR of the two member SUs is fixed to $\bar{\lambda}$. We observe that the OR-rule and the AND-rule achieve their best performance for homogeneous and heterogeneous sensing capacities (PU signal strengths at the sensor) of the two SUs, respectively. The general case is explored below.

Proposition 1. Consider coalition η on channel n and a fixed bottom-layer-coalition-level MD probability constraint $P^n_{\mathrm{MD}}(\eta)$. The FA probability of η for the AND-rule (3.14) [OR-rule (3.15)]

[5] As in [42], we assume AWGN PU-to-SU channels and thus time-invariant λ^{mn} values. In practice, these channels may be subject to fading and the ergodic sensing accuracy probabilities can be obtained by averaging over the fading distribution [44, 58, 59].

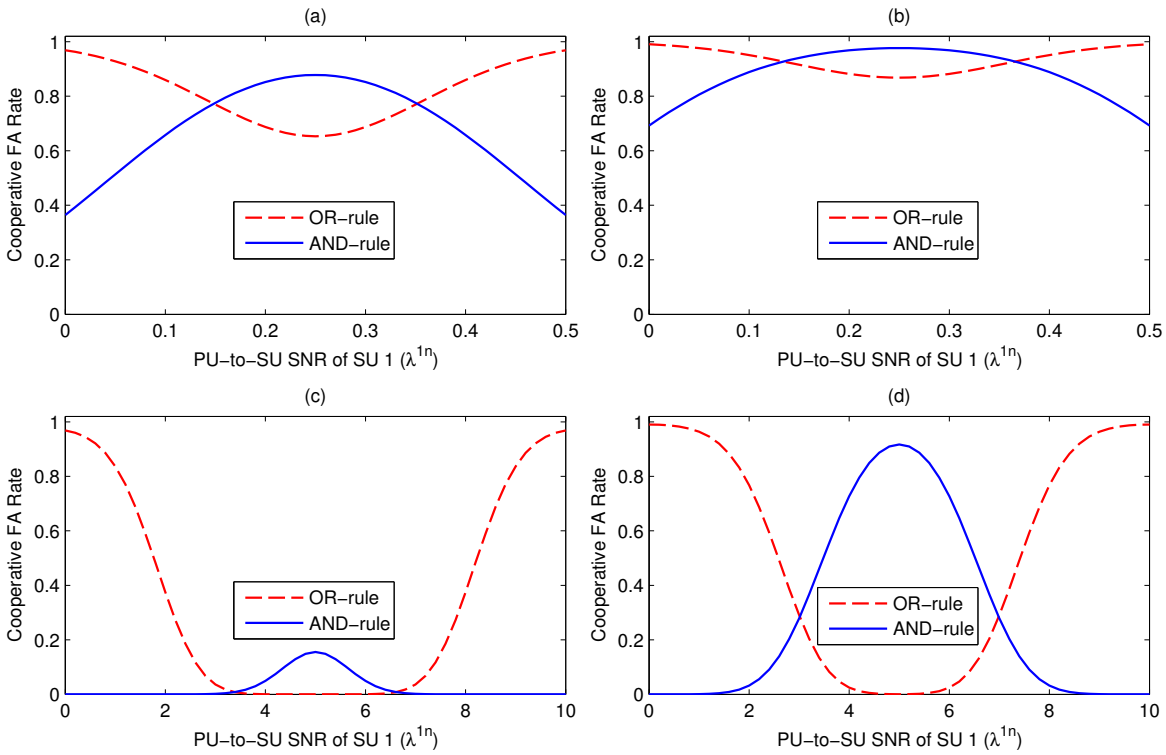

Figure 3.3: Performance comparison of the $P_{\text{FA}}^{n}(\eta)$ for the AND- and OR-rule under the proposed MD constraints; $\eta = \{1, 2\}$; $\bar{\lambda} = 0.5(\lambda^{1n} + \lambda^{2n})$. (a) $\bar{\lambda} = 0.25$ ($-6\,\text{dB}$); $P_{\text{MD}}^{n}(\eta) = 10^{-3}$; $\nu = 100$. (b) $\bar{\lambda} = 0.25$ ($-6\,\text{dB}$); $P_{\text{MD}}^{n}(\eta) = 10^{-4}$; $\nu = 100$. (c) $\bar{\lambda} = 5$ ($7\,\text{dB}$); $P_{\text{MD}}^{n}(\eta) = 10^{-3}$; $\nu = 5$. (d) $\bar{\lambda} = 5$ ($7\,\text{dB}$); $P_{\text{MD}}^{n}(\eta) = 10^{-4}$; $\nu = 5$.

is a quasiconcave (quasiconvex) function [70, Section 3.4], which achieves its global maximum (global minimum) when $\lambda^{mn} = \bar{\lambda}$, $\forall m \in \eta$, subject to an average PU-to-SU SNR constraint

$$\frac{1}{|\eta|} \sum_{m \in \eta} \lambda^{mn} = \bar{\lambda} \tag{3.18}$$

if $\forall m \in \eta$,

$$P_{\text{MD}}^{n}(\eta) < (0.5)^{|\eta|} \tag{3.19}$$

$$\tilde{\phi} > -\frac{\sqrt{\nu}(2\lambda^{mn} + 1)^{\frac{3}{2}}}{3\lambda^{mn} + 2}. \tag{3.20}$$

Proof. See Appendix B.1. □

Note that the constraints (3.19) and (3.20) are mild[6]. For example, they can be easily

[6] (3.19) implies that ϕ (3.16) and $\tilde{\phi}$ (3.17) are both negative since $|\eta| \geq 1$. (3.20) implies that $\tilde{\phi} > -\frac{3\sqrt{\nu}\sqrt{2\lambda^{mn}+1}}{2}$ since $\lambda^{mn} \geq 0$.

satisfied if: (i) $P_{\mathrm{MD}}^n(\eta) \geq 10^{-4}$ and $|\eta| \leq 13$ and (ii) ($\nu \geq 56$ for $\lambda^{mn} \geq 0$) or ($\nu \geq 13$ for $\lambda^{mn} \geq 1$) or ($\nu \geq 2$ for $\lambda^{mn} \geq 10$), i.e., when the MD constraint $P_{\mathrm{MD}}^n(\eta)$ is not extremely stringent, the coalition size $|\eta|$ is not too large, and the number of collected samples for spectrum sensing ν is sufficiently large[7].

Based on these observations, in the remainder of this chapter we will assume the AND fusion rule to study a typical wireless CR network with a moderate number of cooperating SUs on each channel, which experience heterogeneous PU-to-SU channel conditions.

3.3 Two-Layer Coalitional Sensing and Access Game

3.3.1 Grand Coalition Formation and Payoff Allocation at the Bottom Layer

Consider the bottom-layer game (S, U^n) on channel n.

Proposition 2. For the 0/X-model, the game $(S, U_{0/\mathrm{X}}^n)$:

(i) reduces to a characteristic-form game, i.e., the value of a bottom-layer coalition η depends solely on the composition of η [66]: $U_{0/\mathrm{X}}^n(\eta;\rho) = U_{0/\mathrm{X}}^n(\eta;\tilde{\rho}) \triangleq U_{0/\mathrm{X}}^n(\eta)$, for any $\eta \subseteq S$ and any bottom-layer partitions ρ and $\tilde{\rho}$ of S, such that $\eta \in \rho$ and $\eta \in \tilde{\rho}$;

(ii) is superadditive [66], i.e., the SUs benefit from forming larger coalitions. Thus, for any two disjoint bottom-layer coalitions $\eta, \xi \subset S$, $U_{0/\mathrm{X}}^n(\eta \cup \xi) \geq U_{0/\mathrm{X}}^n(\eta) + U_{0/\mathrm{X}}^n(\xi)$;

(iii) from (ii), has efficient grand coalition [68], i.e., the grand coalition value is at least as large as the combined value of all coalitions in any other partition: $\forall \tilde{\rho} \neq \{S\}$, $U_{0/\mathrm{X}}(S) \geq \sum_{\eta \in \tilde{\rho}} U_{0/\mathrm{X}}(\eta)$.

Proof. (i) For any $\eta \subseteq S$ and any bottom-layer partition ρ of S such that $\eta \in \rho$, the value of η is given by [cf. (3.7) and (3.14)]

$$U_{0/\mathrm{X}}^n(\eta;\rho) = \beta^n(1 - P_{\mathrm{FA}}^n(\eta)) \cdot \prod_{m \in S \setminus \eta} P_{\mathrm{FA}}^n(m) \tag{3.21}$$

which does not depend on ρ. (ii) Substituting (3.14) into (3.7) and simplifying, we obtain

$$U_{0/\mathrm{X}}^n(\eta \cup \xi) - U_{0/\mathrm{X}}^n(\eta) - U_{0/\mathrm{X}}^n(\xi) = \beta^n \Big(1 - \prod_{m \in \eta} P_{\mathrm{FA}}^n(m)\Big)\Big(1 - \prod_{m \in \xi} P_{\mathrm{FA}}^n(m)\Big) \prod_{m \in S \setminus \eta \setminus \xi} P_{\mathrm{FA}}^n(m) \tag{3.22}$$

which is nonnegative. □

[7] In practice, low PU-to-SU SNR (e.g., ≤ 1) often requires ν on the order of hundreds to thousands and medium-to-high PU-to-SU SNR (e.g., ≥ 10) often requires less than 10 samples for good performance (see, e.g., [44, 71]).

Proposition 3. Under the 1/X-model, all bottom-layer partitions of S are equally efficient, i.e., for any two partitions ρ and $\tilde{\rho}$ of S, $\sum_{\eta\in\rho} U^n_{1/\mathrm{X}}(\eta;\rho) = \sum_{\eta\in\tilde{\rho}} U^n_{1/\mathrm{X}}(\eta;\tilde{\rho})$.

Proof. Under the 1/X-model, a spectrum opportunity on channel n is wasted if all bottom-layer coalitions make FAs on the PU presence. Thus, for any bottom-layer partition ρ of any S on any channel n [cf. (3.14)]

$$\sum_{\eta\in\rho} U^n_{1/\mathrm{X}}(\eta;\rho) = \beta^n\Big(1-\prod_{\eta\in\rho} P^n_{\mathrm{FA}}(\eta)\Big) = \beta^n\Big(1-\prod_{m\in S} P^n_{\mathrm{FA}}(m)\Big) \tag{3.23}$$

which is independent of ρ. □

Proposition 4. Under the 1/X-model, the bottom-layer game $(S, U^n_{1/\mathrm{X}})$ exhibits nonpositive externalities [72], i.e., a merger between two coalitions cannot improve the values of other coalitions. Formally, for any disjoint coalitions $\eta, \xi, \zeta \subset S$ and any partition ρ of S such that $\eta, \xi, \zeta \in \rho$, the coalition value $U^n_{1/\mathrm{X}}(\eta;\rho) \geq U^n_{1/\mathrm{X}}\big(\eta; \rho\backslash\{\xi\}\backslash\{\zeta\}\cup\{\xi\cup\zeta\}\big)$.

Proof. See Appendix B.2. □

Proposition 5. The grand coalition always forms in the bottom-layer game for the 1/X and 0/X MAC models.

Proof. If $\rho = \{S\}$ is efficient, the grand coalition always forms [66] [68]. We proved in Propositions 2 that the bottom-layer game $(S, U^n_{0/\mathrm{X}})$ is a superadditive characteristic-form game. Thus the grand coalition $\rho = \{S\}$ is efficient and should always form under the 0/X-model.

Moreover, Propositions 3 implies the (weak) efficiency of the grand coalition under the 1/X-model, i.e., $\forall\tilde{\rho} \neq \{S\}$, $U^n_{1/\mathrm{X}}(S;\rho) = \sum_{\eta\in\tilde{\rho}} U^n_{1/\mathrm{X}}(\eta;\tilde{\rho})$. From [68,72], and Proposition 4, the grand coalition also forms under the 1/X-model. □

Proposition 5 implies that all SUs sensing channel n cooperate, and MAC is not utilized. Moreover, it is feasible to divide the value of the grand coalition $U^n(S;\{S\})$ (hereafter referred to as $U^n(S)$ for brevity) while satisfying every member SU with its allocated payoff. Generally, a good payoff allocation rule ensures the stability of and the fairness within the grand coalition [73] by relating the actual individual payoff to the hypothetical payoff that an SU could have obtained by leaving the grand coalition and/or the marginal value it brings into the grand coalition. Therefore, despite the formation of the grand coalition, we need to compute the hypothetical values of smaller bottom-layer coalitions using (3.7) or (3.8) for the two collision models. Fair payoff allocation rules for traditional single-layer coalitional games are extensively studied in the literature assuming (hypothetical) breakdown of the grand coalition, e.g., the Shapley value [66], the Owen value [74], the nucleolus [66], the Nash bargaining solution (NBS) [75,76], etc. In this chapter, we employ the NBS due to its computational efficiency [75].

Proposition 6. For the characteristic-form (cf. Proposition 2) bottom-layer game $(S, U^n_{0/\mathrm{X}})$, NBS assigns a payoff (successful transmission probability) [75]

$$a^{mC}_{\mathrm{NBS},0/\mathrm{X}} = \frac{U^n_{0/\mathrm{X}}(S) - \sum\limits_{i\in S} U^n_{0/\mathrm{X}}(\{i\})}{|S|} + U^n_{0/\mathrm{X}}(\{m\}) \tag{3.24}$$

$\forall m \in S$, where the disagreement point is $\big\{U^n_{0/\mathrm{X}}(\{m\}) : m \in S\big\}$.

The mth component of the disagreement point $U^n_{0/\mathrm{X}}(\{m\})$ represents SU m's minimal expected individual payoff and is given by the hypothetical successful transmission probability obtained if bargaining fails. Since SUs with stronger sensing capabilities have higher singleton values $U^n_{0/\mathrm{X}}(\{m\})$, the NBS (3.24) provides each SU with the allocated payoff commensurate with its sensing contribution, resulting in a fair payoff allocation.

When the 1/X-model is assumed, the selfish individual payoff $U^n_{1/\mathrm{X}}(\{m\};\rho)$ depends not only on that SU's sensing capability, but also on other SUs' reactions when a given SU does not cooperate. In this chapter, we employ the *fine* Nash bargaining solution (fNBS) [76], which implies all SUs stand alone if bargaining is not successful, i.e., if the grand coalition breaks down.

Proposition 7. Under the 1/X model, the payoff of each SU $m \in S$ using fNBS is [76]

$$a^{mC}_{f\mathrm{NBS},1/\mathrm{X}} = \frac{1}{|S|}\Big[U^n_{1/\mathrm{X}}(\{S\}) - \sum_{i\in S} U^n_{1/\mathrm{X}}\big(\{i\};\rho_f\big)\Big] + U^n_{1/\mathrm{X}}\big(\{m\};\rho_f\big) = U^n_{1/\mathrm{X}}\big(\{m\};\rho_f\big) \tag{3.25}$$

where $\rho_f = \{\{j\} : j \in S\}$.

Proof. The first equation is from [76], and the second equation follows from Proposition 3, i.e., $U^n_{1/\mathrm{X}}(\{S\}) = \sum_{i\in S} U^n_{1/\mathrm{X}}(\{i\};\rho_f)$. □

Thus, the allocated payoff probability is simply given by the successful transmission probability that each SU could have obtained individually assuming all other SUs have also formed singletons. However, this does not imply that SUs should deviate from the grand coalition, because each SU is not guaranteed a payoff of $a^{mC}_{f\mathrm{NBS},1/\mathrm{X}}$ if it deviates. In fact, if an SU decides to remain isolated, its payoff is at risk due to the nonpositive externalities (Proposition 4) if other SUs collude. As a result, an SU m might end up with a much worse payoff than its singleton value $U^n_{1/\mathrm{X}}(\{m\};p_f)$ in (3.25). Therefore, every SU has an incentive to join the grand coalition. Moreover, we found that a *coarse* Nash bargaining solution (cNBS) [76] allocation where all other SUs form a coalition and try to reduce the hypothetical individual payoff of the deviating SU, results in similar throughput and energy consumption as that of the fNBS method in Proposition 7, as shown in Appendix B.3.

Algorithm 1 Bottom-layer payoff allocation

Input: $C = (S, n)$, $\{\lambda^{mn} : m \in S\}$, $P_{\text{MD}}^{\text{Ch}}$, ν, β^n
Output: $\{a^{mC} : m \in S\}$

1: $P_{\text{FA}}^n(m) = Q\Big(\sqrt{2\lambda^{mn}+1}Q^{-1}((1-P_{\text{MD}}^{\text{Ch}})^{\frac{1}{|S|}}) + \lambda^{mn}\sqrt{\nu}\Big)$
2: **if** 0/X-MAC **then** $\forall m \in S$:
3: $\quad U_{0/\text{X}}^n(S) = \beta^n(1 - \prod_{i\in S} P_{\text{FA}}^n(i))$
4: $\quad U_{0/\text{X}}^n(\{m\}) = \beta^n(1 - P_{\text{FA}}^n(m)) \prod_{i\in S\setminus\{m\}} P_{\text{FA}}^n(i)$
5: $\quad$ Compute $a_{\text{NBS},0/\text{X}}^{mC}$ using (3.24)
6: **if** 1/X-MAC **then** $\forall m \in S$:
7: $\quad a_{\text{NBS},1/\text{X}}^{mC} = U_{1/\text{X}}^n(\eta = \{m\};\, \rho = \{\{j\} : j \in S\})$ as in (3.8)

Figure 3.4: Bottom-layer payoff allocation.

Note that the allocated payoff probabilities (3.24) and (3.25) are *group-rational* [66]:

$$U^n(S) = \sum_{m\in S} a^{mC}. \tag{3.26}$$

Finally, the conditional transmission probability of an SU $m \in S$ given that a spectrum opportunity is detected successfully is set to $a^{mC}/\sum_{i\in S} a^{iC}$ (see example at the end of Section 3.2.2). From (3.26), the successful transmission probability for SU m sensing channel n is a^{mC}, $\forall m \in S$. The bottom-layer payoff allocation algorithm is summarized in Figure 3.4.

3.3.2 Coalition Formation at the Top Layer

The proposed CR network lacks a central entity that collects global SU information, computes all possible top-layer coalition values, and provides an optimized top-layer partition. Thus, the SUs need to organize themselves into different top-layer coalitions in the top-layer game in a distributed manner. SUs use (3.3) to determine if switching to another channel is advantageous. The proposed coalition formation algorithm (Figure 3.5) employs a distributed switching scheduling scheme to facilitate fast convergence to an SU network partition. At most one switch is allowed in each time slot. Initially, all SUs actively compete for the right to switch using an out-of-band control channel [24]. In every time slot, the winning SU m randomly chooses a potential new channel and notifies other SUs in $\mathcal{M}\backslash\{m\}$ about its decision by broadcasting (on the control channel) (i) a SWITCH signal if (3.3) holds, (ii) a HOLD signal if (3.3) fails and it still plans to continue searching, or (iii) a SLEEP signal when all switching opportunities have been exhausted unsuccessfully, i.e., the current channel is the most preferable for this SU. Competition for the right to switch continues until all SUs are asleep, indicating convergence of

Algorithm 2 Distributed top-layer partition formation

Input: $\mathcal{M}, \mathcal{N}, \beta^{\mathcal{N}}, \gamma^{\mathcal{M}\times\mathcal{N}}, \lambda^{\mathcal{M}\times\mathcal{N}}$
Output: $\mathcal{P}$

Initialization: Each SU m randomly senses a channel n_*^m
$C^n(1) = \{m : n_*^m = n\}$ and $C^n(2) = n$, $\forall n \in \mathcal{N}$
$\mathcal{P} = \{C^1, \ldots, C^N\}$ and Action = SWITCH
while $\mathcal{M}_{\text{Active}} \neq \emptyset$ **(at each time slot)**:
  if Action = SWITCH **then**: $\mathcal{M}_{\text{Active}} = \mathcal{M}$
  if Action $\neq$ HOLD **then**:
    SUs in $\mathcal{M}_{\text{Active}}$ contend for the right to switch
    SU $m \in C^n(1)$ wins and $\mathcal{N}_{\text{Candidate}} = \mathcal{N}\backslash\{n\}$
  SU m randomly chooses another channel $\tilde{n} \in \mathcal{N}_{\text{Candidate}}$
  $\tilde{C}^n = (C^n(1)\backslash\{m\}, n)$, $\tilde{C}^{\tilde{n}} = (C^{\tilde{n}}(1) \cup \{m\}, \tilde{n})$
  SU m plays the bottom-layer game $(\tilde{C}^{\tilde{n}}, U^{\tilde{n}})$ in Figure 3.4
  if (3.3) holds **then**:
    $a^{iC^n} = a^{i\tilde{C}^n}$, $a^{jC^{\tilde{n}}} = a^{j\tilde{C}^{\tilde{n}}}$, $\forall i \in C^n(1)$, $j \in C^{\tilde{n}}(1)$
    $\mathcal{P} = \mathcal{P}\backslash\{C^n\}\backslash\{C^{\tilde{n}}\} \cup \{\tilde{C}^n\} \cup \{\tilde{C}^{\tilde{n}}\}$
    $C^n = \tilde{C}^n$, $C^{\tilde{n}} = \tilde{C}^{\tilde{n}}$, Action = SWITCH
  else:
    SU m stays on channel n and $\mathcal{N}_{\text{Candidate}} = \mathcal{N}\backslash\{\tilde{n}\}$
    if $\mathcal{N}_{\text{Candidate}} \neq \emptyset$ **then**: Action = HOLD
    else: $\mathcal{M}_{\text{Active}} = \mathcal{M}\backslash\{m\}$, Action = SLEEP
  if a slot is sensed idle by $C = (S, n)$ **then** $\forall m \in S$:
    SU m transmits with probability $a^{mC}/\sum_{i\in S} a^{iC}$

Figure 3.5: Distributed top-layer partition formation.

the partition formation process. Note that all SUs (including sleeping SUs) should cognitively monitor the environment changes, e.g., variation of the PU-to-SU SNRs, the PU/SU locations, the number of SUs, the number of channels, etc., and repeat the partition formation algorithm in Figure 3.5 when changes occur. Assuming that these parameters are fixed, the following Proposition holds:

Proposition 8. The proposed coalition formation algorithm (Figure 3.5) converges in at most N^M switches.

Proof. When SU m switches from channel n to $\tilde{n}$, only the payoffs of the SUs on these two channels are affected. Thus

$$U(\tilde{\mathcal{P}}) - U(\mathcal{P}) = \sum_{C\in\tilde{\mathcal{P}}} U^{C(2)}(C(1)) - \sum_{C\in\mathcal{P}} U^{C(2)}(C(1))$$

$$
\begin{aligned}
&= U^n(\tilde{C}^n(1)) + U^{\tilde{n}}(\tilde{C}^{\tilde{n}}(1)) - U^n(C^n(1)) - U^{\tilde{n}}(C^{\tilde{n}}(1)) \\
&= \sum_{i \in \tilde{C}^n(1)} a^{i\tilde{C}^n} + \sum_{i \in \tilde{C}^{\tilde{n}}} a^{i\tilde{C}^{\tilde{n}}} - \sum_{i \in C^n(1)} a^{iC^n} - \sum_{i \in C^{\tilde{n}}(1)} a^{iC^{\tilde{n}}} \\
&> 0
\end{aligned} \tag{3.27}
$$

where $\mathcal{P}$ and $\tilde{\mathcal{P}}$ are the current and new top-layer partitions, respectively, and C^n, $C^{\tilde{n}}$, $\tilde{C}^n$ and $\tilde{C}^{\tilde{n}}$ are defined as in (3.3). The third equation of (3.27) follows from the *group rationality* property in (3.26), and the last inequality is from (3.3). Since the total partition value $U(\mathcal{P})$ strictly increases as the coalition formation process evolves, SUs cannot visit the same top-layer coalition in $\Pi(\mathcal{M}, \mathcal{N})$ twice. Moreover, $U(\mathcal{P})$ can take on only a finite number $|\Pi(\mathcal{M}, \mathcal{N})| = N^M$ of values. Thus, the SUs must converge to a top-layer partition $\mathcal{P}^*$ in no more than N^M transitions. Finally, note that the Nash-stable partition $\mathcal{P}^*$ is not unique due to the short-sightedness [77] of the SUs' actions. □

Variation of the number of SUs/PUs and mobility are explored in Section 3.4.

The computational complexity of the proposed game is dominated by the FA rate computations (line 1 in Figure 3.4). For SU m on channel n [cf. (3.14) and (3.16)], this rate is determined by λ^{mn} and SU population size $|C_t^n(1)|$. Each SU m on channel n maintains three values of its FA rate, corresponding to the current and potential SU populations sizes $|C_t^n(1)| \pm i$, $i = 0, 1$, and this information is exchanged over the control channel as needed. Thus, the initialization step requires $3M$ FA rate computations. When an SU explores whether to switch to channel $\tilde{n}$ using (3.3), it needs to compute its potential FA rate on that channel, corresponding to the updated SU population size $|C_t^{\tilde{n}}(1)| + 1$ and its PU-to-SU SNR $\lambda^{m\tilde{n}}$, resulting in one FA computation in each time slot. In those slots where an SU m actually switches to channel $\tilde{n}$, new coalitions $\tilde{C}_t^n$ and $\tilde{C}_t^{\tilde{n}}$ form [cf. (3.3)], and SU m needs to compute two additional FA rates corresponding to the SU population sizes $|\tilde{C}_t^{\tilde{n}}(1)| \pm 1$ while all other SUs in $\tilde{C}_t^n(1)$ and $\tilde{C}_t^{\tilde{n}}(1)$ have to compute only one additional FA rate each, corresponding to SU population sizes decreased and increased by 2 on their respective channels n and $\tilde{n}$. Since each FA rate computation takes $\mathcal{O}(1)$ time, the total computational complexity of the algorithm until convergence is

$$
\mathcal{O}\Big(3M + T_{\text{Converge}} + \sum_{t \in \mathcal{T}_{\text{Switch}}} (|\tilde{C}_t^n(1)| + |\tilde{C}_t^{\tilde{n}}(1)| + 1)\Big) \tag{3.28}
$$

where $\mathcal{O}(\cdot)$ is the big O notation [78], $\mathcal{T}_{\text{Switch}}$ is the set of time slots in which an SU switches in the interval $[1, T_{\text{Converge}}]$ and T_{Converge} denotes the convergence time, i.e., the time needed to execute the while loop from line 4 to 21 in Figure 3.5.

3.4 Simulation Results

We assume the following simulation setup throughout this section unless otherwise noted: The sensing and slot durations are 5 ms and 100 ms, respectively. The SU sensing power P_S, SU transmission power P_{SU}, PU transmission power P_{PU}, and noise power P_N are 10 mW, 10 mW, 100 mW and 0.1 mW, respectively. All users are randomly placed in a square region of 100 m×100 m, and only path loss effects are considered with the pass loss exponent equal to 2 [64]. The PU-to-SU SNR is given by $\lambda^{mn} = P_{\text{PU}} d_{mn}^{-2}/P_N$, where d_{mn} is the distance between PU n and SU m. Similarly, the SU-to-SU SNR between two SUs m and m' is given by $\gamma^{mm'} = P_{\text{SU}} d_{mm'}^{-2}/P_N$, where $d_{mm'}$ is the SU distance.

In Figure 3.6, we compare the proposed game (i,iii) with the game in [64] (ii,iv) for the two MAC models [cf. (3.7) and (3.8)]. Initially there are $M = 10$ SUs and $N = 5$ PUs. At time slots 2000 and 4000, these parameters change to $(M = 10, N = 6)$ and $(M = 14, N = 6)$, respectively. Each PU uses one channel with $B^n = 10$ MHz exclusively. The channel availability probability is $\beta^n = 0.2$. For fair comparison, the AND-rule combining scheme under the constraints described in Section 3.2.3 is used for both the proposed two-layer game and the game in [64] assuming $\nu = 5$ and $P_{\text{MD}}^{\text{Ch}} = 0.01$. Note that [64] aims to maximize the energy efficiency while the objective of the proposed game is to maximize the expected data rate (3.2). Nevertheless, the proposed game achieves better average energy efficiency and throughput in Figure 3.6(a,d), since in this game the SUs' payoffs increase as they sense closer PUs, resulting in improved sensing accuracy. Moreover, each SU is allocated the access opportunities it deserves and thus is provided with sufficient incentives to participate in the proposed game. In particular, as shown in Figure 3.6(b,c), every SU has higher data rate when playing the proposed game than operating alone (i.e., all SUs are satisfied with their data rates). Despite the fact that the proposed game can have a greater number of dissatisfied SUs in terms of energy efficiency than the game in [64] under the 1/X-model [curves iii vs. iv in Figure 3.6(e)], these SUs experience negligible energy efficiency loss [Figure 3.6(f)], and the overall energy efficiency is significantly higher for the two-layer game [Figure 3.6(d)]. We also note that the changes in the numbers of PUs/SUs at time slots 2000 and 4000 do not cause significant disruptions to these games. Finally, while the overall system throughputs and energy consumption in Figure 3.6(a,d) are very similar under both MAC models, individual SUs report a higher degree of satisfaction under the 0/X-model as shown in Figure 3.6(b,c,e,f) since this model has the maximum noncooperation cost (Section 3.2.2).

In Figure 3.7 we validate the superiority of the AND-rule over the OR-rule for heterogeneous environments (see Section 3.2.3) by comparing the average FA rates of the coalitions formed in the proposed game for the realistic scenario of Figure 3.6. Not surprisingly, we observe significant sensing accuracy degradation using the OR-rule, which can be explained by diverse PU-to-SU

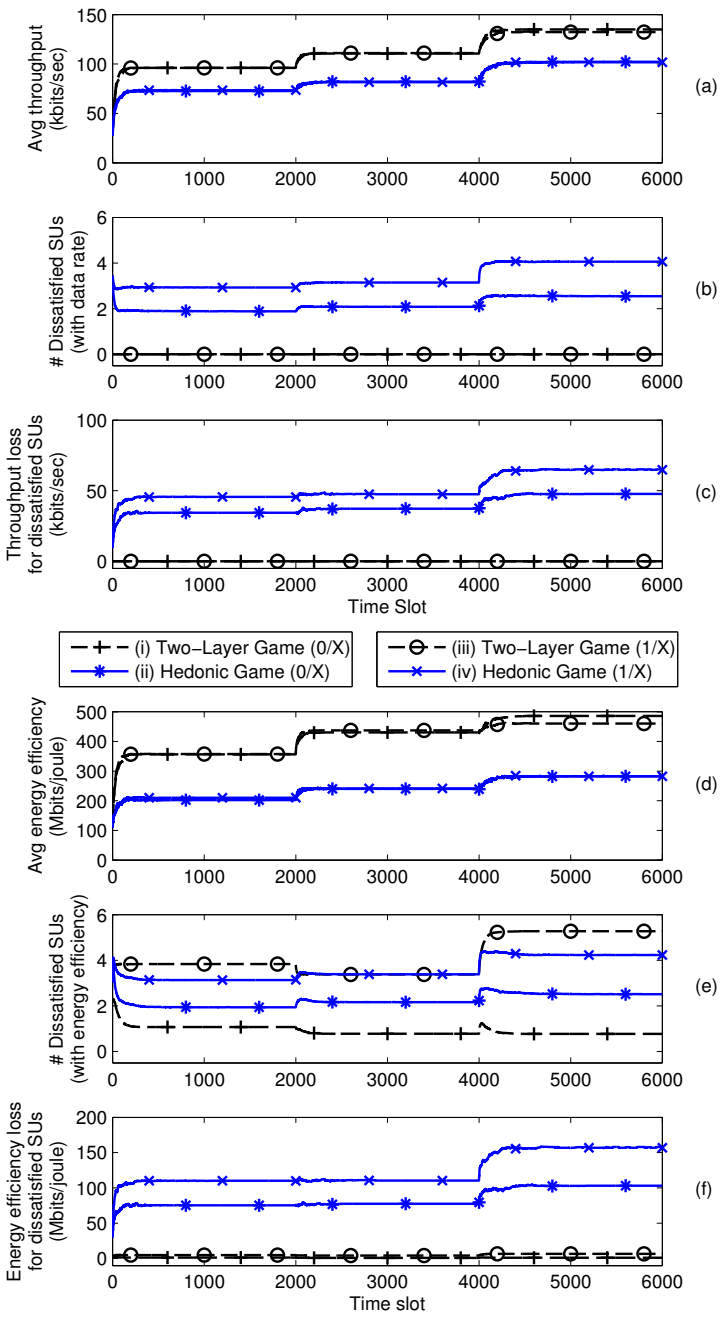

Figure 3.6: Performance comparison of the proposed two-layer game and the hedonic game in [64].

SNRs among the coalition members.

Next, we compare the computational complexity (3.28) and convergence time in Figure 3.8 for varying N values, assuming stable SU/PU population and the 0/X MAC model. Note that

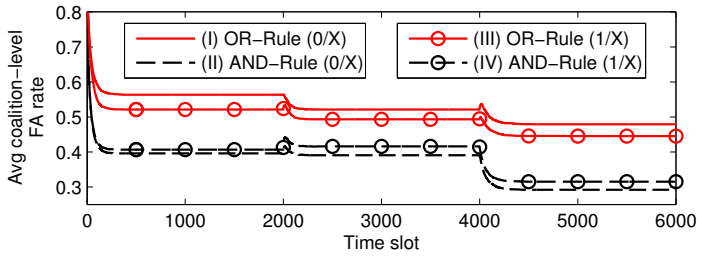

Figure 3.7: Average coalition-level FA rate of the proposed hedonic game.

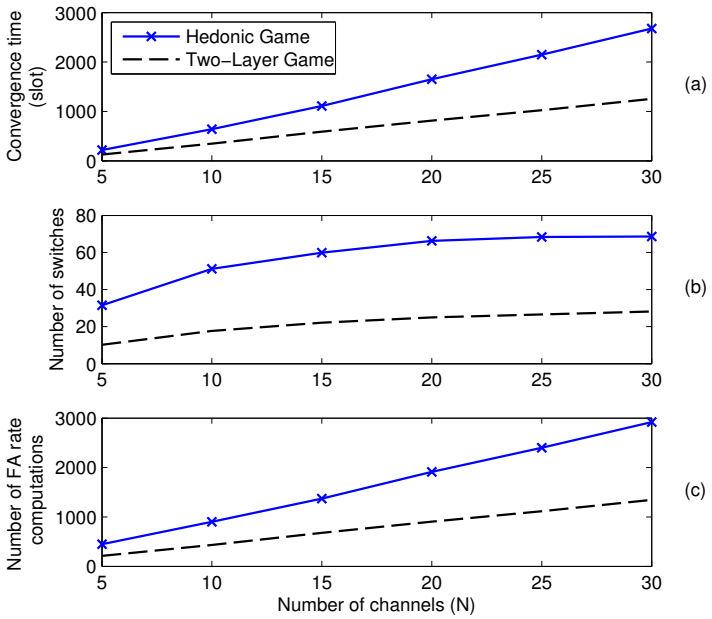

Figure 3.8: Computational complexity vs. N; $M = 10$ SUs; 0/X-model: (a) convergence time T_{Converge} (b) number of switches $|\mathcal{T}_{\text{Switch}}|$ (c) number of FA rate computations (3.28).

when an SU determines whether it should switch to another channel, it needs the knowledge of the updated individual FA rates on the current and new channel for all involved SUs in both the proposed game and the game in [64]. Thus, the complexity analysis in Section 3.3.2 applies to both games. We notice a significant reduction in convergence time and computational complexity when the proposed game is played, due primarily to provision for the social utility improvement in the preference relation (3.3).

Finally, we study the effect of mobility on the performance of the proposed game assuming that the nodes initially achieve a Nash-stable SU network partition. We first consider occasional node position changes in Figure 3.9 assuming each moving SU randomly changes to a different location within the 100 m×100 m square region. As we can see, given that not too many SUs decide to move at the same time, the required reconvergence time and additional computation

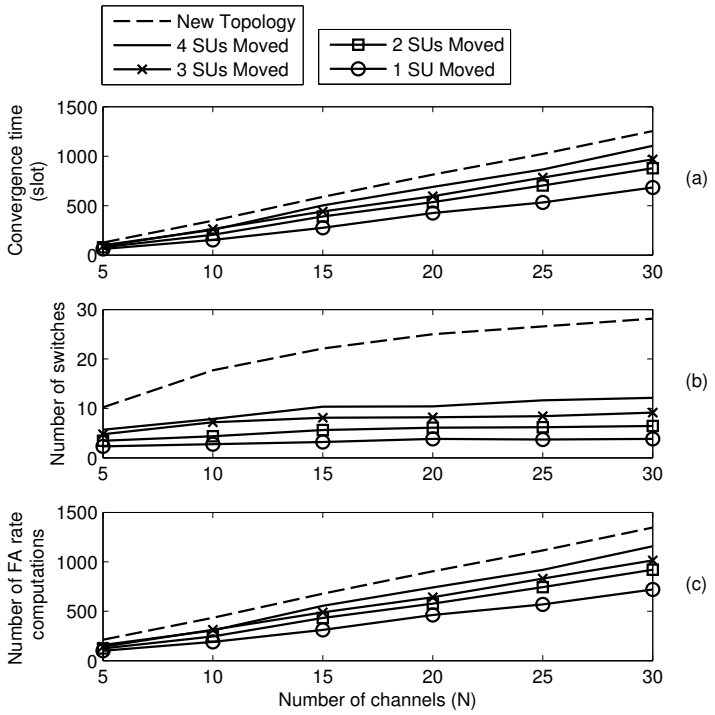

Figure 3.9: Additional computational complexity vs. N; $M = 10$ SUs; 0/X-model: (a) reconvergence time (b) additional number of switches (c) additional number of FA rate computations.

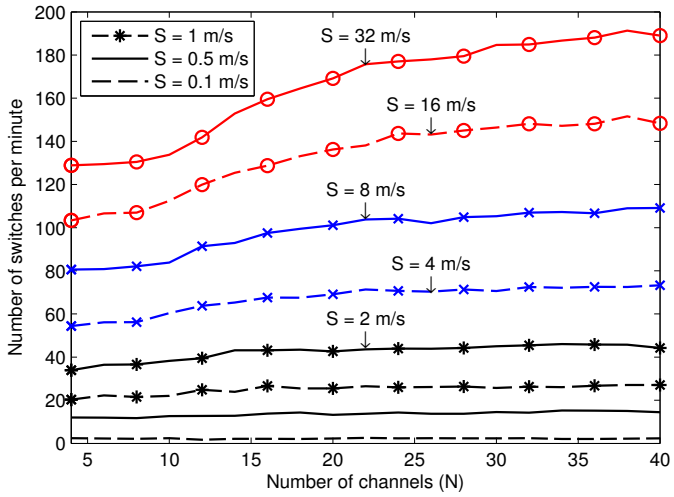

Figure 3.10: Switch frequency vs. number of channels (N) for various traveling speeds (S); $M = 10$ SUs; 0/X-model.

complexity are much smaller than that associated with a completely new topology. Next, assume the SUs continuously move in randomly chosen independent directions at a constant speed S

following the random direction model [79]. When a node reaches the simulation region boundary, it moves in a new randomly chosen direction in the next time slot. Figure 3.10 illustrates the *switch frequency* given by the number of channel switches per minute in the network [58]. We observe that doubling of the mobile speed S results in 10 to 40 additional channel switches per minute. However, for moderate speeds, the switch frequency is insensitive to the numbers of channels in the network. Frequent channel switching increases $|\mathcal{T}_{\text{Switch}}|$ in (3.28) and, thus, results in much larger computational complexity. Moreover, the overhead grows with the mobile speed since the need for message exchange increases. While the proposed game adjusts well to sudden changes in the network settings (see Figure 3.6) and node positions (see Figure 3.9), continuous mobility, as in Figure 3.10, prevents convergence and increases complexity and overhead. To resolve SU competition and provide high throughput in congested mobile CR networks, in Chapter 1–2 we have investigated opportunistic sensing strategies that rely on multichannel diversity by adapting the reward of each SU pair to local CSI prior to sensing.

3.5 Conclusion

The proposed two-layer game provides a comprehensive coalitional game-theoretical framework for cooperative sensing and access in multichannel multi-SU CR networks. Each SU is provided with the transmission opportunities it deserves and, thus, with sufficient incentives to participate in the proposed game. We also present a new cooperative sensing approach under MD constraints for guaranteed PU protection in the heterogeneous environment.

Chapter 4

Single Secondary User with Sequential Sensing Capability

This last chapter is dedicated to the single-SU joint scheduling-and-stopping problem that arises from sequential sensing scenarios. This problem is challenging due to the trade-off between the channel availability and the communication quality when selecting the sensing order, as well as the trade-off between the immediate and the future reward when making stopping decisions. In this chapter, we first develop a reduction approach to simplify the problem. To solve the reduced problem, we employ a fast and accurate greedy algorithm presented in [80]. However, performance and complexity of this algorithm were not investigated in [80]. In this chapter, we strengthen the result in [80] by providing such evidence. Based on this investigation, we propose a near-optimal greedy algorithm, which has the same asymptotic complexity as the greedy approach in [80], and prove a sufficient condition for checking the optimality of an output solution.

4.1 Introduction

In cognitive radio network with slow-varying PU traffic, an SU is able to sense multiple channels before stopping for transmissions. In order to maximize the expected reward, the sensing order and the stopping rule should be designed jointly. In [81], this single-SU joint optimization problem is solved by a combination of the proposed exponential-time dynamic programming (DP) algorithm for finding the optimal sensing order and the optimal stopping rule [82]. To the best of our knowledge, this is the fastest exact algorithm [78] developed to date for solving this problem. While no CSI prior to sensing is assumed in [81], in practice, it is possible to track the CSI and thereby to obtain a priori knowledge of the achievable data rates, as shown in Chapter 1. Under this assumption, an approximation algorithm [78] is proposed in [80]

Table 4.1: Significant Notation in Chapter 4

Notation	Explanation
N	Number of channels.
$\mathcal{N}$	Set of all channels $\{1, \ldots, N\}$.
K	Number of sensing stages $K = \min[\lceil 1/\tau \rceil - 1, N] = N$.
$\underline{\mathbf{s}} = (s_1, s_2, \ldots, s_K)$	Sensing order, which is a permutation of $\mathcal{N}$.
τ	Ratio between the sensing time per channel and the slot duration. Assume $\lceil 1/\tau \rceil - 1 \geq N$.
$c_k = 1 - k\tau$	Remaining time fraction of one time slot after sensing k channels.
θ_n	Availability probability of channel n. Assume $\theta_n \neq 0$, $\forall n$.
R_n	Data rate on channel n. Assume $R_n \neq 0$, $\forall n$.
$\Pi(\mathcal{N})$	Set of all possible permutations of $\mathcal{N}$.
$U_i(s_i, \ldots, s_j)$	Conditional expected reward if the SU proceeds to the ith sensing stage and stops at or before the jth sensing stage, where $i \leq j$.
$U_1(\underline{\mathbf{s}})$	Expected reward (over the stopping decisions) given sensing order $\underline{\mathbf{s}}$.
$\theta^c(\underline{\mathbf{ss}})$	Probability that all channels in subsequence $\underline{\mathbf{ss}}$ are unavailable.
$\mathrm{POS}_{\underline{\mathbf{s}}}(n)$	Position of channel n in the sensing order $\underline{\mathbf{s}}$.
$\mathbb{1}_A$	Indicator function of event A, which is equal to 1 if A occurs and 0 otherwise.

which makes myopic decisions on the next channel to sense by comparing the potentials of remaining channels evaluated at the current position. The work in [80] then uses this simple single-SU algorithm as a subroutine for the proposed multi-SU algorithm without providing an analytical or experimental evaluation for the single-SU setting. Moreover, a simple, yet generally suboptimal, myopic stopping rule is assumed without a justification. In this chapter, we provide this justification and demonstrate superior performance and excellent efficiency of the single-SU greedy search algorithm in [80]. Moreover, we propose a novel two-pass greedy algorithm with improved accuracy at no additional asymptotic complexity cost. To gain a deeper understanding into the reasons for these algorithms' excellent performance, we perform a mathematical analysis that establishes a connection between the potential function and the structure of the optimal solution. Although only the single-SU setting is discussed, we believe the proposed method can serve as an important initial step for designing multi-SU algorithms. Similarly, [12, 13, 80] adapted single-SU algorithms for multi-SU systems.

We note that in the scheduling problem being considered, the SU needs to determine the sensing order under uncertainty on the channel availability. Similar problems have been studied by researchers in the field of operation research and other related fields, e.g., the sequential

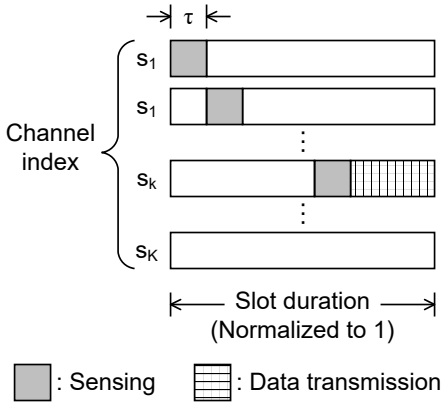

Figure 4.1: Sequential sensing order [81].

scheduling problem [83–85] in which each alternative is associated with a success (or failure) probability, and the traveling agent problem [86] in which each store carries the target item with a certain probability. Our results also yield new insights into solving these problems.

All notation is summarized in Table 4.1, and the rest of this chapter is organized as follows. The system model is introduced in Section 4.2. In Section 4.3, we formulate and reduce the joint stopping rule and sensing order optimization problem. To solve this problem, Section 4.4 introduces several greedy algorithms and presents the running time and space complexity analysis. Finally, analytical and experimental results regarding the ability of the proposed greedy algorithm to find the optimal solution are presented in Section 4.5 and Section 4.6, respectively.

4.2 System Model

Consider a single SU with limited sensing capability seeking for spectrum opportunities by sensing one channel at a time, as illustrated in Figure 4.1. In each time slot, a channel is either busy or idle. These channel availability states can be perfectly revealed through spectrum sensing while the achievable data rates are known a priori (i.e., perfect CSI is assumed). The SU can sense up to $\lceil 1/\tau \rceil - 1$ channels within each time slot, where τ is the ratio between the sensing time and the slot duration. We assume the number of channels N does not exceed the maximum number of sensing stages $\lceil 1/\tau \rceil - 1$, so the actual number of sensing stages is $K = \min[\lceil 1/\tau \rceil - 1, N] = N$. The SU sequentially senses the channels according to a sensing order $\underline{\mathbf{s}} = (s_1, s_2, \ldots, s_K)$ (which is a permutation of the set of all channels $\mathcal{N} = \{1, \ldots, N\}$). Once a channel is sensed idle, the SU may choose to stop probing or proceed to the next channel, but no recall is allowed. In the former case, an effective date rate of $c_k R_{s_k}$ results, where k is the current sensing stage, $c_k = 1 - k\tau$ and R_{s_k} is the data rate on channel s_k. We assume a

block-varying model [1] in which the channel availability probabilities θ_n's and data rates R_n's change from block to block independently with pdfs $f_\theta(x)$ and $f_R(x)$, $\forall n$, where each block consists of one or more slots. The sensing order is determined at the beginning of each block and remains unchanged until the next block.

4.3 Joint Sensing Order and Stopping Rule Optimization: Problem Formulation and Reduction

4.3.1 Optimal Sensing Order with OS

First, when the sensing order $\underline{\mathbf{s}} = (s_1, s_2, \ldots, s_K)$ is fixed, the problem reduces to the classic finite-horizon optimal stopping (OS) problem [82] with the following optimal solution: the SU should stop at the ith stage only if (i) channel s_i is sensed idle and (ii) the data rate achieved by stopping at the ith stage is greater than the expected data rate obtained by proceeding to the next channel. Thus, given that the SU proceeds to the ith sensing stage, the conditional expected reward with OS is

$$U_i^{\mathrm{OS}}(s_i, \ldots, s_K) = \begin{cases} \theta_{s_K} c_K R_{s_K}, & \text{if } i = K \\ \theta_{s_i} \max[c_i R_{s_i}, U_{i+1}^{\mathrm{OS}}(s_{i+1}, \ldots, s_K)] + (1 - \theta_{s_i}) U_{i+1}^{\mathrm{OS}}(s_{i+1}, \ldots, s_K), & \text{otherwise.} \end{cases} \tag{4.1}$$

The expected reward $U_1^{\mathrm{OS}}(\underline{\mathbf{s}})$ can be computed recursively by using (4.1). To improve performance, we can optimize the sensing order [81]:

$$\mathbb{P}1: \quad \underline{\mathbf{s}}^* = \arg \max_{\underline{\mathbf{s}} \in \Pi(\mathcal{N})} U_1^{\mathrm{OS}}(\underline{\mathbf{s}}) \tag{4.2}$$

where $\Pi(\mathcal{N})$ is defined in Table 4.1. Without loss of generality, we assume the optimal sensing order $\underline{\mathbf{s}}^*$ is unique. It is not difficult to extend our analysis to accommodate unusual cases with ties.

4.3.2 Optimal Sensing Order with MS: A Reduction Approach

Next, we introduce the myopic stopping (MS) rule [12, 80] and show reduction of OS to MS in problem $\mathbb{P}1$. In MS, the SU stops at the first sensed available channel and therefore [12]

$$U_1^{\mathrm{MS}}(\underline{\mathbf{s}}) = \sum_{k=1}^{K} \Big[\prod_{l=1}^{k-1} (1 - \theta_{s_l}) \Big] c_k \theta_{s_k} R_{s_k} \tag{4.3}$$

which can also be expressed in a recursive form similar to (4.1):

$$U_i^{\mathrm{MS}}(s_i,\ldots,s_K)=\begin{cases}\theta_{s_K}c_K R_{s_K}, & \text{if } i=K\\ \theta_{s_i}c_i R_{s_i}+(1-\theta_{s_i})U_{i+1}^{\mathrm{MS}}(s_{i+1},\ldots,s_K), & \text{otherwise.}\end{cases} \tag{4.4}$$

We extend the notation $U_i^{\mathrm{MS}}(\cdot)$ for any subsequence $\underline{\mathbf{ss}}=(s_i,\ldots,s_j)$ of $\underline{\mathbf{s}}$ (cf. Table 4.1):

$$U_i^{\mathrm{MS}}(\underline{\mathbf{ss}})=U_i^{\mathrm{MS}}(s_i,\ldots,s_j)\triangleq\sum_{k=i}^{j}\Big[\prod_{l=i}^{k-1}(1-\theta_{s_l})\Big]c_k\theta_{s_k}R_{s_k}. \tag{4.5}$$

For any two partially different sensing orders $\underline{\mathbf{s}}=(\underline{\mathbf{ss}}_1,\underset{\uparrow}{\underline{\mathbf{ss}}_2},\underline{\mathbf{ss}}_3)$ and $\tilde{\underline{\mathbf{s}}}=(\underline{\mathbf{ss}}_1,\underset{\uparrow}{\underline{\widetilde{\mathbf{ss}}}_2},\underline{\mathbf{ss}}_3)$, we have
$\qquad\qquad i\qquad\qquad\qquad\qquad\qquad\qquad\qquad\qquad\qquad i$

$$U_1^{\mathrm{MS}}(\underline{\mathbf{s}})>U_1^{\mathrm{MS}}(\tilde{\underline{\mathbf{s}}})\Leftrightarrow U_i^{\mathrm{MS}}(\underline{\mathbf{ss}}_2)>U_i^{\mathrm{MS}}(\underline{\widetilde{\mathbf{ss}}}_2). \tag{4.6}$$

Proposition 9. OS reduces to MS under the optimal sensing order $\underline{\mathbf{s}}^*$ (4.2), i.e., $U_1^{\mathrm{OS}}(\underline{\mathbf{s}}^*)=U_1^{\mathrm{MS}}(\underline{\mathbf{s}}^*)$.

Proof: The proof is by contradiction. Suppose, given $\underline{\mathbf{s}}^*$, the OS rule (4.1) allows the SU to skip the sensed available channels at some stages, among which stage i is the last skipped stage. Let us split $\underline{\mathbf{s}}^*$ into three parts: $\underline{\mathbf{s}}^*=(\underline{\mathbf{ss}}_1^*,s_i^*,\underline{\mathbf{ss}}_2^*)$ and construct another sensing order $\underline{\mathbf{s}}=(\underline{\mathbf{ss}}_1^*,\underline{\mathbf{ss}}_2^*,s_i^*)$ by moving channel s_i^* to the last position. Due to the optimality of $\underline{\mathbf{s}}^*$, we have

$$U_1^{\mathrm{OS}}(\underline{\mathbf{s}})<U_1^{\mathrm{OS}}(\underline{\mathbf{s}}^*)\Rightarrow U_i^{\mathrm{OS}}(\underline{\mathbf{ss}}_2^*,s_i^*)<U_i^{\mathrm{OS}}(s_i^*,\underline{\mathbf{ss}}_2^*)=U_{i+1}^{\mathrm{OS}}(\underline{\mathbf{ss}}_2^*)=U_{i+1}^{\mathrm{MS}}(\underline{\mathbf{ss}}_2^*) \tag{4.7}$$

where the last two equations are due to the assumption that stage i is the last stage skipped by the OS rule under $\underline{\mathbf{s}}^*$. On the other hand, due to the optimality of the OS rule (4.1), we have

$$U_i^{\mathrm{OS}}(\underline{\mathbf{ss}}_2^*,s_i^*)>U_i^{\mathrm{MS}}(\underline{\mathbf{ss}}_2^*,s_i^*)>U_i^{\mathrm{MS}}(\underline{\mathbf{ss}}_2^*)>U_{i+1}^{\mathrm{MS}}(\underline{\mathbf{ss}}_2^*) \tag{4.8}$$

which contradicts (4.7). □

We emphasize that Proposition 9 is mainly due to perfect CSI knowledge, which helps to resolve the uncertainty regarding the channel quality prior to sensing. Intuitively, when the SU is certain about the amount of reward associated with each transmission opportunity, it would not choose to sense a channel that would later be skipped. This is unlike [81], where the data rate is revealed only after a channel is sensed idle, so the SU may choose to skip a sensed available channel with poor actual communication quality.

Corollary 1. $U_1^{\mathrm{MS}}(\underline{\mathbf{s}}^*) = \max_{\underline{\mathbf{s}}\in\Pi(\mathcal{N})} U_1^{\mathrm{MS}}(\underline{\mathbf{s}})$, where $\underline{\mathbf{s}}^*$ is the optimal sensing order under the OS policy (4.2).

Proof. For any $\underline{\mathbf{s}} \in \Pi(\mathcal{N})$, we have

$$U_1^{\mathrm{MS}}(\underline{\mathbf{s}}^*) = U_1^{\mathrm{OS}}(\underline{\mathbf{s}}^*) > U_1^{\mathrm{OS}}(\underline{\mathbf{s}}) > U_1^{\mathrm{MS}}(\underline{\mathbf{s}}) \tag{4.9}$$

where the first equation is due to Proposition 9, and the two inequalities are due to the optimality of $\underline{\mathbf{s}}^*$ (under OS) and the OS rule (for any fixed sensing order $\underline{\mathbf{s}}$), respectively. □

By Proposition 9 and Corollary 1, problem $\mathbb{P}1$ (4.2) reduces to

$$\mathbb{P}2: \quad \underline{\mathbf{s}}^* = \arg\max_{\underline{\mathbf{s}}\in\Pi(\mathcal{N})} U_1^{\mathrm{MS}}(\underline{\mathbf{s}}). \tag{4.10}$$

Henceforth, we only consider the MS rule and drop the superscript MS in $U_i^{\mathrm{MS}}(\cdot)$. As we can see, the provision of CSI simplifies the stopping rule design and thereby gives rise to the greedy algorithms described next.

4.4 Greedy Algorithms and Complexity Analysis

4.4.1 FG Algorithm

First, we introduce a previously proposed forward-direction greedy (FG) search algorithm [80], which is largely based on the following observation: For any two sensing orders that differ only in two consecutive elements $\underline{\mathbf{s}} = (\underline{\mathbf{ss}}_1, \underset{\substack{\uparrow\\ k}}{n}, \underset{\substack{\uparrow\\ k+1}}{\tilde{n}}, \underline{\mathbf{ss}}_2)$ and $\tilde{\underline{\mathbf{s}}} = (\underline{\mathbf{ss}}_1, \underset{\substack{\uparrow\\ k}}{\tilde{n}}, \underset{\substack{\uparrow\\ k+1}}{n}, \underline{\mathbf{ss}}_2)$ [cf. (4.5)–(4.6)],

$$U_1(\underline{\mathbf{s}}) > U_1(\tilde{\underline{\mathbf{s}}}) \Leftrightarrow U_k(n,\tilde{n}) > U_k(\tilde{n},n) \Leftrightarrow \frac{R_n}{\frac{\tau}{\theta_n}+c_{k+1}} > \frac{R_{\tilde{n}}}{\frac{\tau}{\theta_{\tilde{n}}}+c_{k+1}}. \tag{4.11}$$

The FG algorithm [80], as summarized in Figure 4.2, has K rounds. In the kth round, proper channel assignment for the kth position is determined, and the potential function is defined as

$$g(n,k) \triangleq \frac{R_n}{\frac{\tau}{\theta_n}+c_{k+1}}. \tag{4.12}$$

The remaining channel set $\mathcal{J}$ is updated at the end of each round. The FG algorithm runs in $\mathcal{O}(K)+\mathcal{O}(K-1)+\cdots+\mathcal{O}(1) = \mathcal{O}(K^2)$ time and operates in-place [78], using only $\mathcal{O}(1)$ additional space to store the current best candidate for s_k^{FG} (cf. line 3 in Figure 4.2). Moreover, the FG solution satisfies the following Lemma by construction:

Lemma 1. $\underline{\mathbf{s}}^{\mathrm{FG}} = \underline{\mathbf{s}} = (s_1, s_2, \ldots, s_K)$ if and only if $g(s_i,i) > g(s_j,i)$, $\forall i < j$. □

Algorithm 1 FG algorithm

Output: $\underline{\mathbf{s}}^{\mathrm{FG}} = (s_1^{\mathrm{FG}}, \ldots, s_K^{\mathrm{FG}})$

1: $\mathcal{J} = \mathcal{N}$
2: **for** position $k = 1$ to $K - 1$:
3: $\quad s_k^{\mathrm{FG}} = \arg\max_{n \in \mathcal{J}} g(n, k)$
4: $\quad \mathcal{J} = \mathcal{J} \setminus \{s_k^{\mathrm{FG}}\}$
5: $s_K^{\mathrm{FG}} = \tilde{n}$, where $\tilde{n}$ is the unique element in the singleton set $\mathcal{J}$

Figure 4.2: FG algorithm [80].

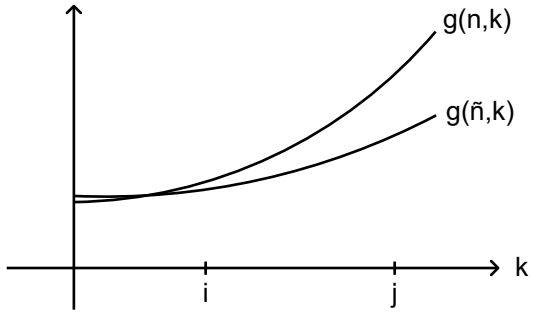

Figure 4.3: Illustration of Lemma 2: a property of the potential function (4.12).

Finally, we show the following property of the potential function (4.12):

Lemma 2. (i) $g(n,i) > g(\tilde{n},i)$ and $g(n,j) > g(\tilde{n},j)$, for some channels $n, \tilde{n}$ and sensing stages $i < j$, if and only if (ii) $g(n,k) > g(\tilde{n},k)$ for all $i \le k \le j$ (see Figure 4.3).

Proof. First, note that (i) is obviously a necessary condition of (ii), because the former is really a special case of the latter evaluated at the end points. Next, we prove that (i) is a sufficient condition of (ii). Suppose (i) is true, which implies [cf. (4.12)]

$$(R_n - R_{\tilde{n}})c_{i+1} > \frac{R_{\tilde{n}}\tau}{\theta_n} - \frac{R_n\tau}{\theta_{\tilde{n}}} \tag{4.13}$$

$$(R_n - R_{\tilde{n}})c_{j+1} > \frac{R_{\tilde{n}}\tau}{\theta_n} - \frac{R_n\tau}{\theta_{\tilde{n}}}. \tag{4.14}$$

Hence, the following inequality holds for any constant $a \in [0,1]$:

$$(R_n - R_{\tilde{n}})[a \cdot c_{i+1} + (1-a) \cdot c_{j+1}] > \frac{R_{\tilde{n}}\tau}{\theta_n} - \frac{R_n\tau}{\theta_{\tilde{n}}}. \tag{4.15}$$

Now, consider any $i \le k \le j$ and let $a = (j-k)/(j-i)$. It is easy to verify that

$$a \cdot c_{i+1} + (1-a) \cdot c_{j+1} = 1 - (k+1)\tau = c_{k+1}. \tag{4.16}$$

Algorithm 2 BG algorithm

Output: $\underline{\mathbf{s}}^{\mathrm{BG}} = (s_1^{\mathrm{BG}}, \ldots, s_K^{\mathrm{BG}})$

1: $\mathcal{J} = \mathcal{N}$
2: **for** position $k = K$ to 2:
3: $\quad s_k^{\mathrm{BG}} = \arg\min_{n \in \mathcal{J}} g(n, k-1)$
4: $\quad \mathcal{J} = \mathcal{J} \setminus \{s_k^{\mathrm{BG}}\}$
5: $s_1^{\mathrm{BG}} = \tilde{n}$, where $\tilde{n}$ is the unique element in the singleton set $\mathcal{J}$

Figure 4.4: BG algorithm.

Algorithm 3 TG algorithm

Output: $\underline{\mathbf{s}}^{\mathrm{TG}}$

1: Run the FG and BG algorithms in Figure 4.2 and Figure 4.4
2: **if** $U_1(\underline{\mathbf{s}}^{\mathrm{FG}}) = U_1(\underline{\mathbf{s}}^{\mathrm{BG}})$ **then**: $\underline{\mathbf{s}}^{\mathrm{TG}} = \underline{\mathbf{s}}^{\mathrm{FG}} = \underline{\mathbf{s}}^*$
3: **else if** $U_1(\underline{\mathbf{s}}^{\mathrm{FG}}) > U_1(\underline{\mathbf{s}}^{\mathrm{BG}})$ **then**: $\underline{\mathbf{s}}^{\mathrm{TG}} = \underline{\mathbf{s}}^{\mathrm{FG}}$
4: **else if** $U_1(\underline{\mathbf{s}}^{\mathrm{FG}}) < U_1(\underline{\mathbf{s}}^{\mathrm{BG}})$ **then**: $\underline{\mathbf{s}}^{\mathrm{TG}} = \underline{\mathbf{s}}^{\mathrm{BG}}$

Figure 4.5: TG algorithm.

Substituting (4.16) into (4.15) and rearranging terms yield

$$\frac{R_n}{\frac{\tau}{\theta_n} + c_{k+1}} > \frac{R_{\tilde{n}}}{\frac{\tau}{\theta_{\tilde{n}}} + c_{k+1}} \Rightarrow g(n,k) > g(\tilde{n},k). \tag{4.17}$$

□

4.4.2 TG Algorithm

In this section, we introduce a novel two-pass greedy (TG) search algorithm by using the FG algorithm as a subroutine in the first pass. For the second pass, we propose a backward-direction greedy (BG) algorithm (Figure 4.4), which is very similar to the FG algorithm (Figure 4.2), except that it runs in the opposite direction and removes the remaining channel with the minimum potential (4.12). The BG algorithm has the same time and space complexity requirements as the FG algorithm and satisfies the following Lemma by construction:

Lemma 3. $\underline{\mathbf{s}}^{\mathrm{BG}} = \underline{\mathbf{s}} = (s_1, s_2, \ldots, s_K)$ if and only if $g(s_i, j-1) > g(s_j, j-1)$, $\forall i < j$. □

Moreover, the following corollary immediately follows from Lemma 1–3:

Corollary 2. $\underline{\mathbf{s}}^{\mathrm{FG}} = \underline{\mathbf{s}}^{\mathrm{BG}} = \underline{\mathbf{s}} = (s_1, s_2, \ldots, s_K)$ if and only if $g(s_i, k) > g(s_j, k)$, $\forall i \leq k \leq j-1$. □

Next, we describe the proposed TG algorithm in Figure 4.5, which simply invokes the FG and BG subroutines and picks the better candidate solution as its output. By doing so, the

error rate is reduced, i.e., $\Pr(\underline{\mathbf{s}}^{\mathrm{TG}} \neq \underline{\mathbf{s}}^*) \leq \min[\Pr(\underline{\mathbf{s}}^{\mathrm{FG}} \neq \underline{\mathbf{s}}^*), \Pr(\underline{\mathbf{s}}^{\mathrm{BG}} \neq \underline{\mathbf{s}}^*)]$. In addition, if the FG and BG solutions match, then it claims that the optimal sensing order has been found. This claim will be proved in Section 4.5.2. Finally, it is easy to see that the TG algorithm maintains the $\mathcal{O}(K^2) = \mathcal{O}(2K^2)$ time complexity and $\mathcal{O}(1) = \mathcal{O}(2)$ space requirement. These are in sharp contrast with the $\mathcal{O}(K \cdot 2^{K-1})$ running time and the $\mathcal{O}(2^K/K)$ average space complexity[1] of the DP-based exact solution in [81].

4.5 Analysis of the Greedy Algorithms

We include in this section several analytical results regarding the ability of the greedy algorithms in Section 4.4 to find the optimal solution. Based on these results, we derive the unusual optimality guarantee when the FG and BG subroutines produce identical solutions as well as an analytical upper bound on the error rate.

4.5.1 Preliminaries

First, we present the supporting lemmas for the main analytical results in Section 4.5.2.

Lemma 4. As illustrated in Figure 4.6, (i) is a necessary and sufficient condition for (ii):

(i) $\mathbb{1}_{G(s_i,s_j;i,j)} = 0, \forall i < j$, where the event $G(s_i, s_j; i, j) \triangleq \{i \leq \mathrm{POS}_{\underline{\mathbf{s}}^*}(s_j) < \mathrm{POS}_{\underline{\mathbf{s}}^*}(s_i) \leq j\}$;

(ii) $\underline{\mathbf{s}}^* = \underline{\mathbf{s}} = (s_1, s_2, \ldots, s_K)$, or equivalently, $\mathrm{POS}_{\underline{\mathbf{s}}^*}(s_k) = k$ for all k.

where $\mathbb{1}_{(\cdot)}$ and $\mathrm{POS}_{\underline{\mathbf{s}}^*}(\cdot)$ are defined in Table 4.1.

Proof. First, we note that (ii) is obviously a sufficient condition of (i), because (ii) implies $\mathrm{POS}_{\underline{\mathbf{s}}^*}(s_i) < \mathrm{POS}_{\underline{\mathbf{s}}^*}(s_j)$, $\forall i < j$. Next, we prove that (i) is a sufficient condition of (ii) by induction on k.

1. **Base case**: we prove $\mathrm{POS}_{\underline{\mathbf{s}}^*}(s_1) = 1$ by contradiction. Suppose $\mathrm{POS}_{\underline{\mathbf{s}}^*}(s_1) = l$, $\exists l > 1$. Then we must have $\mathrm{POS}_{\underline{\mathbf{s}}^*}(s_j) > \mathrm{POS}_{\underline{\mathbf{s}}^*}(s_1)$, $\forall j = l, l+1, \ldots, K$, since otherwise $\mathbb{1}_{G(s_1,s_j;1,j)} = \mathbb{1}_{\{1 \leq \mathrm{POS}_{\underline{\mathbf{s}}^*}(s_j) < \mathrm{POS}_{\underline{\mathbf{s}}^*}(s_1) \leq j\}} = 1$ with $1 < j$, which is not consistent with our assumption that (i) holds true. In other words, we have $K - l + 1$ channels that need to be placed after channel 1 in $\underline{\mathbf{s}}^*$, which leads to a contradiction because channel 1 is located at the lth position and there are only $K - l$ positions following it.
2. **Induction step**: assume $\mathrm{POS}_{\underline{\mathbf{s}}^*}(s_i) = i$, $\forall i \leq k-1$, implying that $\mathrm{POS}_{\underline{\mathbf{s}}^*}(s_k) \geq k$. It is easy to prove that $\mathrm{POS}_{\underline{\mathbf{s}}^*}(s_k) = k$ by mostly the same argument as in the base case. □

[1] The DP solution has K stages, in which the kth stage stores $\binom{K}{K-k}$ state values (cf. [81, Fig. 2]), so it requires $\mathcal{O}\left(\frac{1}{K}\sum_{k=1}^{K}\binom{K}{K-k}\right) = \mathcal{O}(2^K/K)$ space on average.

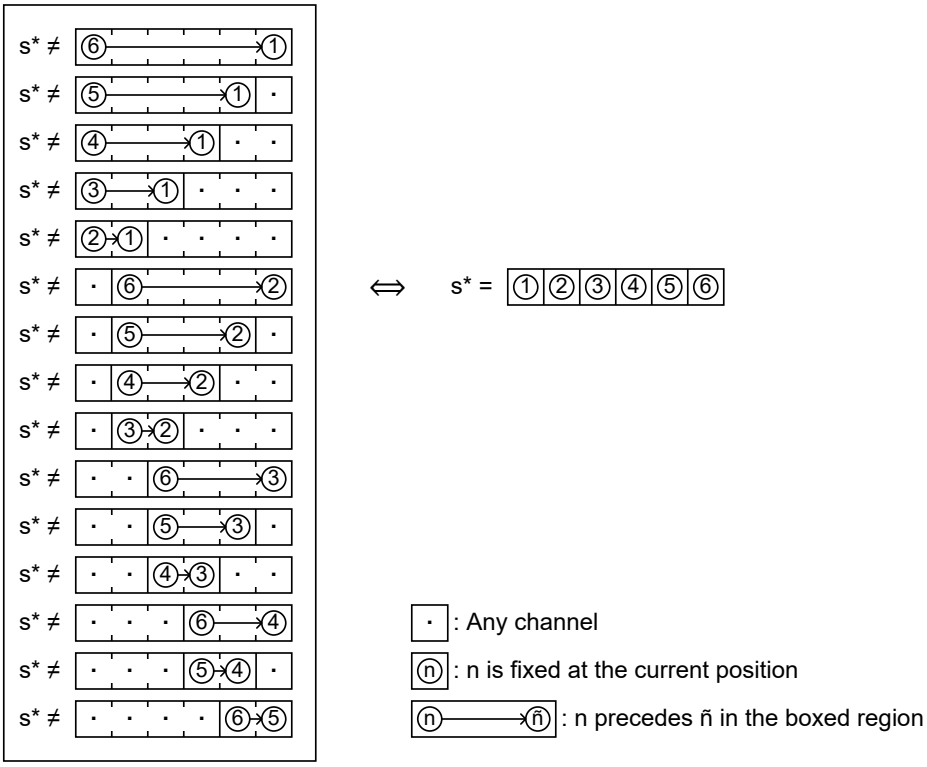

Figure 4.6: Illustration of Lemma 4: a necessary and sufficient condition for optimality; $K = 6$.

Lemma 5. If channel $\tilde{n}$ precedes channel n in the optimal sensing order $\underline{\mathbf{s}}^*$, that is, if

$$\underline{\mathbf{s}}^* = \underline{\mathbf{s}} = (\underline{\mathbf{ss}}_1, \underset{\uparrow}{\tilde{n}}, \underline{\mathbf{ss}}_2, \underset{\uparrow}{n}, \underline{\mathbf{ss}}_3) \tag{4.18}$$
$$\qquad\qquad\quad i \qquad\qquad\quad j$$

$\exists$ stages $i < j$, and subsequences $\underline{\mathbf{ss}}_1$, $\underline{\mathbf{ss}}_2 = (s_{i+1}, \ldots, s_{j-1})$, $\underline{\mathbf{ss}}_3$, then the following inequalities must hold:

$$[c_i - \theta^c(\underline{\mathbf{ss}}_2)c_{j-1}]\theta_{\tilde{n}} R_{\tilde{n}} > \sum_{k=i+1}^{j-1} \Big[\prod_{l=i}^{k-1}(1-\theta_{s_l})\Big](\tau + \theta_{\tilde{n}} c_k)\theta_{s_k} R_{s_k} \tag{4.19}$$

$$\sum_{k=i+1}^{j-1} \Big[\prod_{l=i}^{k-1}(1-\theta_{s_l})\Big](\tau + \theta_n c_{k+1})\theta_{s_k} R_{s_k} > [c_{i+1} - \theta^c(\underline{\mathbf{ss}}_2)c_j]\theta_n R_n \tag{4.20}$$

$$(\theta_n - \theta_{\tilde{n}}) \sum_{k=i+1}^{j-1} \prod_{l=i}^{k-1}(1-\theta_{s_l}) c_k \theta_{s_k} R_{s_k} > [c_i - \theta^c(\underline{\mathbf{ss}}_2)c_j](\theta_n R_n - \theta_{\tilde{n}} R_{\tilde{n}}) + \theta^c(\underline{\mathbf{ss}}_2)c_j \theta_n \theta_{\tilde{n}}(R_n - R_{\tilde{n}}). \tag{4.21}$$

Proof. Since $\underline{\mathbf{s}}^* = \underline{\mathbf{s}}$, we must have [cf. (4.6)]

$$U_1(\underline{\mathbf{s}}) > U_1(\underline{\mathbf{ss}}_1, \underline{\mathbf{ss}}_2, \tilde{n}, n, \underline{\mathbf{ss}}_3) \Rightarrow U_i(\tilde{n}, \underline{\mathbf{ss}}_2, n) > U_i(\underline{\mathbf{ss}}_2, \tilde{n}, n) \tag{4.22}$$

$$U_1(\underline{\mathbf{s}}) > U_1(\underline{\mathbf{ss}}_1, \tilde{n}, n, \underline{\mathbf{ss}}_2, \underline{\mathbf{ss}}_3) \Rightarrow U_i(\tilde{n}, \underline{\mathbf{ss}}_2, n) > U_i(\tilde{n}, n, \underline{\mathbf{ss}}_2) \tag{4.23}$$

$$U_1(\underline{\mathbf{s}}) > U_1(\underline{\mathbf{ss}}_1, n, \underline{\mathbf{ss}}_2, \tilde{n}, \underline{\mathbf{ss}}_3) \Rightarrow U_i(\tilde{n}, \underline{\mathbf{ss}}_2, n) > U_i(n, \underline{\mathbf{ss}}_2, \tilde{n}) \tag{4.24}$$

where [cf. (4.5) and Table 4.1]

$$U_i(\tilde{n}, \underline{\mathbf{ss}}_2, n) = c_i\theta_{\tilde{n}}R_{\tilde{n}} + (1-\theta_{\tilde{n}})U_{i+1}(\underline{\mathbf{ss}}_2) + (1-\theta_{\tilde{n}})\theta^c(\underline{\mathbf{ss}}_2)c_j\theta_n R_n \tag{4.25}$$

$$U_i(\underline{\mathbf{ss}}_2, \tilde{n}, n) = U_i(\underline{\mathbf{ss}}_2) + \theta^c(\underline{\mathbf{ss}}_2)c_{j-1}\theta_{\tilde{n}}R_{\tilde{n}} + \theta^c(\underline{\mathbf{ss}}_2)(1-\theta_{\tilde{n}})c_j\theta_n R_n \tag{4.26}$$

$$U_i(\tilde{n}, n, \underline{\mathbf{ss}}_2) = c_i\theta_{\tilde{n}}R_{\tilde{n}} + (1-\theta_{\tilde{n}})c_{i+1}\theta_n R_n + (1-\theta_{\tilde{n}})(1-\theta_n)U_{i+2}(\underline{\mathbf{ss}}_2) \tag{4.27}$$

$$U_i(n, \underline{\mathbf{ss}}_2, \tilde{n}) = c_i\theta_n R_n + (1-\theta_n)U_{i+1}(\underline{\mathbf{ss}}_2) + (1-\theta_n)\theta^c(\underline{\mathbf{ss}}_2)c_j\theta_{\tilde{n}}R_{\tilde{n}} \tag{4.28}$$

with $(\Delta = -1, 0, 1)$

$$U_{i+1+\Delta}(\underline{\mathbf{ss}}_2) = \sum_{k=i+1}^{j-1} \Big[\prod_{l=i}^{k-1}(1-\theta_{s_l})\Big] c_{k+\Delta}\theta_{s_k}R_{s_k}. \tag{4.29}$$

Substituting (4.25)–(4.29) into (4.22)–(4.24) and simplifying, we obtain (4.19)–(4.21). □

Lemma 6. If $\theta_n > \theta_{\tilde{n}}$, $R_n < R_{\tilde{n}}$, $\theta_n R_n > \theta_{\tilde{n}}R_{\tilde{n}}$ and $g(n,i) > g(\tilde{n},i)$, then the event $E(n,\tilde{n};i) \triangleq \{i = \mathrm{POS}_{\underline{\mathbf{s}}^*}(\tilde{n}) < \mathrm{POS}_{\underline{\mathbf{s}}^*}(n)\}$ must be false.

Proof: We argue by contradiction. Suppose $\mathrm{POS}_{\underline{\mathbf{s}}^*}(\tilde{n}) = i$ and $\mathrm{POS}_{\underline{\mathbf{s}}^*}(n) = j$, $\exists j > i$, that is, suppose $\underline{\mathbf{s}}^* = \underline{\mathbf{s}} = (\underline{\mathbf{ss}}_1, \underset{\uparrow}{\tilde{n}}_{i}, \underline{\mathbf{ss}}_2, \underset{\uparrow}{n}_{j}, \underline{\mathbf{ss}}_3)$ as in (4.18). Then, according to Lemma 5, (4.19)–(4.21) must hold. Since $g(n,i) > g(\tilde{n},i)$, we immediately have [cf. (4.12)]

$$\tau(\theta_n R_n - \theta_{\tilde{n}}R_{\tilde{n}}) > c_{i+1}\theta_n\theta_{\tilde{n}}(R_{\tilde{n}} - R_n) \tag{4.30}$$

$$(\tau + \theta_{\tilde{n}}c_{i+1})(\theta_n R_n - \theta_{\tilde{n}}R_{\tilde{n}}) > (\theta_n - \theta_{\tilde{n}})c_{i+1}\theta_{\tilde{n}}R_{\tilde{n}}. \tag{4.31}$$

Note that $\forall k > i+1$,

$$c_k < c_{i+1} \Rightarrow \frac{\tau + \theta_{\tilde{n}}c_k}{c_k} > \frac{\tau + \theta_{\tilde{n}}c_{i+1}}{c_{i+1}}. \tag{4.32}$$

Thus, we have

$$(\theta_n - \theta_{\tilde{n}}) \sum_{k=i+1}^{j-1} \Big[\prod_{l=i}^{k-1}(1-\theta_{s_l})\Big] c_k\theta_{s_k}R_{s_k}$$

$$
\begin{aligned}
&\overset{(4.31)}{<} \frac{\overbrace{\theta_n R_n - \theta_{\tilde{n}} R_{\tilde{n}}}^{>0}}{\theta_{\tilde{n}} R_{\tilde{n}}} \frac{\tau + \theta_{\tilde{n}} c_{i+1}}{c_{i+1}} \sum_{k=i+1}^{j-1} \Big[\prod_{l=i}^{k-1} (1-\theta_{s_l}) \Big] c_k \theta_{s_k} R_{s_k} \\
&\overset{(4.32)}{<} \frac{\theta_n R_n - \theta_{\tilde{n}} R_{\tilde{n}}}{\theta_{\tilde{n}} R_{\tilde{n}}} \sum_{k=i+1}^{j-1} \Big[\prod_{l=i}^{k-1} (1-\theta_{s_l}) \Big] (\tau + \theta_{\tilde{n}} c_k) \theta_{s_k} R_{s_k} \\
&\overset{(4.19)}{<} [c_i - \theta^c(\underline{\mathbf{ss}}_2) c_{j-1}] (\theta_n R_n - \theta_{\tilde{n}} R_{\tilde{n}}) \\
&= [c_i - \theta^c(\underline{\mathbf{ss}}_2) c_j] (\theta_n R_n - \theta_{\tilde{n}} R_{\tilde{n}}) - \theta^c(\underline{\mathbf{ss}}_2) \tau (\theta_n R_n - \theta_{\tilde{n}} R_{\tilde{n}}) \\
&\overset{(4.30)}{<} [c_i - \theta^c(\underline{\mathbf{ss}}_2) c_j] (\theta_n R_n - \theta_{\tilde{n}} R_{\tilde{n}}) - \theta^c(\underline{\mathbf{ss}}_2) c_{i+1} \theta_n \theta_{\tilde{n}} (\overbrace{R_{\tilde{n}} - R_n}^{>0}) \\
&\leq [c_i - \theta^c(\underline{\mathbf{ss}}_2) c_j] (\theta_n R_n - \theta_{\tilde{n}} R_{\tilde{n}}) - \theta^c(\underline{\mathbf{ss}}_2) c_j \theta_n \theta_{\tilde{n}} (R_{\tilde{n}} - R_n) \qquad (4.33)
\end{aligned}
$$

which contradicts (4.21). □

Lemma 7. If $\theta_n < \theta_{\tilde{n}}$, $R_n > R_{\tilde{n}}$, $\theta_n R_n < \theta_{\tilde{n}} R_{\tilde{n}}$ and $g(n, j-1) > g(\tilde{n}, j-1)$, then the event $F(n, \tilde{n}; j) \triangleq \{\mathrm{POS}_{\underline{\mathbf{s}}^*}(\tilde{n}) < \mathrm{POS}_{\underline{\mathbf{s}}^*}(n) = j\}$ must be false.

Proof: We prove by contraction. Suppose $\mathrm{POS}_{\underline{\mathbf{s}}^*}(\tilde{n}) = i$ and $\mathrm{POS}_{\underline{\mathbf{s}}^*}(n) = j$, $\exists i < j$, that is, suppose $\underline{\mathbf{s}}^* = \underline{\mathbf{s}} = (\underline{\mathbf{ss}}_1, \underset{\uparrow}{\tilde{n}}_{i}, \underline{\mathbf{ss}}_2, \underset{\uparrow}{n}_{j}, \underline{\mathbf{ss}}_3)$ as in (4.18). According to Lemma 5, (4.19)–(4.21) must hold. Since $g(n, j-1) > g(\tilde{n}, j-1)$, we immediately have [cf. (4.12)]

$$
\mathbf{A} \triangleq (\tau + \theta_{\tilde{n}} c_j) \theta_n R_n - (\tau + \theta_n c_j) \theta_{\tilde{n}} R_{\tilde{n}} > 0 \qquad (4.34)
$$

$$
(\tau + \theta_n c_j)(\theta_n R_n - \theta_{\tilde{n}} R_{\tilde{n}}) > (\theta_n - \theta_{\tilde{n}}) c_j \theta_n R_n. \qquad (4.35)
$$

Note that $\forall k < j$,

$$
c_k > c_j \Rightarrow \frac{\tau + \theta_n c_k}{c_k} < \frac{\tau + \theta_n c_j}{c_j}. \qquad (4.36)
$$

Now, multiplying both sides of (4.20) by $(\theta_n R_n - \theta_{\tilde{n}} R_{\tilde{n}})/(\theta_n R_n)$, we get

$$
\begin{aligned}
[c_{i+1} - \theta^c(\underline{\mathbf{ss}}_2) c_j] (\underbrace{\theta_n R_n - \theta_{\tilde{n}} R_{\tilde{n}}}_{<0}) &> \frac{\theta_n R_n - \theta_{\tilde{n}} R_{\tilde{n}}}{\theta_n R_n} \sum_{k=i+1}^{j-1} \Big[\prod_{l=i}^{k-1} (1-\theta_{s_l}) \Big] (\tau + \theta_n c_{k+1}) \theta_{s_k} R_{s_k} \\
&\overset{(4.36)}{>} \frac{\theta_n R_n - \theta_{\tilde{n}} R_{\tilde{n}}}{\theta_n R_n} \frac{\tau + \theta_n c_j}{c_j} \sum_{k=i+1}^{j-1} \Big[\prod_{l=i}^{k-1} (1-\theta_{s_l}) \Big] c_{k+1} \theta_{s_k} R_{s_k} \\
&\overset{(4.35)}{>} (\theta_n - \theta_{\tilde{n}}) \sum_{k=i+1}^{j-1} \Big[\prod_{l=i}^{k-1} (1-\theta_{s_l}) \Big] c_{k+1} \theta_{s_k} R_{s_k}. \qquad (4.37)
\end{aligned}
$$

Thus, we have

$$
\begin{aligned}
&(\theta_n-\theta_{\tilde{n}})\sum_{k=i+1}^{j-1}\Big[\prod_{l=i}^{k-1}(1-\theta_{s_l})\Big]c_k\theta_{s_k}R_{s_k}\\
&=(\overbrace{\theta_n-\theta_{\tilde{n}}}^{<0})\sum_{k=i+1}^{j-1}\Big[\prod_{l=i}^{k-1}(1-\theta_{s_l})\Big](\tau+\theta_n c_{k+1})\theta_{s_k}R_{s_k}\\
&\quad+(\theta_n-\theta_{\tilde{n}})\sum_{k=i+1}^{j-1}\Big[\prod_{l=i}^{k-1}(1-\theta_{s_l})\Big](1-\theta_n)c_{k+1}\theta_{s_k}R_{s_k}\\
&<(\theta_n-\theta_{\tilde{n}})[c_{i+1}-\theta^c(\underline{\mathbf{ss}}_2)c_j]\theta_nR_n+(1-\theta_n)[c_{i+1}-\theta^c(\underline{\mathbf{ss}}_2)c_j](\theta_nR_n-\theta_{\tilde{n}}R_{\tilde{n}})\\
&=[c_i-\theta^c(\underline{\mathbf{ss}}_2)c_j](\theta_nR_n-\theta_{\tilde{n}}R_{\tilde{n}})+\theta^c(\underline{\mathbf{ss}}_2)c_j\theta_n\theta_{\tilde{n}}(R_n-R_{\tilde{n}})-\mathbf{A}-(\overbrace{j-i-1}^{\geq 0})\tau\theta_n\theta_{\tilde{n}}(\overbrace{R_n-R_{\tilde{n}}}^{>0})\\
&<[c_i-\theta^c(\underline{\mathbf{ss}}_2)c_j](\theta_nR_n-\theta_{\tilde{n}}R_{\tilde{n}})+\theta^c(\underline{\mathbf{ss}}_2)c_j\theta_n\theta_{\tilde{n}}(R_n-R_{\tilde{n}}) \qquad (4.38)
\end{aligned}
$$

which contradicts (4.21), where the first inequality is from (4.20) and (4.37), and $\mathbf{A}>0$ as defined in (4.34). □

Lemma 8. If $R_n > R_{\tilde{n}}$ and $\theta_nR_n > \theta_{\tilde{n}}R_{\tilde{n}}$, then channel n must precede channel $\tilde{n}$ in the optimal sensing order $\underline{\mathbf{s}}^*$, i.e., $\mathrm{POS}_{\underline{\mathbf{s}}^*}(n) < \mathrm{POS}_{\underline{\mathbf{s}}^*}(\tilde{n})$.

Proof: We prove by contraction. Suppose $\tilde{n}$ precedes n in $\underline{\mathbf{s}}^*$, that is, suppose $\underline{\mathbf{s}}^* = \underline{\mathbf{s}} = (\underline{\mathbf{ss}}_1, \underset{\uparrow}{\tilde{n}}_{i}, \underline{\mathbf{ss}}_2, \underset{\uparrow}{n}_{j}, \underline{\mathbf{ss}}_3)$ for some $i<j$ as in (4.18). According to Lemma 5, (4.19)–(4.21) must hold. Next, we discuss two cases.

1. $\theta_n < \theta_{\tilde{n}}$. The left-hand and right-hand sides of (4.21) are negative and positive, respectively, which means the inequality (4.21) cannot hold. This is the desired contradiction.
2. $\theta_n > \theta_{\tilde{n}}$. The following inequalities follow from (4.19) and (4.21):

$$
[c_i-\theta^c(\underline{\mathbf{ss}}_2)c_j]\theta_{\tilde{n}}R_{\tilde{n}} > \sum_{k=i+1}^{j-1}\Big[\prod_{l=i}^{k-1}(1-\theta_{s_l})\Big]\theta_{\tilde{n}}c_k\theta_{s_k}R_{s_k} \qquad (4.39)
$$

$$
(\theta_n-\theta_{\tilde{n}})\sum_{k=i+1}^{j-1}\Big[\prod_{l=i}^{k-1}(1-\theta_{s_l})\Big]c_k\theta_{s_k}R_{s_k} > [c_i-\theta^c(\underline{\mathbf{ss}}_2)c_j](\theta_n-\theta_{\tilde{n}})R_{\tilde{n}}. \qquad (4.40)
$$

Dividing (4.39) and (4.40) by $\theta_{\tilde{n}}$ and $(\theta_n-\theta_{\tilde{n}})$, respectively, we immediately get a contradiction. □

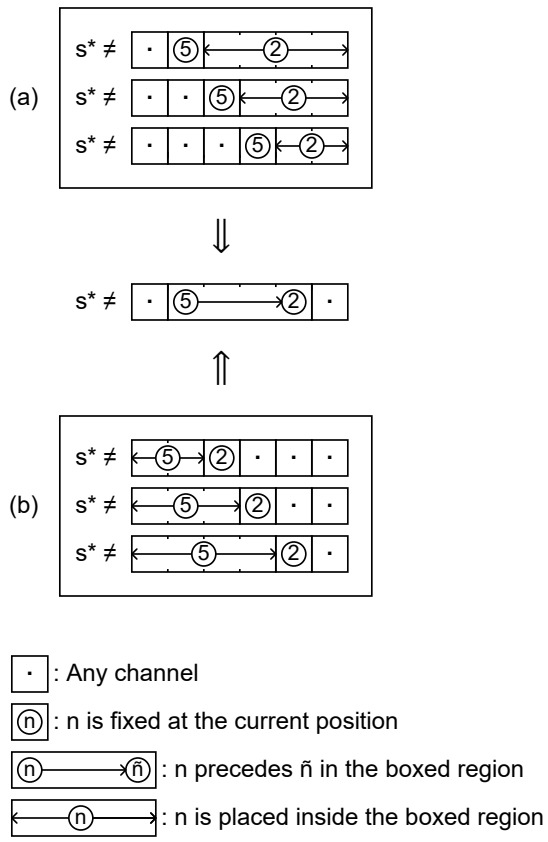

Figure 4.7: An illustrative example for Proposition 10 proof: If (a) $E(2,5,k)$ is false, $\forall 2 \leq k \leq 4$ (**Case 3**), or (b) $F(2,5,k)$ is false, $\forall 3 \leq k \leq 5$ (**Case 4**), then $G(2,5;2,5)$ is false; $K = 6$.

4.5.2 Main Results

Our main analytical results are stated below.

Proposition 10. If the FG and the BG solutions match, then this solution is optimal. That is, if $\underline{\mathbf{s}}^{\mathrm{FG}} = \underline{\mathbf{s}}^{\mathrm{BG}} = \underline{\mathbf{s}} = (s_1, s_2, \ldots, s_K)$, then $\underline{\mathbf{s}}^* = \underline{\mathbf{s}}$.

Proof. We prove the the optimality of $\underline{\mathbf{s}}$ by showing $\mathbb{1}_{G(s_i,s_j;i,j)} = 0$, $\forall i < j$, where the event $G(s_i, s_j; i, j) = \{i \leq \mathrm{POS}_{\underline{\mathbf{s}}^*}(s_j) < \mathrm{POS}_{\underline{\mathbf{s}}^*}(s_i) \leq j\}$ (cf. Lemma 4). First, from Corollary 2, we have $g(s_i, k) > g(s_j, k)$, $\forall i \leq k \leq j-1$, which are covered by the following four cases [cf. (4.12)]:

1. **Case 1**: $\theta_{s_i} > \theta_{s_j}, R_{s_i} > R_{s_j}, \theta_{s_i} R_{s_i} > \theta_{s_j} R_{s_j}$ and **Case 2:** $\theta_{s_i} < \theta_{s_j}, R_{s_i} > R_{s_j}, \theta_{s_i} R_{s_i} > \theta_{s_j} R_{s_j}$. In these two cases, we immediately have $\mathrm{POS}_{\underline{\mathbf{s}}^*}(s_i) < \mathrm{POS}_{\underline{\mathbf{s}}^*}(s_j)$ by applying Lemma 8 and therefore exclude the possibility of the event $G(s_i, s_j; i, j)$.
2. **Case 3**: $\theta_{s_i} > \theta_{s_j}, R_{s_i} < R_{s_j}, \theta_{s_i} R_{s_i} > \theta_{s_j} R_{s_j}$. By Lemma 6, we have $\mathbb{1}_{E(s_i,s_j;k)} = 0$, $\forall i \leq k \leq j-1$, or equivalently $\bigcap_{k=i}^{j-1} \mathbb{1}_{\{k=\mathrm{POS}_{\underline{\mathbf{s}}^*}(s_j) < \mathrm{POS}_{\underline{\mathbf{s}}^*}(s_i)\}} = 0$. As a consequence, $\mathbb{1}_{G(s_i,s_j;i,j)} = \bigcap_{k=i}^{j-1} \mathbb{1}_{\{k=\mathrm{POS}_{\underline{\mathbf{s}}^*}(s_j) < \mathrm{POS}_{\underline{\mathbf{s}}^*}(s_i) \leq j\}}$ must also be zero [see Figure 4.7(a)].

3. **Case 4**: $\theta_{s_i} < \theta_{s_j}, R_{s_i} > R_{s_j}, \theta_{s_i} R_{s_i} < \theta_{s_j} R_{s_j}$. By Lemma 7, we have $\mathbb{1}_{F(s_i,s_j;k)} = 0$, $\forall i+1 \leq k \leq j$, or equivalently $\bigcap_{k=i+1}^{j} \mathbb{1}_{\{\mathrm{POS}_{\underline{\mathbf{s}}^*}(s_j) < \mathrm{POS}_{\underline{\mathbf{s}}^*}(s_i) = k\}} = 0$. As a consequence, $\mathbb{1}_{G(s_i,s_j;i,j)} = \bigcap_{k=i+1}^{j} \mathbb{1}_{\{i \leq \mathrm{POS}_{\underline{\mathbf{s}}^*}(s_j) < \mathrm{POS}_{\underline{\mathbf{s}}^*}(s_i) \leq k\}}$ must also be zero [see Figure 4.7(b)].

To conclude, in all cases, if $g(s_i,k) > g(s_j,k)$, $\forall i \leq k \leq j-1$, then $G(s_i,s_j;i,j)$ is false. Since this statement holds for all $i < j$, we have established the necessary and sufficient condition for $\underline{\mathbf{s}}^* = \underline{\mathbf{s}}$ in Lemma 4. □

Proposition 10 provides a strategy for verifying the correctness of an output solution, and the probability of finding such verifiable optimal solutions is $\Pr(\underline{\mathbf{s}}^{\mathrm{FG}} = \underline{\mathbf{s}}^{\mathrm{BG}})$. Conversely, not all optimal output solutions are verifiable, which leads us to the next proposition.

Proposition 11. Assuming i.i.d. inputs (θ_n's and R_n's), the error rate of the proposed TG algorithm (Figure 4.5) is upper bounded by

$$\begin{aligned}
\Pr(\underline{\mathbf{s}}^{\mathrm{TG}} \neq \underline{\mathbf{s}}^*) &\leq \Pr(\underline{\mathbf{s}}^{\mathrm{FG}} \neq \underline{\mathbf{s}}^{\mathrm{BG}}) \\
&= 1 - \sum_{\underline{\mathbf{s}} \in \Pi(\mathcal{N})} \Pr(\underline{\mathbf{s}}^{\mathrm{FG}} = \underline{\mathbf{s}}^{\mathrm{BG}} = \underline{\mathbf{s}}) \\
&= 1 - |\Pi(\mathcal{N})| \cdot \Pr\left(\underline{\mathbf{s}}^{\mathrm{FG}} = \underline{\mathbf{s}}^{\mathrm{BG}} = (1, \ldots, N)\right) \\
&= 1 - N! \cdot \Pr\Big(\bigcap_{i=1}^{K} \bigcap_{j=i+1}^{K} \bigcap_{k=i}^{j-1} \mathbb{1}_{g(i,k) > g(j,k)}\Big). \qquad (4.41)
\end{aligned}$$

Proof. The first inequality is due to Proposition 10, the second equation is due to the i.i.d. input assumption as well as the symmetric nature of the TG algorithm, and the last equation is from Corollary 2. □

Note that the upper bound (4.41) also applies to $\Pr(\underline{\mathbf{s}}^{\mathrm{FG}} \neq \underline{\mathbf{s}}^*)$ and $\Pr(\underline{\mathbf{s}}^{\mathrm{BG}} \neq \underline{\mathbf{s}}^*)$ (cf. the end of Section 4.4.2) and it can be evaluated numerically based on the distributions of θ_n's and R_n's, before running the TG algorithm. Unfortunately, we were not able to simplify further and express it in closed-form. In the next section, we will take empirical measurements to validate the upper bound (4.41).

4.6 Simulation Results

We consider problem sizes K no less than 4 because otherwise even an exhaustive search for the optimal sensing order can be accomplished in a timely manner, or equivalently, we consider $\tau < 0.25$ and $N \geq 4$ (cf. Table 4.1). Yet the N value does not exceed 20, because otherwise finding the optimal solution using the DP approach [81] (which is the fastest known exact algorithm) becomes computationally intractable (cf. the end of Section 4.4.2). Assuming i.i.d.

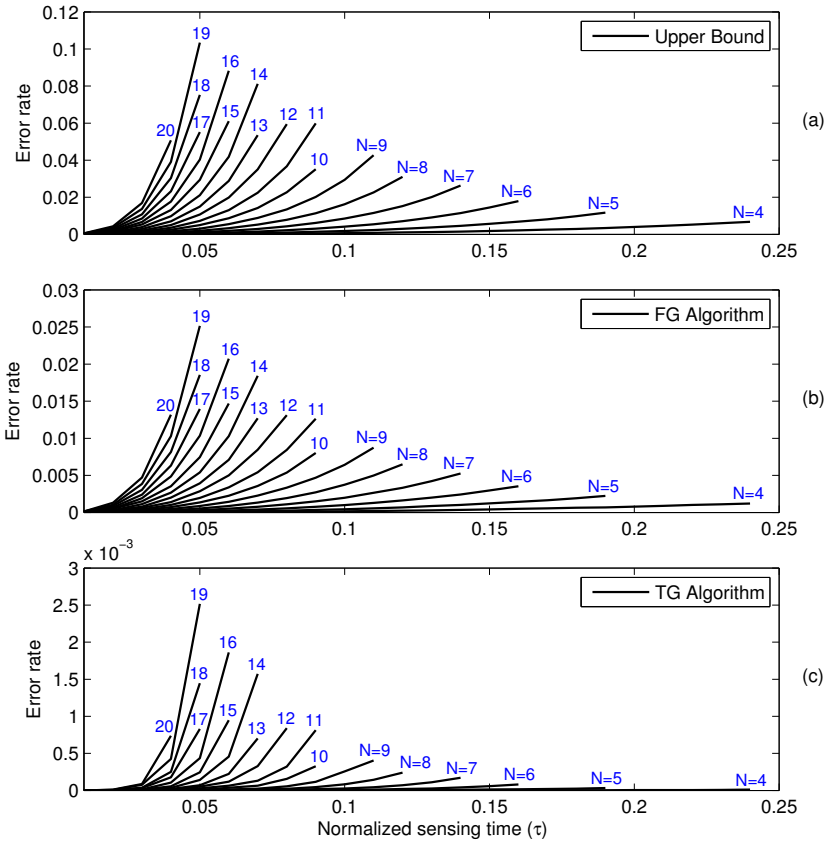

Figure 4.8: Error rate vs. τ vs. N: (a) upper bound (4.41) (b) FG algorithm [80] (c) TG algorithm; i.i.d. Rayleigh fading; uniformly distributed θ_n.

Rayleigh fading, the data rate is given by the channel capacity $R_n = B\log_2(1+\gamma_n)$, where γ_n is exponentially distributed with mean 10, $\forall n$, and the channel bandwidth B is normalized to 1 Hz. Also, assume the channel availability probability θ_n is uniformly distributed on $(0,1)$, $\forall n$.

In Figure 4.8, we compare the empirical error rates of the FG and the TG algorithms and validate the error rate upper bound in (4.41) for various N and τ values with $\lceil 1/\tau \rceil - 1 \geq N$ (cf. Section 4.2). First, we observe that the error rate increases with both N and τ for both algorithms. Next, by comparing Figure 4.8(b) and (c), it is evident that the TG algorithm is significantly more accurate than the FG algorithm. Moreover, in all cases, the empirical probabilities $\tilde{\Pr}(\underline{\mathbf{s}}^{\mathrm{TG}} \neq \underline{\mathbf{s}}^*)$ [in Figure 4.8(c)] and $\tilde{\Pr}(\underline{\mathbf{s}}^{\mathrm{FG}} \neq \underline{\mathbf{s}}^{\mathrm{BG}})$ [in Figure 4.8(a)] are smaller than 2.6×10^{-3} and 0.11, respectively. According to Proposition 10, $\tilde{\Pr}(\underline{\mathbf{s}}^{\mathrm{FG}} = \underline{\mathbf{s}}^{\mathrm{BG}})$ quantifies the portion of time in which the TG algorithm produces a verifiable optimal solution. Consequently, we conclude that the FG algorithm is able to produce an optimal solution for over 99.74% of the time and a verifiable optimal solution for over 89% of the time. The former indicates its near-optimal performance while the latter greatly improves the SU's confidence level.

4.7 Conclusion

In this chapter, we analyze and improve on the previously proposed FG algorithm in [80] for solving the single-SU sensing order selection problem. The potential function is a key element of both our proposed TG algorithm and the FG algorithm in [80], and its relation to the underlying structure of the optimal solution is revealed in our analysis. Moreover, we demonstrate the significant performance improvement of our proposed algorithm and prove an easily verifiable sufficient condition for optimality.

Chapter 5

Contribution and Future Directions

In this thesis, several strategies and algorithms are introduced to guide the distributed decision-making of noncooperative and cooperative SUs under different scenarios. This interdisciplinary work utilizes ideas and/or mathematical tools from diverse fields, including the diversity techniques from wireless communication theory [69], optimal stopping theory [82], coalitional game theory [66], and algorithm design principles [78], to demonstrate their great potential in the ongoing CR research. Moreover, we emphasize that a common theme throughout this thesis is utilization of the CSI, e.g.,

1. CSI-adaptation helps to boost the data rate, to improve sensor reliability, and to randomize sensing decisions of noncooperative SUs (Chapter 1–2);
2. SU's sensing contribution is measured based on the PU-to-SU SNR information (Chapter 3);
3. perfect CSI reduces the OS rule to an extremely simple form (Chapter 4).

Part of this thesis was published or currently under review, including [87–91]. Before concluding this thesis, let us discuss several possible future directions:

SUs with parallel sensing capabilities [41, 92]

While we have focused on sensing one channel at a time, in practice, SUs might be able to sense multiple channels in parallel by using the recently developed wideband sensing techniques [41, 92]. However, extensions to wideband spectrum sensing scenarios are not straightforward. For example, in the cooperative case, an SU can join multiple channel coalitions and, thus, may need to negotiate with multiple (possibly overlapped) sets of SUs simultaneously.

Estimation of and adaptation to fading PU-to-SU CSI under high mobility

Another important direction is to investigate robust fading prediction methods to forecast the PU signal strength at the SU sensor, which is more challenging than predicting the SU-to-

SU CSI (cf. Chapter 1), especially in highly mobile environments, because the PU-to-SU CSI can only be detected noncoherently [69] due to the lack of phase information. Moreover, SUs cannot detect or anticipate the signal strength of a previously silent PU. These difficulties must be addressed carefully.

Cooperative games with Communication Overhead

To facilitate cooperation, SUs exchange information about their sensing reliability and negotiate the payoff allocation, which causes communication overhead and may eventually lead to the nonformation of the grand coalition on each channel. Moreover, delay and uncertainty may arise in reaching a joint agreement on both the coalition structure and payoff allocation in the bottom-layer game. When an SU is uncertain about its expected payoff on a candidate channel, it cannot make an easy switching decision. To accommodate these new characteristics of the game, a more generalized bargaining model as well as innovative solution concepts are required.

More complete analysis on the Two-Pass Greedy algorithm

To better quantify and understand the proposed TG algorithm, tight and closed-form upper bounds on the error rate and the approximation error or, equivalently, the approximation ratio [78] should be explored. Moreover, despite the known NP-hardness status of a few variants [83–86], to the best of our knowledge, whether the computation problem $\mathbb{P}2$ being considered in Chapter 4 [cf. (4.10)] is NP-hard is still an open question.

Multi-Secondary-User sequential sensing under generalized scenarios

Finally, while we only considered single-SU sequential sensing assuming perfect CSI, extensions to multi-SU scenarios with imperfect CSI are certainly desirable. Another possible extension is to consider a large number of channels (N), exceeding the number of sensing stages (K) within one time slot (cf. Section 4.1), in which case, a sensing order becomes a K-permutation [78] of the set of N channels. To reduce the size of the feasible solution space, an initial preprocessing routine can be added to filter out some candidate channels with low potential.

REFERENCES

[1] L. Lai, H. E. Gamal, H. Jiang, and H. V. Poor, "Cognitive medium access: Exploration, exploitation, and competition," *IEEE Trans. Mobile Comput.*, vol. 10, no. 2, pp. 239–253, 2011.

[2] Q. Zhao, L. Tong, A. Swami, and Y. Chen, "Decentralized cognitive MAC for opportunistic spectrum access in ad hoc networks: A POMDP framework," *IEEE J. Sel. Areas Commun.*, vol. 25, no. 3, pp. 589–600, 2007.

[3] I. F. Akyildiz, W. Y. Lee, and K. R. Chowdhury, "CRAHNs: Cognitive radio ad hoc networks," *Ad Hoc Netw.*, vol. 7, no. 5, pp. 810–836, 2009.

[4] K. Liu, Q. Zhao, and Y. Chen, "Distributed sensing and access in cognitive radio networks," in *Proc. IEEE ISSSTA'08*, 2008, pp. 28–31.

[5] Y. Lee, "Modified myopic policy with collision avoidance for opportunistic spectrum access," *Electron. Lett.*, vol. 46, no. 12, pp. 871–872, 2010.

[6] A. Anandkumar, N. Michael, A. K. Tang, and A. Swami, "Distributed algorithms for learning and cognitive medium access with logarithmic regret," *IEEE J. Sel. Areas Commun.*, vol. 29, no. 4, pp. 731–745, 2011.

[7] K. Liu and Q. Zhao, "Distributed learning in multi-armed bandit with multiple players," *IEEE Trans. Signal Process.*, vol. 58, no. 11, pp. 5667–5681, 2010.

[8] Y. Xu, J. Wang, Q. Wu, A. Anpalagan, and Y. D. Yao, "Opportunistic spectrum access in unknown dynamic environment: A game-theoretic stochastic learning solution," *IEEE Trans. Wireless Commun.*, vol. 11, no. 4, pp. 1380–1391, 2012.

[9] V. Asghari and S. Aïssa, "Adaptive rate and power transmission in spectrum-sharing systems," *IEEE Trans. Wireless Commun.*, vol. 9, no. 10, pp. 3272–3280, 2010.

[10] A. Bagayoko, I. Fijalkow, and P. Tortelier, "Power control of spectrum-sharing in fading environment with partial channel state information," *IEEE Trans. Signal Process.*, vol. 59, no. 5, pp. 2244–2256, 2011.

[11] A. W. Min and K. G. Shin, "Exploiting multi-channel diversity in spectrum-agile networks," in *Proc. IEEE INFOCOM'08*, 2008, pp. 56–60.

[12] H. T. Cheng and W. Zhuang, "Simple channel sensing order in cognitive radio networks," *IEEE J. Sel. Areas Commun.*, vol. 29, no. 4, pp. 676–688, 2011.

[13] J. Zhao and X. Wang, "Channel sensing order in multi-user cognitive radio networks," in *Proc. IEEE DySPAN'12*, 2012, pp. 397–407.

[14] Y. Wang, Y. Xu, L. Shen, C. Xu, and Y. Cheng, "Two-dimensional POMDP-based opportunistic spectrum access in time-varying environment with fading channels," *J. Commun. Netw.*, vol. 16, no. 2, pp. 217–226, 2014.

[15] Q. Zhao and B. M. Sadler, "A survey of dynamic spectrum access," *IEEE Signal Process. Mag.*, vol. 24, no. 3, pp. 79–89, 2007.

[16] A. J. Gibson and L. Arnett, "Statistical modelling of spectrum occupancy," *Electron. Lett.*, vol. 29, no. 25, pp. 2175–2176, 1993.

[17] S. Geirhofer, L. Tong, and B. M. Sadler, "Dynamic spectrum access in the time domain: Modeling and exploiting white space," *IEEE Commun. Mag.*, vol. 45, no. 5, pp. 66–72, 2007.

[18] Y. Xu, A. Anpalagan, Q. Wu, L. Shen, Z. Gao, and J. Wang, "Decision-theoretic distributed channel selection for opportunistic spectrum access: Strategies, challenges and solutions," *IEEE Commun. Surveys Tuts.*, vol. 15, no. 4, pp. 1689–1713, 2013.

[19] C. Zhang and K. G. Shin, "What should secondary users do upon incumbents' return?" *IEEE J. Sel. Areas Commun.*, vol. 31, no. 3, pp. 417–428, 2013.

[20] X. Zhou, G. Y. Li, Y. H. Kwon, and A. C. K. Soong, "Detection timing and channel selection for periodic spectrum sensing in cognitive radio," in *Proc. IEEE GLOBECOM'08*, 2008, pp. 1–5.

[21] S. T. Chung and A. J. Goldsmith, "Degrees of freedom in adaptive modulation: A unified view," *IEEE Trans. Commun.*, vol. 49, no. 9, pp. 1561–1571, 2001.

[22] J. Jia, Q. Zhang, and X. Shen, "HC-MAC: A hardware-constrained cognitive MAC for efficient spectrum management," *IEEE J. Sel. Areas Commun.*, vol. 26, no. 1, pp. 106–117, 2008.

[23] J. Mo, H. S. W. So, and J. Walrand, "Comparison of multichannel MAC protocols," *IEEE Trans. Mobile Comput.*, vol. 7, no. 1, pp. 50–65, 2008.

[24] B. F. Lo, "A survey of common control channel design in cognitive radio networks," *Physical Commun.*, vol. 4, no. 1, pp. 26–39, 2011.

[25] D. G. Brennan, "Linear diversity combining techniques," *Proc. IEEE*, vol. 91, no. 2, pp. 331–356, 2003.

[26] F. F. Digham, M. S. Alouini, and M. K. Simon, "On the energy detection of unknown signals over fading channels," *IEEE Trans. Commun.*, vol. 55, no. 1, pp. 21–24, 2007.

[27] S. Chen and L. Tong, "Low-complexity distributed spectrum sharing among multiple cognitive users," in *Proc. IEEE MILCOM'10*, 2010, pp. 2274–2279.

[28] D. L. Goeckel, "Adaptive coding for time-varying channels using outdated fading estimates," *IEEE Trans. Commun.*, vol. 47, no. 6, pp. 844–855, 1999.

[29] A. Duel-Hallen, "Fading channel prediction for mobile radio adaptive transmission systems," *Proc. IEEE*, vol. 95, no. 12, pp. 2299–2313, 2007.

[30] H. Su and X. Zhang, "Cross-layer based opportunistic MAC protocols for QoS provisionings over cognitive radio wireless networks," *IEEE J. Sel. Areas Commun.*, vol. 26, no. 1, pp. 118–129, 2008.

[31] M. Lei, A. Duel-Hallen, and H. Hallen, "Reliable adaptive modulation and interference mitigation for mobile radio slow frequency hopping channels," *IEEE Trans. Commun.*, vol. 56, no. 3, pp. 352–355, 2008.

[32] C. D. Meyer, *Matrix analysis and applied linear algebra.* SIAM, 2000.

[33] *Universal Mobile Telecommunications System (UMTS); Selection procedures for the choice of radio transmission technologies of the UMTS*, ETSI Std. TR 101 112 V3.1.0, 1997.

[34] P. Dent, G. E. Bottomley, and T. Croft, "Jakes fading model revisited," *Electron. Lett.*, vol. 29, no. 13, pp. 1162–1163, 1993.

[35] A. Tajer and X. Wang, "Beacon-assisted spectrum access with cooperative cognitive transmitter and receiver," *IEEE Trans. Mobile Comput.*, vol. 9, no. 1, pp. 112–126, 2010.

[36] M. C. Gursoy and S. Gezici, "On the interplay between channel sensing and estimation in cognitive radio systems," in *Proc. IEEE GLOBECOM'11*, 2011, pp. 1–5.

[37] A. J. Goldsmith and S. G. Chua, "Variable-rate variable-power MQAM for fading channels," *IEEE Trans. Commun.*, vol. 45, no. 10, pp. 1218–1230, 1997.

[38] M. Gudmundson, "Correlation model for shadow fading in mobile radio systems," *Electron. Lett.*, vol. 27, no. 23, pp. 2145–2146, 1991.

[39] A. Ghasemi and E. S. Sousa, "Asymptotic performance of collaborative spectrum sensing under correlated log-normal shadowing," *IEEE Commun. Lett.*, vol. 11, no. 1, pp. 34–36, 2007.

[40] P. Agrawal and N. Patwari, "Correlated link shadow fading in multi-hop wireless networks," *IEEE Trans. Wireless Commun.*, vol. 8, no. 8, pp. 4024–4036, 2009.

[41] Z. Quan, S. Cui, H. V. Poor, and A. H. Sayed, "Collaborative wideband sensing for cognitive radios," *IEEE Signal Process. Mag.*, vol. 25, no. 6, pp. 60–73, 2008.

[42] E. C. Y. Peh and Y. C. Liang, "Optimization for cooperative sensing in cognitive radio networks," in *Proc. IEEE WCNC'07*, 2007, pp. 27–32.

[43] Z. Quan, S. J. Shellhammer, W. Zhang, and A. H. Sayed, "Spectrum sensing by cognitive radios at very low SNR," in *Proc. IEEE GLOBECOM'09*, 2009, pp. 1–6.

[44] A. Ghasemi and E. S. Sousa, "Collaborative spectrum sensing for opportunistic access in fading environments," in *Proc. IEEE DySPAN'05*, 2005, pp. 131–136.

[45] S. H. Song, K. Hamdi, and K. B. Letaief, "Spectrum sensing with active cognitive systems," *IEEE Trans. Wireless Commun.*, vol. 9, no. 6, pp. 1849–1854, 2010.

[46] H. H. Choi, K. Jang, and Y. Cheong, "Adaptive sensing threshold control based on transmission power in cognitive radio systems," in *Proc. CrownCom'08*, 2008, pp. 1–6.

[47] X. Ling, B. Wu, H. Wen, P. H. Ho, Z. Bao, and L. Pan, "Adaptive threshold control for energy detection based spectrum sensing in cognitive radios," *IEEE Wireless Commun. Lett.*, vol. 1, no. 5, pp. 448–451, 2012.

[48] Y. E. Lin, K. H. Liu, and H. Y. Hsieh, "On using interference-aware spectrum sensing for dynamic spectrum access in cognitive radio networks," *IEEE Trans. Mobile Comput.*, vol. 12, no. 3, pp. 461–474, 2013.

[49] F. T. Foukalas, G. T. Karetsos, and L. F. Merakos, "Capacity optimization through sensing threshold adaptation for cognitive radio networks," *Optim. Lett.*, vol. 6, no. 7, pp. 1499–1511, 2012.

[50] S. J. Kim, N. Jain, G. B. Giannakis, and P. A. Forero, "Joint link learning and cognitive radio sensing," in *Proc. 45th Asilomar Conf. Signals, Syst., Comput.*, 2011, pp. 1415–1419.

[51] Z. Quan, S. Cui, and A. H. Sayed, "An optimal strategy for cooperative spectrum sensing in cognitive radio networks," in *Proc. IEEE GLOBECOM'07*, 2007, pp. 2947–2951.

[52] E. Dall'Anese, S. J. Kim, and G. B. Giannakis, "Channel gain map tracking via distributed kriging," *IEEE Trans. Veh. Technol.*, vol. 60, no. 3, pp. 1205–1211, 2011.

[53] A. Jovicic and P. Viswanath, "Cognitive radio: An information-theoretic perspective," *IEEE Trans. Inf. Theory*, vol. 55, no. 9, pp. 3945–3958, 2009.

[54] J. So and N. H. Vaidya, "Multi-channel MAC for ad hoc networks: Handling multi-channel hidden terminals using a single transceiver," in *Proc. ACM MobiHoc'04*, 2004, pp. 222–233.

[55] I. F. Akyildiz, B. F. Lo, and R. Balakrishnan, "Cooperative spectrum sensing in cognitive radio networks: A survey," *Physical Commun.*, vol. 4, no. 1, pp. 40–62, 2011.

[56] Y. Gu, W. Saad, M. Bennis, M. Debbah, and Z. Han, "Matching theory for future wireless networks: Fundamentals and applications," *IEEE Commun. Mag.*, vol. 53, no. 5, pp. 52–59, 2015.

[57] B. Wang, K. J. R. Liu, and T. C. Clancy, "Evolutionary cooperative spectrum sensing game: How to collaborate?" *IEEE Trans. Commun.*, vol. 58, no. 3, pp. 890–900, 2010.

[58] W. Saad, Z. Han, T. Basar, M. Debbah, and A. Hjorungnes, "Coalition formation games for collaborative spectrum sensing," *IEEE Trans. Veh. Technol.*, vol. 60, no. 1, pp. 276–297, 2011.

[59] W. Wang, B. Kasiri, J. Cai, and A. S. Alfa, "Distributed cooperative multi-channel spectrum sensing based on dynamic coalitional game," in *Proc. IEEE GLOBECOM'10*, 2010, pp. 1–5.

[60] J. Rajasekharan, J. Eriksson, and V. Koivunen, "Cooperative game-theoretic modeling for spectrum sensing in cognitive radios," in *Proc. 44th Asilomar Conf. Signals, Syst., Comput.*, 2010, pp. 165–169.

[61] Q. Shi, C. Comaniciu, and K. Jaffrs-Runser, "An auction-based mechanism for cooperative sensing in cognitive networks," *IEEE Trans. Wireless Commun.*, vol. 12, no. 8, pp. 3649–3661, 2013.

[62] W. Saad, Z. Han, R. Zheng, A. Hjorungnes, T. Basar, and H. V. Poor, "Coalitional games in partition form for joint spectrum sensing and access in cognitive radio networks," *IEEE J. Sel. Topics Signal Process.*, vol. 6, no. 2, pp. 195–209, 2012.

[63] T. Wang, L. Song, Z. Han, and W. Saad, "Distributed cooperative sensing in cognitive radio networks: An overlapping coalition formation approach," *IEEE Trans. Commun.*, vol. 62, no. 9, pp. 3144–3160, 2014.

[64] X. Hao, M. H. Cheung, V. W. S. Wong, and V. C. M. Leung, "Hedonic coalition formation game for cooperative spectrum sensing and channel access in cognitive radio networks," *IEEE Trans. Wireless Commun.*, vol. 11, no. 11, pp. 3968–3979, 2012.

[65] C. Jiang, Y. Chen, K. J. R. Liu, and Y. Ren, "Network economics in cognitive networks," *IEEE Commun. Mag.*, vol. 53, no. 5, pp. 75–81, 2015.

[66] W. Saad, Z. Han, M. Debbah, A. Hjorungnes, and T. Basar, "Coalitional game theory for communication networks," *IEEE Signal Process. Mag.*, vol. 26, no. 5, pp. 77–97, 2009.

[67] A. Bogomolnaia and M. O. Jackson, "The stability of hedonic coalition structures," *Game Econ. Behav.*, vol. 38, no. 2, pp. 201–230, 2002.

[68] I. E. Hafalir, "Efficiency in coalition games with externalities," *Games Econ. Behav.*, vol. 61, no. 2, pp. 242–258, 2007.

[69] A. J. Goldsmith, *Wireless communications*. Cambridge Univ. Press, 2005.

[70] S. Boyd and L. Vandenberghe, *Convex optimization*. Cambridge Univ. Press, 2009.

[71] Y. C. Liang, Y. Zeng, E. C. Y. Peh, and A. T. Hoang, "Sensing-throughput tradeoff for cognitive radio networks," *IEEE Trans. Wireless Commun.*, vol. 7, no. 4, pp. 1326–1337, 2008.

[72] E. Maskin, "Bargaining, coalitions and externalities," *Presidential Address to the Econometric Society*, 2003.

[73] G. Bacci, S. Lasaulce, W. Saad, and L. Sanguinetti, "Game theory for networks: A tutorial on game-theoretic tools for emerging signal processing applications," *IEEE Signal Process. Mag.*, vol. 33, no. 1, pp. 94–119, 2016.

[74] G. Owen, *Values of games with a priori unions*, ser. Mathematical economics and game theory. Springer, 1977, pp. 76–88.

[75] K. Avrachenkov, J. Elias, F. Martignon, G. Neglia, and L. Petrosyan, "A Nash bargaining solution for cooperative network formation games," in *Networking'11*, 2011, pp. 307–318.

[76] T. Kawamori and T. Miyakawa, "Nash bargaining solution under externalities," *Osaka Univ. Econ. Work. Paper Series*, 2012.

[77] H. Konishi and D. Ray, "Coalition formation as a dynamic process," *J. Econ. Theory*, vol. 110, no. 1, pp. 1–41, 2003.

[78] T. H. Cormen, C. E. Leiserson, R. L. Rivest, and C. Stein, *Introduction to algorithms.* Cambridge, MA: MIT Press, 2009.

[79] T. Camp, J. Boleng, and V. Davies, "A survey of mobility models for ad hoc network research," *Wireless Commun. Mobile Comput.*, vol. 2, no. 5, pp. 483–502, 2002.

[80] J. Huang, H. Zhou, Y. Chen, B. Chen, and R. Kong, "Distributed and centralized schemes for channel sensing order setting in multi-user cognitive radio networks," *Wireless Personal Commun.*, vol. 75, no. 2, pp. 1391–1410, 2014.

[81] H. Jiang, L. Lai, R. Fan, and H. V. Poor, "Optimal selection of channel sensing order in cognitive radio," *IEEE Trans. Wireless Commun.*, vol. 8, no. 1, pp. 297–307, 2009.

[82] T. S. Ferguson. Optimal stopping and applications. Website. [Online]. Available: http://www.math.ucla.edu/~tom/Stopping/Contents.html

[83] C. C. Y. Kwan and Y. Yuan, "The present value issue in a sequential selection problem," *Decis. Sci.*, vol. 24, no. 5, pp. 1057–1067, 1993.

[84] T. Ünlüyurt, "Sequential testing of complex systems: A review," *Discrete Appl. Math.*, vol. 142, no. 1, pp. 189–205, 2004.

[85] B. D. Reyck and R. Leus, "R&D project scheduling when activities may fail," *IIE Trans.*, vol. 40, no. 4, pp. 367–384, 2008.

[86] K. Moizumi and G. Cybenko, "The traveling agent problem," *Math. Control Signals Syst.*, vol. 14, no. 3, pp. 213–232, 2001.

[87] Y. Lu and A. Duel-Hallen, "Channel-adaptive sensing strategy for cognitive radio ad hoc networks," in *Proc. IEEE CCNC'13*, 2013, pp. 466–471.

[88] Y. Lu and A. Duel-Hallen, "Channel-adaptive spectrum detection and sensing strategy for cognitive radio ad-hoc networks," in *Proc. 51st Allerton Conf. Commun., Control, Comput.*, 2013, pp. 1408–1414.

[89] Y. Lu and A. Duel-Hallen, "A two-layer coalitional game among rational cognitive radio users," in *Proc. CISS'15*, 2015, pp. 1–6.

[90] Y. Lu and A. Duel-Hallen, "Channel-aware spectrum sensing and access for mobile cognitive radio ad hoc networks," *IEEE Trans. Veh. Technol.*, vol. 65, no. 4, pp. 2471–2480, 2016.

[91] Y. Lu and A. Duel-Hallen, "Game-theoretic framework for cooperative sensing and fair spectrum access in multichannel cognitive radio networks," submitted.

[92] H. Sun, A. Nallanathan, C. X. Wang, and Y. Chen, "Wideband spectrum sensing for cognitive radio networks: A survey," *IEEE Wireless Commun.*, vol. 20, no. 2, pp. 74–81, 2013.

[93] W. C. Waterhouse, "Do symmetric problems have symmetric solutions?" *Amer. Math. Monthly*, vol. 90, no. 6, pp. 378–387, 1983.

APPENDICES

Appendix A

A.1 Properties of Analytical Throughputs for $M = N = 2$ in Section 1.3.2

First, note that for $M = N = 2$, the average expected individual throughput (1.10) can be expanded as

$$\begin{aligned} H_\pi^m = &\sum_{n=1}^{2} \Pr[n_*^m = n, n_*^{m'} = n'] \mathbb{E}[H^{mn} | n_*^m = n, n_*^{m'} = n'] \\ &+ \sum_{n=1}^{2} \frac{1}{2} \Pr[n_*^m = n, n_*^{m'} = n] \mathbb{E}[H^{mn} | n_*^m = n, n_*^{m'} = n] \end{aligned} \tag{A.1}$$

where $m \neq m'$, $n \neq n'$ and the expectation is over γ^{mn}. We also note that if the sensing decisions are made individually without negotiating before sensing, the following properties hold $\forall n, n'$ and $m \neq m'$:

$$\Pr[n_*^m = n, n_*^{m'} = n'] = \Pr[n_*^m = n] \Pr[n_*^{m'} = n'] \tag{A.2}$$

$$\mathbb{E}[H^{mn} | n_*^m = n, n_*^{m'} = n'] = \mathbb{E}[H^{mn} | n_*^m = n]. \tag{A.3}$$

Policies (i,ii,v,vi) in Table A.1 satisfy these two conditions (A.2)–(A.3). Moreover, for policies that do not exploit CSI, (i–v), the following property is justified $\forall n$, n' and $m \neq m'$:

$$\mathbb{E}[H^{mn} | n_*^m = n, n_*^{m'} = n'] = \mathbb{E}[H^{mn}]. \tag{A.4}$$

Finally, γ^{mn} is exponentially distributed with pdf $f_{\gamma^{mn}}(x) = \frac{1}{\bar{\gamma}} \exp(-\frac{x}{\bar{\gamma}})$ assuming i.i.d. Rayleigh fading. The cdf and pdf of $H^{mn} = \beta^n \log_2(1 + \gamma^{mn})$ in (1.12) and (A.5) follow from simple changes of variables.

$$f_{H^{mn}}(x) = \frac{\ln 2}{\beta^n \bar{\gamma}} \exp\left(\frac{-1}{\bar{\gamma}} \left(2^{x/\beta^n} - 1 \right) \right) 2^{x/\beta^n}. \tag{A.5}$$

A.2 Derivation of Throughputs in Table A.1 ($M = N = 2$) for Section 1.3.2

(i) *Random Selection*. This is a naïve approach where sensing decisions are made at random: $\forall m$,

$$\Pr[n_*^m = 1] = \Pr[n_*^m = 2] = 1/2. \tag{A.6}$$

Combining (A.1), (A.2), (A.4) and (A.6), we arrive at H^m_{Random} in Table A.1.

(ii) *Myopic Sensing* [2]. SUs always sense the channel that is more likely to be available, so $\forall m$,

$$n_*^m = \begin{cases} 1, & \text{if } \beta^1 > \beta^2 \\ 2, & \text{if } \beta^1 < \beta^2. \end{cases} \tag{A.7}$$

A combination of (A.1), (A.2), (A.4) and (A.7) leads to H^m_{My} in Table A.1.

(iii) *Myopic Policy with TDFS* [7]. SUs take turns sensing their favorite channels. Without loss of generality, we assume the TDFS schedules of the two SUs are such that SU 1 senses its favorite channel in odd time slots and its second favorite channel in even time slots, while SU 2 does the opposite. In the myopic policy, each SU's favorite channel is just the channel with higher β [cf. (A.7)], so we have

$$n_*^1 = \begin{cases} \arg\max_n \beta^n, & \text{if } t \text{ is odd} \\ \arg\min_n \beta^n, & \text{if } t \text{ is even} \end{cases} \quad \text{and} \quad n_*^2 = \begin{cases} \arg\min_n \beta^n, & \text{if } t \text{ is odd} \\ \arg\max_n \beta^n, & \text{if } t \text{ is even.} \end{cases} \tag{A.8}$$

Thus,

$$\begin{cases} \Pr[n_*^m = 1, n_*^{m'} = 2] = \Pr[n_*^m = 2, n_*^{m'} = 1] = 1/2 \\ \Pr[n_*^m = 1, n_*^{m'} = 1] = \Pr[n_*^m = 2, n_*^{m'} = 2] = 0 \end{cases} \tag{A.9}$$

where $m \neq m'$. Plugging (A.4) and (A.9) into (A.1) gives $H^m_{\text{My-TDFS}}$ in Table A.1.

(iv) *Myopic Policy with FCFS*. Each SU is equally likely to win the right to sense the channel with higher availability probability or to switch to sensing the channel with lower availability. It is easy to show that (A.9) still holds, so $H^m_{\text{My-FCFS}} = H^m_{\text{My-TDFS}}$.

(v) *Randomized Policy* [4]. Each SU m senses channel n with probability

$$\Pr[n_*^m = n] = \beta^n/(\beta^1 + \beta^2). \tag{A.10}$$

The expression for $H^m_{\text{Randomized}}$ in Table A.1 can be obtained by using (A.10) and (A.1)–(A.4).

(vi) *CSI-aided Myopic Policy*. The sensing decisions are made by (1.1) with the reward given by (1.5). When $N = M = 2$, $B^n = 1\,\text{Hz}$ and $\theta^{mn}(t) = \beta^n$ for all m, n, the sensing policy

becomes

$$n_*^m = \arg\max_n H^{mn} \tag{A.11}$$

where $m = 1, 2$, following from the definition of H^{mn} in (1.6). Using the conditions (A.2)–(A.3) in (A.1) and from (A.11), we obtain

$$\begin{aligned} H_{\text{CSI}}^m = &\sum_{n=1}^{2} \Pr[H^{mn} > H^{mn'}] \Pr[H^{m'n'} > H^{m'n}] \mathbb{E}[H^{mn} | H^{mn} > H^{mn'}] \\ &+ \sum_{n=1}^{2} \frac{1}{2} \Pr[H^{mn} > H^{mn'}] \Pr[H^{m'n} > H^{m'n'}] \mathbb{E}[H^{mn} | H^{mn} > H^{mn'}] \end{aligned} \tag{A.12}$$

with

$$\begin{aligned} \Pr[H^{mn} > H^{mn'}] = F_{H^{mn'} - H^{mn}}(0) &= \int_0^\infty F_{H^{mn'}}(x) f_{H^{mn}}(x) dx \\ &\triangleq \begin{cases} F_\Delta^m, & \text{if } n = 1, n' = 2 \\ 1 - F_\Delta^m, & \text{if } n = 2, n' = 1 \end{cases} \end{aligned} \tag{A.13}$$

and

$$\begin{aligned} \Pr[H^{mn} > H^{mn'}] \mathbb{E}[H^{mn} | H^{mn} > H^{mn'}] &= \Pr[H^{mn} > H^{mn'}] \int_0^\infty x f_{H^{mn}}(x | H^{mn} > H^{mn'}) dx \\ &\triangleq I_{nn'}^m \end{aligned} \tag{A.14}$$

where

$$f_{H^{mn}}(x | H^{mn} > H^{mn'}) = \frac{f_{H^{mn}}(x) F_{H^{mn'}}(x)}{\Pr[H^{mn} > H^{mn'}]}. \tag{A.15}$$

Substituting (A.13) and (A.14) into (A.12) and further simplifying, we obtain H_{CSI}^m in Table A.1.

(vii) *CSI-aided Myopic Policy with TDFS.* Applying the TDFS schedule in (iii) to the CSI-aided myopic policy [cf. (A.11)], we have

$$n_*^1 = \begin{cases} \arg\max_n H^{1n}, & \text{if } t \text{ is odd} \\ \arg\min_n H^{1n}, & \text{if } t \text{ is even} \end{cases} \quad \text{and} \quad n_*^2 = \begin{cases} \arg\min_n H^{2n}, & \text{if } t \text{ is odd} \\ \arg\max_n H^{2n}, & \text{if } t \text{ is even.} \end{cases} \tag{A.16}$$

Next, average over the achievable throughput of SU 1 at odd and even slots,

$$H_{\text{CSI-TDFS}}^1 = \frac{1}{2} H_{\text{CSI-TDFS}}^1(\text{odd}) + \frac{1}{2} H_{\text{CSI-TDFS}}^1(\text{even}) \tag{A.17}$$

with [cf. (A.1)]

$$
\begin{aligned}
H^1_{\text{CSI-TDFS}}(\text{odd}) &= \sum_{n=1}^{2} \Pr[n^1_* = n, n^2_* = n' | \text{odd } t] E[H^{1n} | n^1_* = n, n^2_* = n', \text{odd } t] \qquad \text{(A.18)} \\
&+ \sum_{n=1}^{2} \frac{1}{2} \Pr[n^1_* = n, n^2_* = n | \text{odd } t] \mathbb{E}[H^{1n} | n^1_* = n, n^2_* = n, \text{odd } t] \\
&= \sum_{n=1}^{2} \Pr[H^{1n} > H^{1n'}, H^{2n} > H^{2n'}] \mathbb{E}[H^{1n} | H^{1n} > H^{1n'}, H^{2n} > H^{2n'}] \\
&+ \sum_{n=1}^{2} \frac{1}{2} \Pr[H^{1n} > H^{1n'}, H^{2n'} > H^{2n}] \mathbb{E}[H^{1n} | H^{1n} > H^{1n'}, H^{2n'} > H^{2n}] \\
&= \sum_{n=1}^{2} \Pr[H^{1n} > H^{1n'}] \Pr[H^{2n} > H^{2n'}] \mathbb{E}[H^{1n} | H^{1n} > H^{1n'}] \\
&+ \sum_{n=1}^{2} \frac{1}{2} \Pr[H^{1n} > H^{1n'}] \Pr[H^{2n'} > H^{2n}] \mathbb{E}[H^{1n} | H^{1n} > H^{1n'}]
\end{aligned}
$$

where $n \neq n'$, the second equation is from (A.16) and the last step is from the i.i.d. fading assumption, i.e., H^{mn} and $H^{m'n'}$ are independent $\forall n, n'$ and $m \neq m'$. Similarly,

$$
\begin{aligned}
H^1_{\text{CSI-TDFS}}(\text{even}) &= \sum_{n=1}^{2} \Pr[H^{1n} < H^{1n'}] \Pr[H^{2n'} > H^{2n}] \mathbb{E}[H^{1n} | H^{1n} < H^{1n'}] \qquad \text{(A.19)} \\
&+ \sum_{n=1}^{2} \frac{1}{2} \Pr[H^{1n} < H^{1n'}] \Pr[H^{2n} > H^{2n'}] \mathbb{E}[H^{1n} | H^{1n} < H^{1n'}]
\end{aligned}
$$

where $n \neq n'$ and [cf. (A.14)]

$$
\Pr[H^{mn} < H^{mn'}] \mathbb{E}[H^{mn} | H^{mn} < H^{mn'}] = \mathbb{E}[H^{mn}] - I^m_{nn'}. \qquad \text{(A.20)}
$$

Combining (A.13)–(A.14) and (A.17)–(A.20) results in the expression of $H^m_{\text{CSI-TDFS}}$ in Table A.1 for $m = 1$. The $m = 2$ case is proven similarly.

(viii) *CSI-aided Myopic Policy with FCFS.* As discussed in Section 1.3.1, FCFS MAC serves to resolve congestion as needed before sensing while providing fairness to SUs. Hence, when the CSI-aided myopic policy [cf. (A.11)] is used in conjunction with FCFS MAC, $\Pr[n^m_* = n, n^{m'}_* = n] = 0$ holds. Moreover, $[n^m_* = n, n^{m'}_* = n']$ if and only if one of the

following mutually exclusive events occurs:

$$\begin{cases} H^{mn} > H^{mn'} \quad \text{and} \quad H^{m'n'} > H^{m'n} \\ H^{mn} > H^{mn'} \quad \text{and} \quad H^{m'n} > H^{m'n'} \quad \text{and} \quad m \text{ wins the competition in FCFS} \\ H^{mn} < H^{mn'} \quad \text{and} \quad H^{m'n'} > H^{m'n} \quad \text{and} \quad m \text{ loses the competition in FCFS} \end{cases} \tag{A.21}$$

where $m \neq m'$ and $n \neq n'$. As discussed in Section 1.3.1, we assume perfect sensing request resolution in FCFS such that both SUs are equally likely to win, and thus (A.1) expands as

$$\begin{aligned} H^m_{\text{CSI-FCFS}} = &\sum_{n=1}^{2} \Pr[H^{mn}>H^{mn'}, H^{m'n'}>H^{m'n}]\mathbb{E}[H^{mn}|H^{mn}>H^{mn'}, H^{m'n'}>H^{m'n}] \\ &+ \sum_{n=1}^{2} \frac{1}{2} \Pr[H^{mn}>H^{mn'}, H^{m'n}>H^{m'n'}]\mathbb{E}[H^{mn}|H^{mn}>H^{mn'}, H^{m'n}>H^{m'n'}] \\ &+ \sum_{n=1}^{2} \frac{1}{2} \Pr[H^{mn}<H^{mn'}, H^{m'n'}>H^{m'n}]\mathbb{E}[H^{mn}|H^{mn}<H^{mn'}, H^{m'n'}>H^{m'n}]. \end{aligned} \tag{A.22}$$

Using the i.i.d. fading assumption, we can simplify (A.22) similarly to the last step in (A.18). Then, substituting into (A.13)–(A.14) and (A.20) and simplifying, we obtain $H^m_{\text{CSI-FCFS}}$ in Table A.1.

(ix) *Centralized Policy*. The maximum network throughput is achieved by assigning the two SUs to different channels: $\forall m \neq m'$,

$$n^m_* = \begin{cases} 1, & \text{if } H^{m1} + H^{m'2} > H^{m'1} + H^{m2} \\ 2, & \text{if } H^{m'1} + H^{m2} > H^{m1} + H^{m'2}. \end{cases} \tag{A.23}$$

Substituting the above into (A.1) yields

$$\begin{aligned} H^m_{\text{Opt}} &= \Pr[H^{m1} > H^{m2} + H^{m'1} - H^{m'2}]\mathbb{E}[H^{m1}|H^{m1} > H^{m2} + H^{m'1} - H^{m'2}] \\ &\quad + \Pr[H^{m2} > H^{m1} + H^{m'2} - H^{m'1}]\mathbb{E}[H^{m2}|H^{m2} > H^{m1} + H^{m'2} - H^{m'1}] \\ &= \int_0^\infty x f_{H^{m1}}(x) F_{H^{m2}+H^{m'1}-H^{m'2}}(x)dx + \int_0^\infty x f_{H^{m2}}(x) F_{H^{m1}+H^{m'2}-H^{m'1}}(x)dx \end{aligned} \tag{A.24}$$

where the last step uses the same approach as in (A.14) and results in H^m_{Opt} in Table A.1.

Table A.1: Summary of Sensing Strategies for $N = M = 2$

No	**Strategy π**	**CSI-Adaptation (Y/N)**	**MAC (Before/After Sensing)**
i	Random selection	N	After
ii	Myopic [2]	N	After
iii	Myopic with TDFS [7]	N	Before
iv	Myopic with FCFS	N	Before
v	Randomized [4]	N	After
vi	CSI-aided myopic (Section 1.2)	Y	After
vii	CSI-aided myopic with TDFS	Y	Before
viii	CSI-aided myopic with FCFS	Y	Before
ix	Centralized	Y	Before

Expected Individual Throughput H_π^m
(i) $H^m_{\text{Random}} = \frac{3}{8}\left(E[H^{m1}] + E[H^{m2}]\right)$
(ii) $H^m_{\text{My}} = \begin{cases} E[H^{m1}]/2, & \text{if } \beta^1 > \beta^2 \\ E[H^{m2}]/2, & \text{if } \beta^1 < \beta^2 \end{cases}$
(iii) $H^m_{\text{My-TDFS}} = (E[H^{m1}] + E[H^{m2}])/2 \geq H^m_{\text{My}}$
(iv) $H^m_{\text{My-FCFS}} = H^m_{\text{My-TDFS}}$
(v) $H^m_{\text{Randomized}} = \sum_{n=1}^{2} \left(\frac{\beta^1\beta^2 + \beta^n\beta^n/2}{(\beta^1+\beta^2)^2} \right) E[H^{mn}] \leq H^m_{\text{My-TDFS}}$
(vi) $H^m_{\text{CSI}} = (1 - \frac{1}{2}F^{m'}_\Delta)I^m_{12} + (\frac{1}{2} + \frac{1}{2}F^{m'}_\Delta)I^m_{21}$
(vii) $H^m_{\text{CSI-TDFS}} = (\frac{1}{4} + \frac{1}{4}F^{m'}_\Delta)(I^m_{12} + E[H^{m2}] - I^m_{21}) + (\frac{1}{2} - \frac{1}{4}F^{m'}_\Delta)\left(I^m_{21} + E[H^{m1}] - I^m_{12}\right)$
(viii) $H^m_{\text{CSI-FCFS}} = (1-\frac{1}{2}F^{m'}_\Delta)I^m_{12} + (\frac{1}{2}-\frac{1}{2}F^{m'}_\Delta)\left(E[H^{m1}]-I^m_{12}\right) + (\frac{1}{2}+\frac{1}{2}F^{m'}_\Delta)I^m_{21} + \frac{1}{2}F^{m'}_\Delta\left(E[H^{m2}]-I^m_{21}\right)$
(ix) $H^m_{\text{Opt}} = \int_0^\infty x f_{H^{m1}}(x) F_{H^{m2}+H^{m'1}-H^{m'2}}(x)dx + \int_0^\infty x f_{H^{m2}}(x) F_{H^{m1}+H^{m'2}-H^{m'1}}(x)dx$

A.3 Performance Analysis for $N, M \geq 2$ in Section 1.3.2

Next, we generalize the throughput formulas to arbitrary $N, M \geq 2$ as listed in Table 1.2 included in Section 1.3. In this section, we assume nonhomogeneous channel availabilities and without loss generality, let $\beta^1 > \ldots > \beta^N$. Note that policies (i,ii,v,vi) satisfy the following two properties [cf. (A.2)–(A.3)] $\forall m, n$:

$$\Pr[n_*^m = n, J_n^m = j-1] = \Pr[n_*^m = n] \Pr[J_n^m = j-1] \tag{A.25}$$

$$E[H^{mn} | n_*^m = n, J_n^m = j-1] = E[H^{mn} | n_*^m = n]. \tag{A.26}$$

Moreover, the following property is justified for policies (i–v) [cf. (A.4)] $\forall m, n$:

$$E[H^{mn} | n_*^m = n, J_n^m = j-1] = E[H^{mn}]. \tag{A.27}$$

(i) *Random Selection*. $\forall m, n, j \leq M$,

$$\Pr[n_*^m = n] = 1/N \tag{A.28}$$

and

$$\Pr[J_n^m = j-1] = \binom{M-1}{j-1} \left(\frac{1}{N}\right)^{j-1} \left(1 - \frac{1}{N}\right)^{M-j}. \tag{A.29}$$

Combining (1.10), (A.25), (A.27)–(A.29), we arrive at H^m_{Random} in Table 1.2.

(ii) *Myopic Sensing* [2]. Since $\arg\max_n \beta^n = 1$, the sensing decision $\forall m$ is simply

$$n_*^m = 1 \tag{A.30}$$

and thus $\forall m$,

$$\Pr[J_n^m = j-1] = \begin{cases} 1, & \text{if } j = M \text{ and } n = 1 \\ 0, & \text{otherwise.} \end{cases} \tag{A.31}$$

A combination of (1.10), (A.25), (A.27), (A.30) and (A.31) leads to H^m_{My} in Table 1.2.

(iii) *Myopic Policy with TDFS* [7]. Assume $N \geq M$. Since all SUs have the same channel preference, TDFS resolves contention perfectly prior to sensing, and all SUs share the M best channels with higher β values (i.e., channels 1 to M) in a time division manner. Thus $\forall m$,

$$\Pr[n_*^m = n, J_n^m = j-1] = \begin{cases} 1/M, & \text{if } j = 1 \text{ and } n \leq M \\ 0, & \text{otherwise.} \end{cases} \tag{A.32}$$

Substituting (A.27) and (A.32) into (1.10) gives $H^m_{\text{My-TDFS}}$ in Table 1.2.

(iv) *Myopic Policy with FCFS.* (A.32) still holds, so $H^m_{\text{My-FCFS}} = H^m_{\text{My-TDFS}}$.

(v) *Randomized Policy* [4]. Each SU m senses channel n with probability

$$\Pr[n^m_* = n] = \beta^n / \sum_k \beta^k \tag{A.33}$$

and $\forall m, n, j \leq M$,

$$\Pr[J^m_n = j-1] = \binom{M-1}{j-1} \left(\frac{\beta^n}{\sum_k \beta^k}\right)^{j-1} \left(1 - \frac{\beta^n}{\sum_k \beta^k}\right)^{M-j}. \tag{A.34}$$

The expression for $H^m_{\text{Randomized}}$ in Table 1.2 can be obtained by using (A.33)–(A.34), (1.10) and (A.25)–(A.27).

(vi) *CSI-aided Myopic Policy.* The sensing decisions are made by (1.1) with the reward (1.5). Assuming $\theta^{mn}(t) = \beta^n$, $\forall m, n$, the sensing policy becomes

$$n^m_* = \arg\max_n H^{mn} \tag{A.35}$$

which follows from the definition of H^{mn} (1.6) and

$$\Pr[J^m_n = j-1] = \binom{M-1}{j-1} (q_n)^{j-1} (1-q_n)^{M-j} \tag{A.36}$$

for all m, n and $j \leq M$, where q_n (1.13) has the same value for all m because both the channel availability β^n and the average SNR $\bar{\gamma}^{mn} = \bar{\gamma}$ are SU-invariant. Using (A.25)–(A.26) in (1.10) and from (A.35)–(A.36), we obtain H^m_{CSI} in Table 1.2.

(vii) *CSI-aided Myopic Policy with TDFS.* In this case, $\Pr[n^m_* = n]$, or the probability of sensing a certain channel n has different values for different m. Therefore, it is difficult to quantify the probability of SU m sensing channel n and competing with $j-1$ neighboring SUs on that channel, i.e., the $\Pr[n^m_* = n, J^m_n = j-1]$ term in (1.10). Thus, closed-form expression is not available for $H^m_{\text{CSI-TDFS}}$.

(viii) *CSI-aided Myopic Policy with FCFS.* It is hard to compute $E[H^{mn} | n^m_* = n, J^m_n = j-1]$ in (1.10) because the event of $[n^m_* = n]$ may occur when H^{mn} is the largest, or the second largest, $\cdots$, or the Mth largest depending on other SUs' sensing decisions, the outcome of sensing request resolution in previous rounds of SU competition, and the number of remaining SUs that have not successfully reserved any channel in FCFS MAC. Therefore, we could not obtain $H^m_{\text{CSI-FCFS}}$ in closed-form.

(ix) *Centralized Policy.* The centralized sensing strategy can be formulated as an optimization problem for general $N, M \geq 2$, but its performance is very difficult to express in closed-form.

A.4 Proofs for Diversity Gain Analysis in Section 1.3.2

In a homogeneous environment where all channels have the same availability and fading statistics for all SUs, each SU senses one of the channels with equal probability under the CSI-aided sensing policy: $\forall m, n$,

$$q_n = \Pr[n_*^m = n] = \Pr[\arg\max_n H^{mn} = n] = 1/N. \tag{A.37}$$

Substituting (A.37) into H_{CSI}^m in Table 1.2 and simplifying, we complete the proof of (1.15).

Next, we prove that g^{MN} in (1.16) is a decreasing function of M assuming $M = N$,

$$\begin{aligned} g^{MM} =& M \sum_{j=1}^{M} \frac{1}{j} \frac{(M-1)!}{(j-1)!(M-j)!} \left(\frac{1}{M}\right)^j \left(1-\frac{1}{M}\right)^{M-j} \\ =& \sum_{j=0}^{M} \binom{M}{j} \left(\frac{1}{M}\right)^j \left(1-\frac{1}{M}\right)^{M-j} - \left(1-\frac{1}{M}\right)^M \\ =& \Pr(X \le M) - \left(1-\frac{1}{M}\right)^M \end{aligned} \tag{A.38}$$

where X follows binomial distribution with parameters M and $1/M$, i.e., $X \sim B(M, 1/M)$. It is easy to show that $\Pr(X \le M) = 1$, so g^{MM} reduces to

$$g^{MM} = 1 - \left(1-\frac{1}{M}\right)^M. \tag{A.39}$$

Taking the derivative of g^{MM},

$$\frac{dg^{MM}}{dM} = -\left(1-\frac{1}{M}\right)^M \cdot \left(\frac{1}{M-1} + \ln\left(1-\frac{1}{M}\right)\right) \tag{A.40}$$

where $\forall M \ge 2$,

$$\frac{d\left(\frac{1}{M-1} + \ln\left(1-\frac{1}{M}\right)\right)}{dM} = \frac{1}{M-1}\left(\frac{1}{M} - \frac{1}{M-1}\right) < 0. \tag{A.41}$$

From (A.41), $\left(\frac{1}{M-1} + \ln\left(1-\frac{1}{M}\right)\right)$ is a decreasing function of M, and thus

$$\frac{1}{M-1} + \ln\left(1-\frac{1}{M}\right) > \lim_{M\to\infty}\left(\frac{1}{M-1} + \ln\left(1-\frac{1}{M}\right)\right) = 0. \tag{A.42}$$

From (A.42) it follows that $dg^{MM}/dM < 0$ in (A.40) and thus g^{MM} is a decreasing function of M.

Appendix B

B.1 Proof of Proposition 1 in Section 3.2.3

Quasiconcavity of $P^n_{\mathrm{FA,AND}}(\eta)$

We show the quasiconcavity of $P^n_{\mathrm{FA,AND}}(\eta)$ by proving its logconcavity [70, Section 3.5.1], that is, we prove that

$$\log\left[P^n_{\mathrm{FA,AND}}(\eta)\right] = \sum_{m\in\eta} \log\left[Q\left(g(\lambda^{mn})\right)\right] \tag{B.1}$$

is concave, where

$$g(\lambda) \triangleq \sqrt{2\lambda+1}\phi + \sqrt{\nu}\lambda. \tag{B.2}$$

Taking the second derivative of $g(\lambda)$, we obtain

$$g''(\lambda) = \frac{-\phi}{(2\lambda+1)^{3/2}} > 0 \tag{B.3}$$

where the PU-to-SU SNR $\lambda \geq 0$ and $\phi < 0$ (see footnote 6 on page 48), so $g(\lambda)$ is convex. Next, we note that the logarithm of the Q-function, i.e., $\log(Q(\lambda))$, is concave [70, Section 3.5.1] and decreasing. Therefore, $\log\left[Q\left(g(\lambda)\right)\right]$ is concave [70, Section 3.2.4] in λ and, thus, $\log[P^n_{\mathrm{FA,AND}}(\eta)]$ in (B.1) is concave in $(\lambda^{mn} : m \in \eta)$.

Quasiconvexity of $P^n_{\mathrm{FA,OR}}(\eta)$

We prove the quasiconvexity of $P^n_{\mathrm{FA,OR}}(\eta)$ by proving the concavity of

$$\log\left[1 - P^n_{\mathrm{FA,OR}}(\eta)\right] = \sum_{m\in\eta} \log\left[1 - Q\left(\tilde{g}(\lambda^{mn})\right)\right] \tag{B.4}$$

where

$$\tilde{g}(\lambda) \triangleq \sqrt{2\lambda+1}\tilde{\phi} + \sqrt{\nu}\lambda. \tag{B.5}$$

Taking the derivative of $1 - Q(\tilde{g}(\lambda))$ we obtain

$$\frac{d\left[1 - Q\left(\tilde{g}(\lambda)\right)\right]}{d\lambda} = \frac{1}{\sqrt{2\pi}} \cdot \exp\left(-\frac{\tilde{g}^2(\lambda)}{2}\right) \cdot \tilde{g}'(\lambda) \triangleq \frac{1}{\sqrt{2\pi}} \cdot \tilde{f}(\lambda) \cdot \tilde{g}'(\lambda). \tag{B.6}$$

Next, we prove the log-concavity of $\tilde{f}(\lambda)$ and $g'(\lambda)$ in (B.6):

$$\frac{d^2[\log \tilde{f}(\lambda)]}{d\lambda^2} = -\frac{\tilde{\phi}\sqrt{\nu}(3\lambda + 2)}{(2\lambda + 1)^{\frac{3}{2}}} - \nu < 0 \tag{B.7}$$

where the last inequality is from condition (3.20), so $\tilde{f}(\lambda)$ is log-concave. The function $\tilde{g}'(\lambda)$ is also log-concave because $\tilde{g}'(\lambda)\tilde{g}'''(\lambda) < \tilde{g}''(\lambda)^2$ [70, Section 3.5.2] as verified below (cf. footnote 6 on page 48):

$$\tilde{g}'(\lambda)\tilde{g}'''(\lambda) - \tilde{g}''(\lambda)^2 = \frac{2\tilde{\phi}^2}{(2\lambda + 1)^3} + \frac{3\tilde{\phi}\sqrt{\nu}}{(2\lambda + 1)^{5/2}} < 0. \tag{B.8}$$

Since multiplication, integration, and positive scaling preserve log-concavity, $\log\left[1 - Q\left(\tilde{g}(\lambda)\right)\right)$ is concave in λ [cf. (B.6)] and thus $\log\left[1 - P^n_{\mathrm{FA,OR}}(\eta)\right]$ in (B.4) is concave in $(\lambda^{mn} : m \in \eta)$. It is clear that the logconcave function $1 - P^n_{\mathrm{FA,OR}}(\eta)$ is also quasiconcave [70, Section 3.5.1] and thus $P^n_{\mathrm{FA,OR}}(\eta)$ must be quasiconvex.

Global maximum (minimum)

Because the logarithm is a strictly increasing function, the constrained optimization problems considered in Proposition 1 are equivalent to the following convex optimization problems in standard form [70, Section 4.2]:

$$\begin{aligned} \mathbb{P}1: \ \text{maximize} \quad & \log\left[P^n_{\mathrm{FA,AND}}(\eta)\right] \\ \text{subject to} \quad & (3.18) \end{aligned}$$

and

$$\begin{aligned} \mathbb{P}2: \ \text{maximize} \quad & \log\left[1 - P^n_{\mathrm{FA,OR}}(\eta)\right] \\ \text{subject to} \quad & (3.18) \end{aligned}$$

where the objective functions in $\mathbb{P}1$ and $\mathbb{P}2$ are both concave [cf. (B.1) and (B.4)] and the constraint (3.18) is an affine function [70, Section 4.2]. An important property for such problems is that any locally optimal point is also globally optimal [70, Section 4.2]. Moreover, we note that the objective functions and the constraints in $\mathbb{P}1$ and $\mathbb{P}2$ are symmetric, so they should both achieve a local (and thus global) maximum at $(\lambda^{mn} = \bar{\lambda} : m \in \eta)$ according to [93].

B.2 Proof of Proposition 4 in Section 3.3.1

Without loss of generality, we assume $\xi = \xi_1$ and $\zeta = \xi_2$ are the bottom-layer coalitions to be merged and denote the resulted bottom-layer partition as $\tilde{\rho} = \rho\backslash\{\xi_1\}\backslash\{\xi_2\} \cup \{\xi_1 \cup \xi_2\}$ with $|\tilde{\rho}| = |\rho| - 1$. Expanding the bottom-layer coalition value $U^n_{1/\mathrm{X}}(\eta;\rho)$ in (3.8) over all possible values of (X_{ξ_1}, X_{ξ_2}) in $\{0,1\}^2$ yields (B.9) [cf. (3.5)].

$$\frac{U^n_{1/\mathrm{X}}(\eta;\rho)}{\beta^n(1-P^n_{\mathrm{FA}}(\eta))} = \sum_{\tilde{\mathbf{x}}\in\{0,1\}^{|\rho|-3}} \left\{ \sum_{(x_1,x_2)\in\{0,1\}^2} \frac{|\eta| \Pr(X_{\xi_1}=x_1)\Pr(X_{\xi_2}=x_2)\prod_{i=1}^{|\rho|-3}\Pr(X_{\xi_{i+2}}=\tilde{x}_i)}{|\eta| + J_{\{\xi_1,\xi_2\}}(x_1,x_2) + J_{\rho\backslash\{\eta\}\backslash\{\xi_1\}\backslash\{\xi_2\}}(\tilde{\mathbf{x}})} \right\} \tag{B.9}$$

$$\frac{U^n_{1/\mathrm{X}}(\eta;\tilde{\rho})}{\beta^n(1-P^n_{\mathrm{FA}}(\eta))} = \sum_{\tilde{\mathbf{x}}\in\{0,1\}^{|\rho|-3}} \left\{ \sum_{x_1\in\{0,1\}} \frac{|\eta| \Pr(X_{\xi_1\cup\xi_2}=x_1)\prod_{i=1}^{|\rho|-3}\Pr(X_{\xi_{i+2}}=\tilde{x}_i)}{|\eta| + J_{\{\xi_1\cup\xi_2\}}(x_1) + J_{\tilde{\rho}\backslash\{\eta\}\backslash\{\xi_1\cup\xi_2\}}(\tilde{\mathbf{x}})} \right\} \tag{B.10}$$

$$U^n_{1/\mathrm{X}}(\eta;\rho) - U^n_{1/\mathrm{X}}(\eta;\tilde{\rho}) = \beta^n(1-P^n_{\mathrm{FA}}(\eta)) \cdot \sum_{\tilde{\mathbf{x}}\in\{0,1\}^{|\rho|-3}} \left\{ \prod_{i=1}^{|\rho|-3} \Pr(X_{\xi_{i+2}}=\tilde{x}_i) \cdot A(\tilde{\mathbf{x}}) \right\}. \tag{B.11}$$

Similarly, the bottom-layer coalition value $U^n_{1/\mathrm{X}}(\eta;\tilde{\rho})$ after the merger is derived in (B.10) by expanding over all possible $X_{\xi_1\cup\xi_2}$ values. Noting that $\rho\backslash\{\eta\}\backslash\{\xi_1\}\backslash\{\xi_2\} = \tilde{\rho}\backslash\{\eta\}\backslash\{\xi_1\cup\xi_2\}$ and $P^n_{\mathrm{FA}}(\xi_1\cup\xi_1) = P^n_{\mathrm{FA}}(\xi_1)P^n_{\mathrm{FA}}(\xi_2)$ [cf. (3.14)], we subtract (B.10) from (B.9) and simplify to obtain (B.11) where [cf. (3.4)–(3.9)]

$$\begin{aligned} A(\tilde{\mathbf{x}}) = {} & \Big(\frac{1}{b_1(\tilde{\mathbf{x}})} - \frac{1}{b_{12}(\tilde{\mathbf{x}})}\Big)|\eta| P^n_{\mathrm{FA}}(\xi_2)\Big(1-P^n_{\mathrm{FA}}(\xi_1)\Big) \\ & + \Big(\frac{1}{b_2(\tilde{\mathbf{x}})} - \frac{1}{b_{12}(\tilde{\mathbf{x}})}\Big)|\eta| P^n_{\mathrm{FA}}(\xi_1)\Big(1-P^n_{\mathrm{FA}}(\xi_2)\Big) \end{aligned} \tag{B.12}$$

with

$$\begin{aligned} b_1(\tilde{\mathbf{x}}) &= |\eta| + |\xi_1| + \textstyle\sum_{i=1}^{|\rho|-3}(1-\tilde{x}_i)|\xi_{i+2}| \\ b_2(\tilde{\mathbf{x}}) &= |\eta| + |\xi_2| + \textstyle\sum_{i=1}^{|\rho|-3}(1-\tilde{x}_i)|\xi_{i+2}| \\ b_{12}(\tilde{\mathbf{x}}) &= |\eta| + |\xi_1| + |\xi_2| + \textstyle\sum_{i=1}^{|\rho|-3}(1-\tilde{x}_i)|\xi_{i+2}|. \end{aligned} \tag{B.13}$$

It is easy to show that $A(\tilde{\mathbf{x}}) \geq 0$ in (B.12), and thus the expression in (B.11) must be nonnegative.

B.3 *Coarse* Nash Bargaining Solution Result in Section 3.3.1

In Figure B.1, we provide the cNBS [76] simulation result as mentioned in Section 3.3.1 with the same simulation setup as in Figure 3.6. We observe that:

1. the network throughput and energy consumption stay almost unchanged;
2. the number of dissatisfied SUs are smaller under the cNBS payoff allocation due to the nonpositive externality in the 1/X-model (cf. Proposition 4).

In cNBS, when an SU threatens other SUs on the same channel that it will (hypothetically) leave the grand coalition in the payoff negotiation process, all other SUs collude to work against this (hypothetically) deviating SU and thereby to suppress his component of the disagreement point. However, such payoffs of different SUs are not compatible and, thus, the result shown in Figure B.1 does not mean that the cNBS payoff allocation rule is more fair and/or more applicable than the other allocation rules.

Finally, various payoff allocation rules proposed for coalition games in the literature apply to our proposed bottom-layer game, but a comparison of these rules and/or different disagreement point choices is out of the scope of this thesis.

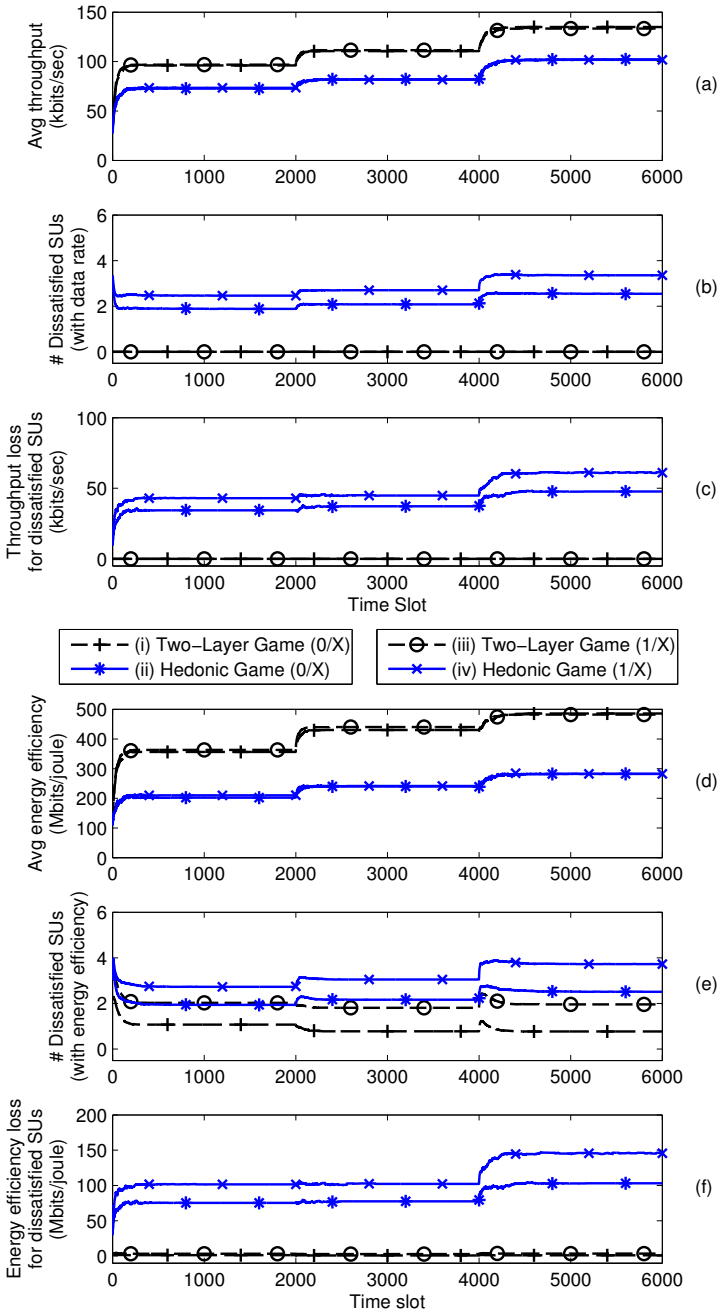

Figure B.1: Performance comparison of the proposed two-layer game and the hedonic game in [64] using the cNBS payoff allocation [76] in the 1/X-model.